



FMUC FACULDADE DE MEDICINA
UNIVERSIDADE DE COIMBRA


FUNDAÇÃO CALOUSTE GULBENKIAN
Instituto Gulbenkian de Ciência



INFLUENZA A VIRUS MODULATION OF MITOCHONDRIA DYNAMICS

Maria Inês Martins Veríssimo

Dissertação de Mestrado apresentada à Faculdade de
Medicina da Universidade de Coimbra em Investigação
Biomédica

2016

Orientador | Maria João Amorim, PhD

Co-orientador | Cláudia Pereira, PhD

Supervisor | Marta Alenquer, PhD

ACKNOWLEDGEMENTS

I would like to thank Maria João for seeing something in me and for giving me the opportunity to work at the Instituto Gulbenkian de Ciência within her team. This has given me the chance to learn a great number of laboratorial techniques, develop critical thinking and experience how science of excellence is made. I want to thank Maria João for all the teaching moments, her patience and dedication. Furthermore, I also learned from Maria João the empowerment role of woman in science and society.

Just as importantly, I want to thank Marta for tacking me under her wing since the beginning. Thank you for everything you taught me, for all the support throughout this year, for the “tough love” when I need it and for being a role model and showing me that, in life, you don’t always have to follow the norm to be successful.

I would further like to acknowledge the remaining members of the Cell Biology of Viral Infection lab. Sílvia, Zoé and Bárbara thank you for all the help and availability. Thank you for teaching me the meaning of professionalism and what it truly means to work in a lab as a team. Thank you to Filipe for the help in the final stages of my thesis. And Ana, I guess all I can say is thank you for being a true friend.

To my parents, words are never enough to thank you for all that you have done for me. Thank you for the unconditional support and for all the investment in my education. Thank you for giving me the space to make my own mistakes and the pillar to hold on to when I fall.

To Xavier, I am sorry that I have put 200km between us, but being apart only proved how strong we can be together. Thank you for giving me and us the space to grow and for the support, understanding and sharing of laughter and stress.

Lastly, but not least, I want to thank my close friends and apologize for the important moments I have missed. Thank you for listening and always being there for the good and the bad.

ABSTRACT

Mitochondria were originally described as the power house of the cell, but their importance expanded as their role in controlling several death processes was discovered. Recently, this organelle also emerged as the central player in a number of cellular innate immune responses, in particular interferon (IFN) responses, which constitute the first line of defence against intracellular pathogens. Mitochondria thus operate in response to cellular insults, ultimately deciding its fate. Interestingly, all mitochondria functions are intimately related to dynamic changes in their morphology and distribution. Morphological changes operate by fusion and fission events that are regulated by dynamin-like large GTPases, some of them already existing within the mitochondria (mitofusins) whilst others requiring active recruitment (dynamin-related protein 1, Drp1). The emerging view is that trafficking of cytoplasmic Drp1 to the mitochondria is a crucial regulatory step in mitochondrial responses. It has been demonstrated that many viruses interfere with mitochondria dynamics to favour infection at specific steps.

Influenza A virus (IAV) is an important human pathogen responsible for acute respiratory disease, which provokes yearly epidemics and occasional pandemics. Pathogenicity of infection has been associated with the ability to modulate immune responses. One report suggested that IAV decreases innate immunity activation by inducing mitochondria fragmentation. However, the knowledge on the mitochondria-IAV interplay remains largely unexplored. This thesis aims to study the effects of IAV infection in mitochondria dynamics, by elucidating the changes in mitochondria morphology during infection and determining the host and viral factors involved. The ultimate goal is to understand the mechanisms by which the IAV modulates mitochondria dynamics and elucidate the functional relevance of this process. Our results indicate that infection leads to mitochondria fragmentation of two types: complete fragmentation and fragmented mitochondria localised at the periphery. We further assessed that at least three viral components modulate mitochondria shape, the viral proteins NS1, PB1-F2 (and/or PB1-N40) and vRNPs. In addition we have tested the role of two host GTPases in the process: Drp1 and Arl17. Our results strongly suggest that Drp1 is implicated in mitochondria fragmentation during IAV infection whilst Arl17, although essential for infection, might operate at the level of mitochondria quality control.

SUMÁRIO

A mitocondria foi inicialmente identificada e descrita pelas suas funções no metabolismo celular e pelo seu papel na produção de grandes quantidades de energia na forma de ATP. A relevância deste organelo aumentou à medida que se descobriu que a mitocondria desempenha um papel fundamental em diversos processos de morte celular e, mais recentemente, em vários mecanismos de resposta imune inata da célula, particularmente, na activação de interferão que constitui a primeira linha de defesa contra agentes patogénicos intracelulares. A mitocondria adapta as suas funcionalidades em resposta a um estímulo celular e, em última análise, decide o destino da célula. Todas as funções mitocondriais estão relacionadas com alterações dinâmicas na sua morfologia e distribuição celular. A morfologia mitocondrial é alterada por processos de fissão e fusão que são regulados por GTPases, algumas, como as mitofusinas, estão presentes na mitocondria e outras, como a Drp1, necessitam de ser recrutadas para o organelo. A Drp1 é uma proteína citoplasmática e o seu recrutamento para a mitocondria é visto como um passo regulador das respostas e funções mitocondriais. A literatura descreve a forma como diversos vírus alteram a dinâmica mitocondrial de modo a favorecer a progressão da infecção.

O vírus influenza A (IAV) é um importante agente patogénico em humanos e é responsável por epidemias sazonais e pandemias ocasionais. A patogenicidade da infecção está directamente relacionada com a capacidade do vírus modular a resposta imune da célula e uma das formas de o fazer é induzindo a fragmentação da mitocondria de modo a diminuir a activação da resposta imune inata. No caso do IAV, há ainda muito por explicar em relação à interacção entre a mitocondria e o vírus. Por isso mesmo, os objectivos desta tese são o estudo dos efeitos da infecção pelo IAV na dinâmica mitocondrial, identificando alterações morfológicas da mitocondria e determinando se as alterações observadas são provocadas pelo vírus ou, pelo contrário, pela resposta da célula à infecção. O objectivo último deste estudo é perceber os mecanismos que o IAV utiliza para modular a dinâmica mitocondrial e elucidar qual a função deste processo. Os nossos resultados indicam que a infecção pelo IAV leva a um aumento da segmentação mitocondrial que pode ser uma fragmentação completa do organelo ou uma fragmentação localizada na periferia da célula. A nossa análise indica que pelo menos três componentes virais modulam a morfologia mitocondrial: as proteínas virais NS1 e PB1-F2 e/ou complexos virais denominados ribonucleoproteínas. Este estudo também envolveu a análise do papel de duas GTPases celulares na modulação da mitocondria durante a infecção: a Drp1 e a Arl17. Os nossos resultados sugerem que a Drp1 está implicada na fragmentação da mitocondria enquanto a Arl17 parece estar a actuar a nível do controlo da qualidade da mitocondria, não deixando, contudo, de ser essencial para a infecção.

CONTENTS

1. Introduction	1
1.1 Mitochondrial Functions and dynamics	1
1.2 Mitochondria in innate immunity	2
1.3 Influenza Viruses	4
1.4 Influenza A: The Virion.....	5
1.5 Influenza A: Replication cycle.....	7
1.5.1 Viral entry.....	8
1.5.2 Transcription and Replication	8
1.5.3 Viral Assembly and Budding.....	9
1.6 Objectives of the work.....	11
2. Methods	12
3. Results – Characterization of mitochondria modulation in PR8 infection and identification of viral factors involved	17
3.1 Building up a working hypothesis.....	17
3.2 Characterization of mitochondria’s morphology throughout a time course of IAV infection: mitochondria becomes more fragmented in PR8 infected cells over time .	19
3.3 Viral proteins that modulate mitochondrial dynamics: NS1 and PB1-F2 participate in shaping mitochondrial morphology in PR8 infected cells	23
3.4. Pulling the system to a maximum: targeting vRNPs to mitochondria increases mitochondrial fission.....	29
4. Results – Host factors involved in mitochondria modulation in PR8 infection.....	35
4.1. Building up a working hypothesis.....	35
4.2. Drp1 is required for normal viral production	38
4.3. IFN β 1 mRNA levels accompanied viral progression.....	40
4.4. Arl17 is required for normal viral production.....	41
4.5. Depleting Arl17 causes mitochondrial fractioning.....	42
4.6. Depletion of Arl17 delays nuclear export of NP	48
5. Discussion	49
6. Future perspectives	54
7. References.....	56
8. Supplementary data.....	60

LIST OF TABLES AND FIGURES

Table 2.1: Description of seeding specificities for each immunofluorescence experiment.....	13
Table 2.2: Reagents. Primary and secondary antibodies, siRNAs, plasmids, primers, transfection and cloning reagents used in the procedures described below.	15
Fig. 1.1 Mitochondrial dynamics are associated with different mitochondrial functions.	2
Fig. 1.4 Influenza A virus.....	6
Fig. 1.5 Influenza A virus replication cycle.....	7
Fig. 3.1 Quantification of mitochondrial distribution during IAV infection.....	18
Fig. 3.2 Classification system of mitochondria morphology.	20
Fig. 3.3 Mitochondria morphology changes during PR8 infection.	21
Fig. 3.4 PR8 infection induces mitochondria fragmentation.....	22
Fig. 3.5 Predicted modulation of mitochondrial morphology by NS1 and PB1-F2 viral proteins.....	23
Fig. 3.6 Characterization of Δ NS1 and Δ 8 viruses.....	24
Fig. 3.7 Δ NS1 viral infection mildly increases mitochondria fragmentation.	26
Fig. 3.8 Δ 8 viral infection modestly increases mitochondria fragmentation.	27
Fig. 3.9 PR8 WT viral infection leads to higher fragmentation levels at the mitochondria than Δ NS1 and Δ 8 viruses infection.	28
Fig. 3.10 The MitoRab11 method used to recruit vRNPs to the mitochondria and study mitochondrial morphology.....	30
Fig.3.11 Mitochondria morphology changes during PR8 infection when using the MitoRab11 method to obligatorily bind vRNPs to mitochondria.	32
Fig. 3.12 Using the MitoRab11 method to obligatorily bind vRNPs to mitochondria during PR8 infection increases mitochondrial fragmentation.	33
Fig. 4.1 Predicted working model for vRNP-mitochondria association at the cell periphery via Drp1 intermediate.	35
Fig. 4.2 The analysis of a large screen testing ARF proteins for their potential to disturb recruitment of vRNPs identified Arl17 as a potential mitochondrial modulator in infection.	37
Fig. 4.3 Schematic model for predicted Drp1 role in IAV infection.	38
Fig. 4.4 Drp1 depletion causes a decrease in viral production.....	39
Fig. 4.5 Drp1 depletion did not increase activation of innate immunity.	40

Fig. 4.6 | Arl17 has a mitochondria targeting signal. Illustrative image of Arl17 protein. 41

Fig. 4.7 | Arl17 depletion causes a decrease in viral production. 42

Fig. 4.8 | Arl17 depletion increases mitochondrial fragmentation..... 44

Fig. 4.9 | Infection in Arl17 depleted cells does not lead to significant changes in mitochondrial fragmentation. 45

Fig. 4.10 | Infection causes mitochondrial fragmentation in an Arl17 independent manner. 46

Fig. 4.11 | Infection in Arl17 depleted cells is stalled at the nucleus. 48

Fig. 5.11 | Models proposed for the role of mitochondria fragmentation and localization at the periphery, modulated by viral infection. 51

Fig. S1 | Segmentation of mitochondria using the SQUASSH automated tool..... 60

Fig. S2 | Rescue assay in HeLa cells. 61

Abbreviations

A549	Alveolar 549 cells
ARF	ADP-ribosylation factor
ARL	ARF-like
BSA	Bovine serum albumin
CA	Constitutively active
CARDS	Caspase activation and recruitment domains
DN	Dominant negative
DNA	Deoxyribonucleic acid
Drp1	Dynamin 1-like protein
GAP	Gtpase activating protein
GAPDH	Glyceraldehyde 3-phosphate dehydrogenase protein
GEF	Guanine exchange factor
H or HA	Hemagglutinin
IAV	Influenza A virus
IFN	Interferon
IMM	Inner mitochondria membrane
IRF3	Interferon regulatory factor 3
IRF7	Interferon regulatory factor 7
M1	Matrix protein 1
M2	Matrix protein 2
MAVS	Mitochondrial antiviral-signaling protein
MDCK	Madin-Darby canine kidney cells
Mff	Mitochondrial fission factor
Mfn1	Mitofusin 1
Mfn2	Mitofusin 2
MiD49	Mitochondrial dynamics proteins 49
MiD51	Mitochondrial dynamics proteins 51
MOI	Multiplicity of infection
N or NA	Neuraminidase
NEP	Nuclear export protein
NLR	NOD-like receptors
NLRP3	NLR family pyrin domain containing 3
NP	Nucleoprotein
OMM	Outer mitochondria membrane
OPA1	Optic atrophy 1
p.i.	Post-infection
PA	Polymerase acidic protein
PB1	Polymerase basic subunit 1
PB2	Polymerase basic subunit 2

PFU	Plaque forming unit
PRR	Pattern recognition receptor
qRT PCR	Quantitative real time polymerase chain reaction
RD	Regulatory domain
RIG-I	Retinoic acid-inducible gene 1
RLR	RIG-I-like receptor
RNA	Ribonucleic acid
ROS	Reactive oxygen species
TLR	Toll-like receptor
TRADD	TNFR1-associated death domain protein
TRAF1	TNF receptor-associated factor 1
TRIM25	Tripartite motif containing 25
UTR	Untranslated region
vRNA	Viral RNA
vRNP	Viral ribonucleoprotein
WT	Wild-type

1. Introduction

1.1 | Mitochondrial functions and dynamics

Mitochondria are maternally inherited, multifunctional, semi-autonomous, cytoplasmic organelles that originated from symbiotic bacteria and have, since then, evolved with their host¹. Mitochondria possess their own circular genome that encodes 13 proteins essential in mitochondrial respiratory complexes, 22 transfer RNAs and 2 ribosomal RNAs. Yet, the majority of mitochondrial proteins are encoded by nuclear genes, synthesized in the cytoplasm and transported to the mitochondria². Structurally, mitochondria have four main compartments: the outer mitochondrial membrane (OMM), the matrix that is enclosed by the inner mitochondrial membrane (IMM) and the inner membrane space³.

Mitochondria take part in fundamental reactions in the cell. These organelles participate in catabolism, anabolism and signaling. Mitochondria uptake substrates from the cytoplasm and use them in fatty acid oxidation, the citric acid cycle, the electron transport chain and respiration⁴. Mitochondria are involved in the synthesis of amino acid, lipid, nucleotide, heme and NADPH, which is subsequently used to produce ATP in the electron transport chain⁴. The generation of reactive oxygen species (ROS) in this process can activate important signal transduction pathways like that of MAP kinase⁵, whilst excessive ROS production may lead to cell death⁶. Mitochondria sequester and selectively release calcium mediating cellular signaling and have a vital role in apoptosis by mediating the release of cytochrome c, a fundamental step in the apoptosome formation⁷. Mitochondria also act as signaling platforms for innate immunity and antiviral signaling through the regulation of mitochondrial anti-viral signaling (MAVS) proteins (described in detail in section 1.2)⁸.

Mitochondria are highly dynamic organelles, continuously changing their distribution within the cell and their shape through combined action of fission and fusion events. The key regulator of mitochondrial fission is the GTPase dynamin-related protein 1 (Drp1). Drp1 resides primarily in the cytoplasm and is actively recruited to the mitochondria outer membrane, where the adaptor proteins fission 1 (Fis1), mitochondrial fission factor (Mff) and mitochondrial dynamics 49 and 51 (MiD49 and MiD51) function as receptors for Drp1. Activation and trafficking of Drp1 to the mitochondria is a complex regulatory step, involving different post-translational modifications⁹, which has recently been proposed to be regulated by Rab11a¹⁰. Membrane-bound Drp1 oligomerizes as a ring and, in the presence of GTP, constricts, causing the scission of both outer and inner mitochondrial membranes. Recent studies suggest that this process is assisted by endoplasmic reticulum (ER) tubules and actin filaments located in close proximity to Drp1 constriction sites¹¹.

Mitochondrial fusion occurs in a brief kiss-and-run pattern. Fusion of the OMM is mediated by Mitofusins 1 and 2 (Mfn1 and Mfn2), whilst the Optic atrophy protein 1 (OPA1) is responsible for the fusion of the IMM ¹². Cycles of mitochondria fusion and fission coordinate mitochondrial distribution. Division of the mitochondria network into smaller organelles facilitates their transport along the microtubules by motor proteins ^{13,14}.

Many mitochondrial functions described have been linked with changes in their morphology and position. Fragmentation stages have been associated with mitosis, mitophagy and apoptotic processes whilst elongation relates to an increase in bioenergetics and innate immune response ¹⁵ (Fig.1.1). Also, mitochondria have been reported to cluster at the perinuclear region in response to hepatitis B infection or at sites with high demand of ATP ¹⁶.

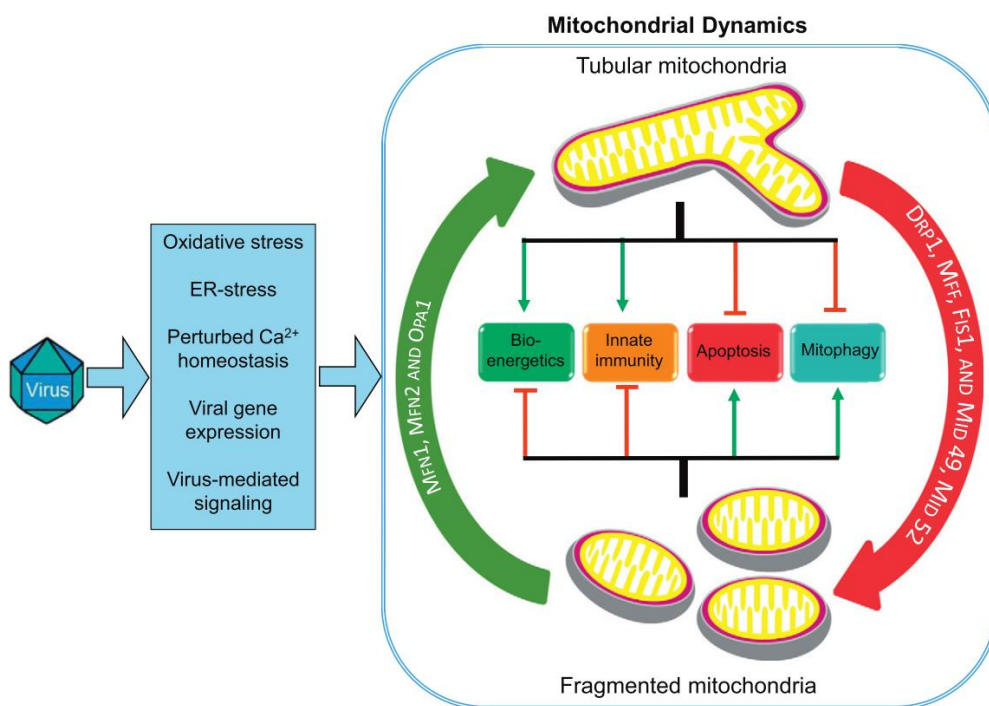


Fig. 1.1 | Mitochondrial dynamics are associated with different mitochondrial functions. Mitochondria elongation relies Mfn 1 and Mfn 2 to fuse the OMM and on OPA1 to mediate fusion of the inner mitochondrial membrane. Elongated mitochondria relates with processes of activation of innate immunity and increased bio-energetics. Fission relies on Drp1, fission 1 (Fis1), Mff and MiD49 and MiD51. Fragmented mitochondria relates to an increase in mitophagy and apoptosis. Viruses can modulate the mitochondrial dynamics thus interfering with mitochondrial functions. (Image from Khan et al., 2015 ¹⁵)

1.2 | Mitochondria in innate immunity

Broadly conserved microbial components can be detected by eukaryotic cells that trigger an initial response to infection. Recognition of foreign material is made by specific sensors known as pattern-recognition receptors (PRR) that scan for nucleic acids in unusual places or bearing uncommon features, such as 5' triphosphate ends, dsRNA, dsDNA, genomic DNA, ssRNA. Three major families of PRR have been characterized: the transmembrane Toll-like receptors (TLR), and the cytosolic retinoic acid-inducible gene-I (RIG-I)-like receptors (RLR) and Nod-like

receptors (NLRs). The first two trigger type I interferon (IFN) to activate the transcription of a range of inflammatory and defense mechanisms and NLR triggers the caspase 1 inflammasome^{17,18}.

In recent years, an emerging role for mitochondria in innate immunity, in particular in responses mediated by RLR and NLR receptors, has become evident. Mitochondrial antiviral signaling (MAVS) protein has been shown to trigger a type I interferon response upon binding to the dsRNA cytosolic sensors RIG-I and melanoma differentiation-associated gene-5 (MDA5), both members of the RLR family^{19–22}.

RIG-I and MDA-5 are helicases with ATPase activity. They contain a C-terminal regulatory domain (RD) and two caspase activation and recruitment domains (CARDs) in the N-terminus. In uninfected cells, RIG-I is maintained in a closed, inactive conformation by intramolecular interactions between the RD and CARD domains²³. The C-terminal RD of RIG-I recognizes and binds 5'-triphosphate uncapped RNA structures. Upon viral RNA binding, RIG-I is polyubiquitinated by the E3 ubiquitin ligases TRIM25 and RIPLET, resulting in the exposure of the CARDs domain and its oligomerization and translocation from the cytoplasm to the mitochondrial outer membrane, where RIG-I binds MAVS via CARD-CARD interactions. Upon activation, MAVS oligomerizes and recruits a number of downstream signal effectors, including the tumour necrosis factor receptor associated factors (TRAF) 2 and 6, and the TNFR1-associated death domain protein (TRADD), which activate the transcription factor NF- κ B, ultimately resulting in pro-inflammatory cytokine release^{23,24}. MAVS also interacts with several molecules that lead to the activation of the interferon response factors IRF3 and IRF7 and, consequently, to the induction of type I interferon regulated genes^{23,24}.

The activation of these pathways represents a first line of defence against infection and promotes an impairment of viral progression. Nevertheless, MAVS have to be tightly regulated in order to maintain a functional antiviral innate response. Cellular factors can regulate MAVS by post-translational modifications, by protein-protein interactions and by alterations in mitochondrial dynamics²³. Initial evidence for the role of mitochondrial dynamics in MAVS signalling came from studies demonstrating that cells infected with Sendai virus or transfected with poly (I:C) resulted in elongation of mitochondria²⁵. This study also showed that phosphorylation of IRF3 was delayed in cells with fragmented mitochondria and that RLR signalling was attenuated by mitochondrial fragmentation but was enhanced upon mitochondrial fusion²⁵. A later study showed that MFN1 acts as a positive regulator of MAVS mediated antiviral signalling by a redistribution of MAVS to form aggregates. The interaction of MFN1 with MAVS is thought to increase mitochondrial fusion as a way to facilitate MAVS aggregation²⁴.

In addition to their role in mediating responses triggered by RLR receptors, mitochondria are also involved in the activation of NLR family pyrin domain-containing 3 (NLRP3) inflammasomes. NLRP3 inflammasomes are activated by accumulation of ROS generated through mitochondrial respiration, or by cytosolic mitochondrial DNA that are released from damaged organelles. Activation of this

pathway induces, in a caspase 1-dependent manner, the secretion of inflammasome-dependent cytokines including IL-1 β and IL-18¹⁸. Furthermore, MFN2 was also shown to be required for NLRP3 inflammasome activation upon RNA virus infection²⁶.

Several successful viral infections have been reported to take over the mitochondrial dynamics mechanisms in order to inhibit antiviral signaling. For instance, hepatitis C virus (HCV) enhances mitochondrial fission through Drp1 activation²⁷. By translocating Parkin protein to the mitochondria, HCV accentuates mitophagy thus inhibiting innate immune responses and apoptosis^{15,28}. Hepatitis B virus also inhibits innate immunity and apoptosis by enhancing mitochondrial fragmentation and mitophagy through phosphorylation of Drp1 and up-regulation of mitophagy associated proteins Parkin and PINK1¹⁶.

Epstein-Barr virus (EBV) enhances mitochondrial fission through induction of Drp1 expression, affecting cell migration and avoiding apoptosis¹⁵. Pseudorabies virus increases mitochondrial fragmentation by altering functioning of Miro protein which is responsible for mitochondrial mobility, thus affecting calcium signaling and mitochondrial motility¹⁵. Measles virus and Newcastle disease virus induce mitophagy to reduce the levels of MAVS and cripple innate immunity^{29,30}. Severe acute respiratory syndrome-coronavirus (SARS-CoV) enhances mitochondrial fusion by reducing Drp1 levels in order to use the cell's ubiquitination and proteosomal degradation system to degrade MAVS, TRAF3 and TRAF6³¹.

Regarding influenza A virus (IAV), very little is known about the interplay between this virus and mitochondria. A recent study indicates that incoming viral ribonucleoproteins (vRNPs) associate with mitochondria by attaching to RIG-I, and suppress type I IFN signalling mediated by MAVS³². Furthermore, Influenza A virus protein PB1-F2 also seems to be involved in impairing innate immunity by interfering with mitochondrial dynamics. This viral protein has been shown to translocate into mitochondrial inner membrane space via TOM40 channels and induce mitochondrial fission due to dissipation of membrane potential^{15,33}. This process was dependent on Drp1 and correlated with defective RIG-I signaling and impaired activation of NLRP3 inflammasomes³³.

1.3 | Influenza Viruses

Influenza viruses are infectious agents responsible for what is commonly referred to as flu. These viruses infect a large variety of vertebrates and, in humans, are one of the main causes of acute respiratory disease, being associated with yearly epidemics and sporadic deadly pandemics (World Health Organization). There are four types of influenza viruses: A, B, C³⁴ and D³⁵. Influenza A virus (IAV) is the most relevant type for human health and, besides humans, it also infects pigs, bats, horses and wild birds, which are the primary reservoir of most influenza A viruses. Influenza B viruses infect humans and seals. Infections cause symptoms less severe than those attributed to influenza A and are associated with less severe outbreaks and

pandemics. Influenza A and B types are both considered during annual vaccine design. Influenza C and D types cause mild infections in pigs, but, out of the two, only influenza C viruses infect humans ³⁴.

There is a vast diversity of influenza A viruses, separated into several subtypes labelled accordingly to the presence of different types of the viral surface proteins hemagglutinin (H or HA) and neuraminidase (N or NA). There are 18 different hemagglutinin identified (H1 – H18) and 11 neuraminidase subtypes (N1 – N11) with different host distributions ³⁶. Each subtype presents restricted viral growth to specific hosts, but some of the IAV outbreaks with worst outcomes for human health were originated when specific IAV subtypes shifted hosts and became able to infect humans. Current epidemic strains circulating in humans are H3N2 and H1N1. These strains were responsible for pandemic events in 1968 and 2009, respectively, and have since become established in the human population. H3N2 is most commonly known as Hong Kong flu. It originally infected birds and was responsible for infections in 1 to 3 million people with 700 000 deaths worldwide ³⁷. H1N1 known as swine or Mexican flu, originally infected birds and pigs and caused 18 000 deaths worldwide³⁸.

The shift in viral hosts is a result of two events that modulate viral adaptation: antigenic drifts and antigenic shifts. The first arises from constant mutations on account of the error prone RNA polymerase the virus encodes, which reshapes the viral antigens and allows continued infections in the same host. Antigenic shift occurs when the same cell is co-infected with two different strains and the genome of the viruses mix and become reassorted, producing a new combination of HA and NA subtypes present in the surface of the virion. When these changes take place, the hosts' immune defences developed against HA and NA are no longer capable of recognizing the new antigens and thus infection spreads ³⁹.

Latest reports from the World Health Organization (WHO) show that, for the time period from the 16th May 2016 to 29th May 2016, more than 61285 specimens were analyzed, 4320 (7%) were positive for influenza viruses, of which 1276 (29.5%) were typed as influenza A and 3044 (70.5%) as influenza B. Of the sub-typed influenza A viruses, 540 (71%) were influenza A (H1N1) and 221 (29%) were influenza A (H3N2).

1.4 | Influenza A: The Virion

Influenza A viruses belong to the *Orthomyxoviridae* family. Structurally, the virion presents an envelope derived from the host's cell membrane, which contains 3 viral proteins at the surface: hemagglutinin (HA), neuraminidase (NA) and matrix protein 2 (M2). The inner core encloses the viral genome and 2 proteins: matrix protein 1 (M1) and nuclear export protein (NEP) also named non-structural protein 2 (NS2) (Fig. 1.4) ³⁶.

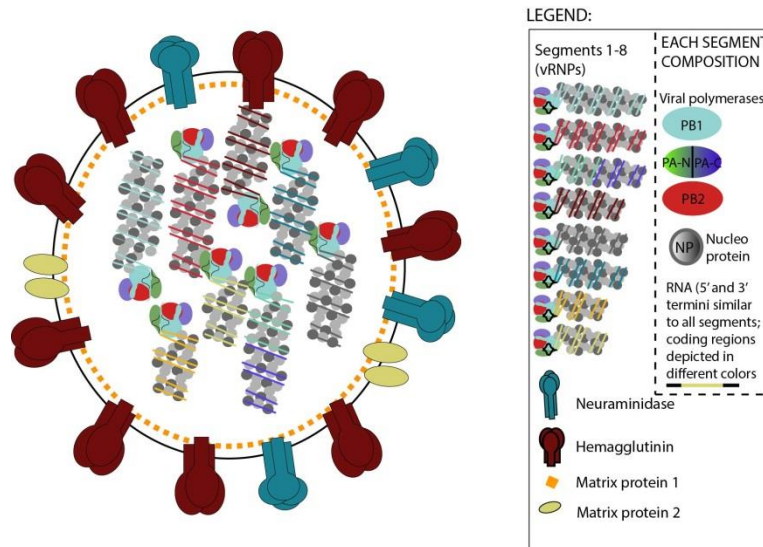


Fig. 1.4 | Influenza A virus. The viral particle has an envelope derived from the host lipid bilayer with surface proteins hemagglutinin (HA), neuraminidase (NA) and matrix protein 2 (M2). The core bridged by matrix protein 1 (M1) contains the segmented genome: 8 segments of negative-sense RNA coated with nucleoprotein (NP), and the viral polymerase complex³⁶. The viral RNA is coated by NP at the ratio of 1 NP: 24 nucleotides. The extremities are complementary and form a double-stranded structure, bound by the polymerase complex PA, PB1 and PB2. The segments adopt a cork-screw conformation with a loop region opposed to the polymerase. (Image made by Dr. MJ Amorim)

IAV genome is composed by eight independent RNA segments, single stranded and negative sense, all organized in the same fashion with the middle antisense coding region flanked by two small untranslated regions. These UTRs are highly conserved and show partial complementarity which leads to base pairing, required for viral polymerase binding³⁶.

The eight RNA segments encode ten essential proteins and eight accessory proteins⁴⁰. The first three segments encode the three subunits of the viral polymerase: polymerase basic protein 2 (PB2), polymerase basic protein 1 (PB1) and polymerase acidic (PA). Segment five encodes for the nucleoprotein (NP), whilst segments four and six express the surface viral proteins hemagglutinin (HA) and neuraminidase (NA), respectively. Matrix protein 1 and 2 (M1 and M2) are encoded by segment 7. Non-structural proteins 1 and 2 (NS1 and NS2) are encoded by segment 8. Several segments are capable of producing more than one protein. For instance, segment 2 has three different open reading frames (ORFs), one coding for the viral polymerase subunit PB1, another coding for the much smaller viral protein PB1-F2 that, as described in section 1.2, localizes to the mitochondria, inducing fission, and yet another one coding for PB1-N40 that is less abundant in infection and which function in infection is currently unknown^{41,42}. Another example includes the alternatively spliced transcripts, M2 and NEP, obtained from segment 7 and 8, respectively. They exist in lower abundance than M1 and NS1 transcripts coded in the same segments⁴³. In segment 3, a ribosomal frameshift results in a second protein PA-X⁴⁰. The relevance of this protein is still to be understood, although mutant viruses lacking the peptide show reduced levels of replication and pathogenicity. Other proteins have been identified, but require characterization during infection (M42⁴⁴, M3⁴⁵, PA-N155⁴⁶, PA-N182⁴⁶ and PB2-S1⁴⁷).

The viral genome is coated by several copies of NP, which bind the phosphate backbone of the RNA strand every twenty four nucleotides, without sequence specificity. The trimeric RNA-dependent RNA polymerase binds to both terminal sequences of the single-stranded genome. This RNA-protein complex is called viral ribonucleoprotein (vRNP). Inside the virion, vRNPs are arranged in a 7+1 conformation. ⁴⁸.

1.5 | Influenza A: Replication cycle

Briefly, IAV enters the cell in an endosome, the viral genome is released to the cytoplasm and is transported to the nucleus where it undergoes transcription and replication. After *de novo* synthesis of viral genome and proteins, viral components are transported through the cytoplasm to the plasma membrane, to form a new virion as depicted in Figure 1.5. IAV lifecycle will be discussed in detail below, accordingly to the following divisions of stages in the viral lifecycle: 1) viral entry, 2) transcription and replication and 3) assembly and budding.

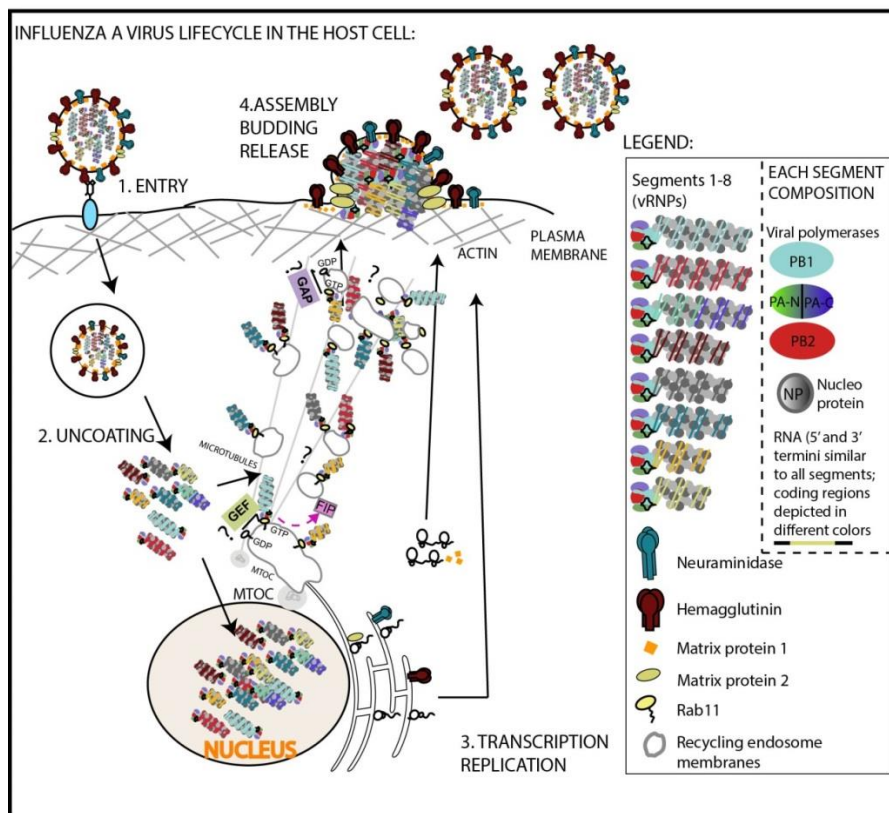


Fig. 1.5 | Influenza A virus replication cycle. IAV enters the cell by receptor mediated endocytosis through the binding of HA to sialic acid residues at the plasma membrane. After internalization, the acidity inside the endosome increases resulting in the fusion of the viral envelope and the endosomal membrane, and in the release of vRNPs to the cytoplasm. Upon translocation of vRNPs into the nucleus, transcription and replication occur and the newly-synthesized segments are exported to the cytoplasm. vRNPs are accumulated near the microtubule organizing centre and are loaded onto Rab11 vesicles and transported using the recycling endosome towards the plasma membrane, where the virus assembles its components and buds out. The binding of vRNPs to Rab11 vesicles compromises the host recycling pathway and leads to the coalescence of the vesicles in the cytoplasm. Eventually, each of the segments needs to be incorporated into the budding particle created with host membrane and decorated with HA, NA and M2 and interiorly with M1. Adapted from ⁴⁹.

1.5.1 | Viral entry

HA binds to molecules of sialic acid present in glycoproteins at the cell surface and the virus enters the cell through endocytosis⁵⁰. The virus is transported from early to late endosomes, in an actin and microtubule-dependent manner^{51,52}. Inside the endosome, during maturation, pH decreases due to v-ATPase activity which triggers a conformational change in HA that leads to fusion of the membranes of the virus and the endosome⁵⁰. The progressive decrease in pH activates viral protein M2, which acts as a proton pump to acidify the virus inner core, weakening the affinity between matrix protein M1 and vRNPs. Endosomal and viral membranes fuse and vRNPs are released into the cytoplasm⁵⁰.

vRNPs then travel towards the nucleus. In order to enter this compartment, viral proteins must have nuclear localization signals (NLSs) that bind to importins in the cytoplasm, but, at this point, each vRNP relies only on the NP nuclear localization signals. Importins belong to a family of nuclear transport receptors that travel through the nuclear pore complexes (NPCs) in the nuclear envelope. Once non-canonical importins $\alpha 1$ and $\alpha 5$ have crossed into the nucleus and bind Ran-GTP, the vRNPs are released^{53–55}.

1.5.2 | Transcription and Replication

In the nucleus, the viral genome is transcribed and replicated into positive sense mRNA and cRNA, respectively⁴³. Host transcription occurring within the nucleus ensures the “cap-snatching” mechanism by which the viral polymerase cleaves and takes for itself sequences from newly formed host mRNAs that include the 5'cap structure. Besides acting as a primer for the viral polymerase, this guarantees mRNA processing and translation of viral proteins through host pathways. Replication occurring within the nucleus allows for new vRNPs to form shielded from cytoplasmic proteins that detect foreign genetic material and trigger an antiviral response⁵⁶.

vRNPs diffuse through the nucleoplasm and begin to transcribe and later to replicate their genome. In order for transcription to begin, the viral polymerase subunits must come together with the 5' end of the host mRNA, which resembles a hook structure, and binds to the PA and PB1 subunits. PB2 and PA are involved in the “cap-snatching” mechanism^{56,57}. PB2 has a cap-binding domain which faces the endonuclease domain of PA⁵⁸, thus capturing and cleaving the host's cap structure. PB1 is the subunit that presents the polymerase active site and accounts for the addition of new nucleotides to form the viral mRNA until it reaches a short polyU sequence located almost at the end of each segment^{57,59}. When the mRNA exits the polymerase complex, it undergoes the host's pathways of processing and translation. New viral proteins are formed, some of which have to be imported to the nucleus to form new vRNPs⁶⁰.

Replication peaks later in infection and it produces a full-length cRNA that has to be copied again to amplify the viral genome. The 3' end of the vRNA template needs to be released of the vRNP-

associated polymerase and bind a newly synthesized RNA polymerase. The polymerase needs GTP to initiate elongation of the cRNA and the 5' end of the new cRNA needs to bind the polymerase. Once this process is complete, NP proteins start binding to the cRNA and replication continues generating an encapsidated cRNA in a 5' to 3' direction. A similar process then turns cRNA into vRNA ⁶¹.

At this stage of infection vRNPs leave the nucleus, which means that viral proteins must have nuclear export signals (NESs) that bind to exportin-Ran-GTP complexes. Proteins M1 and NEP are responsible for this process. Once the exportin CRM1 reaches the cytoplasm and unbinds Ran-GTP the vRNP-M1-NEP chain complexes are released⁶²⁻⁶⁶. The virus has developed a way of timing nuclear export by controlling segment 8 transcription. Only 10-15% of segment 8 transcripts code for NEP as a result of a weak splicing site which delays the synthesis and accumulation of the protein^{67,68}. The remaining 85-90% of transcripts code for viral NS1 earlier in infection that among other functions blocks interferon response by direct inhibition of RIG-I ⁶⁹. This inhibition allows vRNPs to better escape viral RNA host sensors on the way to the plasma membrane.

1.5.3 | Viral Assembly and Budding

In the cytoplasm, vRNPs concentrate around the pericentriolar recycling endosome, near the microtubule organizing centre. Here they interact with recycling endosomes and bind to those that are Rab11a positive ⁷⁰⁻⁷³. This is an important step in the virus lifecycle as it allows for the vRNPs to be trafficked through the microtubule network, alongside the recycling endosomes, towards the plasma membrane where new virions can be released. vRNP binding to Rab11a vesicles competes with Rab11a effectors ⁷⁴. Such competition decreases the levels of Rab11a effectors present at the vesicles, which stalls the host recycling process ⁷⁴. Slowing down vesicular sorting, leads to an agglomeration of vesicles carrying different vRNPs which allows for the close contact between segments ⁷⁴, perhaps facilitating intersegment interaction that might aid in selective packaging of the vRNPs before reaching the plasma membrane, by a process yet unknown.

Assembly of vRNPs and viral proteins at the plasma membrane occurs at lipid raft domains that are able to limit protein diffusion ^{75,76}. Envelope proteins HA and NA are targeted to these regions, whereas the M2 protein is excluded from these domains ^{60,76}. HA and NA presence in lipid rafts may serve to provide a local alteration in membrane curvature that starts the budding process. The cytoplasmic tails of HA and NA may then serve as docking sites for M1 that recruits vRNPs to the budding sites ⁷⁷. The delayed expression of M2 may allow for the initiation of budding, and for proper virion assembly, before the mechanism of scission and virion release is provided. At the budding neck, M2 may exert its own positive membrane curvature providing the final force needed to mediate membrane scission and the release of the budding virion⁶⁰. Following the completion of membrane scission, the virion may still be coupled to the cell membrane due to the

interaction of HA with cell-surface sialic acid. NA is then able to play the final role in virus budding by cleaving sialic acid off the cell surface and freeing the budded virion ⁷⁵. The virus then needs to undergo one last step of maturation in order to proceed into the next round of infection, by cleavage of viral protein HA by extracellular proteases ^{78,79}. This modification is fundamental for membrane fusion between endosomal and virus membranes upon entry ⁷⁸.

1.6 | Objectives of the work

Mitochondria play fundamental roles in eukaryotic cells and are highly dynamic organelles. Mitochondria react to external stimuli changing morphology and motility and adapting its functionality, which can lead to activation of an antiviral status, mitophagy and apoptosis¹⁹. In addition, cellular function induces mitochondria damage that is repaired using a quality control system, essential in maintaining a fully functional mitochondrial network⁸⁰. The quality control system also relies on fission and fusion machineries, changing mitochondria morphology and motility.

Viruses have the ability to take over the host's machinery, including that controlling mitochondria morphology and motility¹⁵. Several viruses have been reported to alter mitochondrial dynamics through increased mitochondrial fission as a means to avert innate immunity and antiviral signaling¹⁵. When it comes to IAV, not much is known about the mechanisms it uses to modulate the mitochondrial machinery. One report indicated that mitochondrial fragmentation increased in IAV infection, on account of the PB1-F2 viral protein³³ and another showed that mitochondria bind incoming vRNPs to avoid being recognized by innate immunity mechanisms³². However, how mitochondria behave during the course of infection is far from well understood.

Altogether, this study aims to characterize mitochondrial morphology in IAV infection and to identify potential viral and host factors that modulate mitochondria during infection. Subsequently, we aim at determining the functional relevance of mitochondria reaction to infection and of viral modulation of mitochondrial dynamics. This thesis is divided into two main chapters of results where the following topics will be assessed:

- I. Investigate whether infection induces fragmentation of mitochondria and point out viral factors responsible for this alteration;
- II. Investigate mitochondrial host mechanisms taken over by IAV virus.

2. Methods

Cell lines | Three different cell lines were used throughout this work: 1) HeLa cells originated from cervix adenocarcinogenic epithelia, 2) Madin-Darby canine kidney epithelial cells (MDCK) and 3) human alveolar basal epithelial cells originated from lung carcinoma (A549). HeLa cells were used to study mitochondrial morphology by immunofluorescence due to their extended shape and larger cytosolic portion. MDCK cells were used in viral titration assays by plaque forming due to their high adherence to the substrate and resistance to the presence of trypsin. A549 cells were used for ARL17 depletion as they represent a better model to study human lung epithelia.

Cell culture | All cell lines were cultured in Dulbecco Modified Eagle medium (DMEM) (Life Technologies), supplemented with 10% fetal bovine serum (V/V), 200mM glutamine, 100U/ml penicillin and 10µg/ml streptomycin. Cells were grown at 37°C in a humidified atmosphere containing 5% CO₂.

Infection | Infections were carried out with reverse genetics-derived A/Puerto Rico/8/34 (PR8; H1N1) grown in chicken eggs with the exception of PR8 Δ8 and PR8 ΔNS1 that were grown in MDCK (the PR8 WT virus used in parallel with mutated viruses was also grown in MDCK cells).

The viruses were added at a multiplicity of infection (MOI) specified in each case, in serum-free DMEM (Life Technologies) or in OptiMEM Reduced Serum Media (Life Technologies), in the case of cells previously transfected. After 45 min of infection, cells were overlaid with serum-free DMEM supplemented with 0.14% (w/v) bovine serum albumin (BSA).

In the particular case of Drp1 depleted cells a multicycle infection was performed. PR8 was added to cells at a MOI of 0.001 and 45 min later cells were overlaid with serum-free DMEM supplemented with 0.14% (w/v) BSA and 1µg/mL TPCK trypsin that would allow for HA to be cleaved upon viral exit and thus carry on a new cycle of infection.

Cloning | pMitoCherryRab11aDN was derived from two other pre-existing plasmids: pMitoCherryRab11aCA and pCherry-Rab11aDN. Both plasmids were digested with NheI and XhoI restriction enzymes (Table 2.2). The TOM20-Cherry insert from pMitoCherryRab11aCA was isolated. The Cherry tag was detached from pCherry-Rab11aDN and the remaining plasmid was used as the vector. Both the insert and the vector were purified by agarose gel. Upon vector ligation, the new plasmids were used to transform E. coli TOP10 by heat-shock. Bacteria were plated and incubated overnight at 37°C in plates with agarose-LB media supplemented with kanamycin, the antibiotic granting specific resistance. Clones were screened for the presence of the insert by PCR and restriction digestions. Positive clones were purified using with NZYMiniprep kit.

Plasmid transfection | 5x10⁴ HeLa cells were transfected with 250ng of pCherry, pMitoCherryRab11aWT, pMitoCherryRab11aCA and pMitoCherryRab11aDN using

Lipofectamine LTX, accordingly to manufacturer's instructions (Table 2.2). Cells were immediately infected with an MOI of 20 and kept at 37°C and 5% CO₂ for 14 hours.

siRNA silencing | Cells were transfected with FlexiTube siRNA (Qiagen) targeting endogenous human Drp1 (Table 2.2) or ARL17 (Table 2.2). DharmaFECT-1 (Dharmacon) was used as a transfection agent accordingly to manufacturer's instructions (Table 2.2). Cells were incubated for 36 hours at 37°C and 5%CO₂ before infection with PR8. A non-targeting RNA sequence was used as a negative control (Table 2.2).

Rescue Assay | 3x10⁴ HeLa cells were transfected for 36 hours with siRNAs targeting ARL17 or control siNT, and, in parallel with 500ng of pGFP or pARL17-GFP using Lipofectamine®2000 accordingly to manufacturer's guidelines (Table 2.2). Cells were infected with PR8 (MOI of 5) and incubated for 10 hours at 37°C and 5%CO₂. After this time, supernatants were collected for plaque assays, cells were lysed in Laemmli buffer for western blotting.

Immunofluorescence | Cells were seeded on glass coverslips (TRADE), as detailed in Table 2.1, transfected, when indicated, and then infected. After the indicated time post-infection cells were fixed in 4% (v/v) paraformaldehyde for 20 min at 37°C, then washed in 1% (w/v) NCS-PBS and permeabilised in 0.2% Triton X-100-PBS for 7 min. Blocking and washing steps between each procedure were performed using 1% (v/v) NCS-PBS. Staining of proteins of interest was performed through incubation with primary antibodies (Table 2.2) for 1 hour followed by incubation with secondary host-specific or isotype-specific antibodies conjugated with Alexa 488, 568 or 647 (Table 2.2) during 45 min at room temperature. The cell nucleus was stained using Hoechst incubated with the secondary antibodies at a dilution of 1:1000. Coverslips were mounted using Dako® mounting media. Images were acquired on a Leica SP5 Upright confocal using a 63x 1.40-0.60NA oil immersion objective illuminated with Diode, Argon, DPSS 561 and HeNe 633 lasers.

Table 2.1: Description of seeding specificities for each immunofluorescence experiment.

Experiment name	Number of cells seeded	Cell line	Coverslip size
PR8 WT, Δ8, ΔNS1 infections	10 ⁵	HeLa	20mm
MitoRab11 transfection	5x10 ⁴	HeLa	13mm
Arl17 depletion	5x10 ⁴	A549	13mm

RNA extraction | Quick spin column purification of total RNA directly from TRIzol® was performed accordingly to manufacturer instructions using Direct-Zol™ RNA MiniPrep kit from Zymo Research.

cDNA synthesis | cDNA was obtained upon RNA extraction through a Reverse Transcription reaction accordingly to Transcriptor First Strand cDNA Synthesis kit from Roche.

qRT-PCR | Quantification of gene expression of specific genes was obtained with iTaq™ Universal SYBR® Green Supermix from BioRad. Forward and reverse primers (4µM) indicated in table 2.2 were used to amplify the gene of interest and GAPDH as a control. Standard DNA dilutions (1:5) were made using a mix of the mock NT samples. Real-Time gene expression was measured using CFX 384 Touch™ Real-Time PCR Detection System from BioRad as follows: 10min at 95°C, 40 cycles consisting of 15s at 95°C and 1min at 60°C. Each condition was normalized to its GAPDH sample values.

Plaque assay | Supernatant samples collected from each set of experiments were serial diluted (1:10) in serum free media. Confluent MDCK monolayers were then infected with the 10⁻¹ to 10⁻⁶ dilutions and were kept at 37°C and 5% CO₂ atmosphere. One hour post-infection cells were overlaid with a 1:2 serum free media and 4% Avicel solution with 0.14% BSA and 1µg/ml TPCK trypsin and cells were kept at the previous conditions for 36 hours. At this time, cell were fixed and stained using a 4% PFA – 0.2% toluidine blue solution. Plaque forming units were then counted for each dilution and viral titers were calculated. Results are expressed as mean ± standard deviation. D'Agostino Pearson test was performed to assess normal distribution of the replicates. Statistical significance analysis was conducted by unpaired t-test with 95% confidence.

Western blot | Upon harvest, cell samples were kept in Laemmli buffer at -20°C. Proteins were separated by electrophoresis in 12.5% polyacrylamide gels and transferred to a nitrocellulose membrane at 200mA for 45 min, using filter papers soaked in two sets of buffers. Closer to the negative pole, a 0,3M Tris and 20% (v/v) ethanol solution was used and on the opposite pole, a 25mM Tris and 20% (v/v) ethanol solution. Upon transfection, membranes were blocked in 5% (w/v) skimmed milk diluted in 0.2% (v/v) tween-PBS (PBS-T) for 30 min. Staining of the proteins of interest was performed using primary antibodies (Table 2.2) for 1 hour followed by incubation with host-specific secondary antibodies conjugated to fluorochromes LiCor 800 or 680 (Table 2.2) for 30 min, both at room temperature. Washing steps between membrane incubations were carried out using PBS-T. Membranes were then scanned using LiCor Biosciences Odyssey near-infrared platform.

Mitochondrial morphology analysis | Images obtained by immunofluorescence were divided into three categories: 1) Network-like; 2) Network-like but presenting clear fragments at the periphery; 3) Fragmented (no network visible). For bigger accuracy, images of cells within category number 2) were further divided into two subcategories: 2.1.) Network-like presenting more than 10 fragments at the periphery, but fewer than 40; 2.2.) Network-like presenting more than 40 fragments at the periphery. Over 100 images were counted per condition. Results in each rank were presented as percentages of the total of cells analyzed.

Table 2.2: Reagents. Primary and secondary antibodies, siRNAs, plasmids, primers, transfection and cloning reagents used in the procedures described above.

Primary Antibodies	Brand, Reference	Host	Dilutions
PB1	Homemade, ⁷⁰	Rabbit	Western blot: 1:1000
GAPDH	Sicgen®, #AB0049-200	Goat	Western blot: 1:2000
NS1	Homemade, ⁷⁰	Rabbit	Western blot: 1:500
Lamin B1	Abcam®, #ab16048	Rabbit	Western blot: 1:3000
M1	Abcam®, #ab20910	Goat	Western blot: 1:500
GFP	Sicgen®, #AB0020-200	Goat	Western blot: 1:2000
NP	Homemade, ⁷⁰	Rabbit	Western blot: 1:1000; Immunofluorescence: 1:1000
TOM 20	Sigma®, #WH0009804M1	Mouse (IgG1)	Immunofluorescence: 1:100
Secondary Antibodies	Brand, Reference	Host	Dilutions
Alexa Fluor® Anti-Rabbit 488	Life technologies®, #A-11008	Goat	Immunofluorescence: 1:1000
Alexa Fluor® Anti-Mouse 488	Life technologies®, #A-11001	Goat	Immunofluorescence: 1:1000
Alexa Fluor® Anti-Mouse IgG1 647	Life technologies®, #A-21240	Goat	Immunofluorescence: 1:1000
Alexa Fluor® Anti-Rabbit 568	Life technologies®, #A-21069	Goat	Immunofluorescence: 1:1000
IRDye 800CW Donkey Anti-Goat	Li-Cor®, #926-32214	Donkey	Western blot: 1:10 000
IRDye 680RD Donkey Anti-Rabbit	Li-Cor®, #926-68073	Donkey	Western blot: 1:10 000
siRNAs	Brand, Reference		Concentrations
siDrp1 #4, #10	Qiagen , # SI02661365, # SI04320092		Final concentration: 25nM
siARL17 #2, #3	Qiagen , # SI04198033, # SI04310495		Final concentration: 25nM
siNT (Non-targeting)	Qiagen , # SI03650325		Final concentration: 25nM
Transfection Reagents	Brand, Reference		Concentrations
Lipofectamine® LTX	Life technologies®, #15338100		Final concentration: 0.10% (v/v)
DharmaFECT-1	Dharmacon®, #T-2001		Final concentration: 0.20% (v/v)
Lipofectamine® 2000	Life technologies®, #11668027		Final concentration: 0.15% (v/v)
Cloning Reagents	Brand		Specifications
XhoI	New England Biolabs, # R0146S		10 units per reaction
NheI	New England Biolabs, # R0131L		10 units per reaction
Quick Ligase	New England Biolabs, # M2200S		10 units per reaction
NZY Miniprep kit	NZYtech, #MB01001		Used according to manufacturer's instructions
Primers	Sequence		
Drp1-Forward	GCGGTGGTGCTAGAATTTGT		
Drp1-Reverse	TCATTAGCCCACAAGCATCA		
IFBβ1-Forward	CCTGAAGGCCAAGGAGTACA		
IFNβ1-Reverse	AAGCAATTGTCCAGTCCCAG		

Primers	Sequence
Arl17-Forward	ACAGCTGGAAAAACCACCATC
Arl17-Reverse	AACATCCCAGACAGCGAAGG
GAPDH-Forward	CTCTGCTCCTCCTGTTGAC
GAPDH-Reverse	ACCAAATCCGTTGACTCCGAC

Plasmids	Description	Source
pCherry	pmCherry-C1 plasmid with resistance to kanamycin, expressing an mCherry fluorescent tag under a CMV promoter.	Invitrogen©
pMitoRab11a-WT	Tom20 mitochondrial sorting signal cloned in the N-terminus of mCherry in pCherryRab11a-WT plasmid with resistance to kanamycin, under a CMV promoter.	A Nascimento – CBV, IGC
pMitoRab11a-CA	Tom20 mitochondrial sorting signal cloned in the N-terminus of mCherry in pCherryRab11a-CA plasmid with resistance to kanamycin, under a CMV promoter. Rab11 has a single substitution in Q70L.	M Alenquer – CBV, IGC
pMitoRab11a-DN	Tom20 mitochondrial sorting signal cloned in the N-terminus of Cherry in pCherryRab11a-DN plasmid with resistance to kanamycin, under a CMV promoter. Rab11a has with single substitution in S25N. Rab11 has a single substitution in Q70L.	M Veríssimo – CBV, IGC
pGFP	pEGFP-N1 with resistance to kanamycin, expressing an EGFP fluorescent tag under a CMV promoter.	Invitrogen©
pARL17-GFP	ADP Ribosylation factor 17 coding sequence, in a pEGFP-N1 backbone, with resistance to kanamycin, expressing ARL17 with a C-terminal fluorescent tag, under a CMV promoter.	Kindly given by J Mota – ITQB

3. Results

Characterization of mitochondria modulation in PR8 infection and identification of viral factors involved

3.1 | Building up a working hypothesis

Prior to my arrival, the Cell Biology of Viral Infection (CBV) lab observed that, at late stages of infection, vRNPs associate with fragmented mitochondria at the cell periphery. An increase in fragmented mitochondria near the cell periphery indicates that infection disrupts mitochondrial dynamics at two different levels: localization and morphology.

The cell-to-cell variation in mitochondria dynamics in any given sample is extremely high and, therefore, to acquire a statistically meaningful result on viral-induced mitochondria alterations, many cells must be analyzed per sample, picked randomly to limit the bias of analysis, and treated equally. To analyze the accumulation of mitochondria at the periphery, Dr. M. Alenquer (CBV lab) and the IGC imaging facility, created an automated tool able to quantify the intracellular distribution of organelles. The software converted a confocal image from polar to a Cartesian system. The conversion of a confocal image into a 2D organelle distribution map enabled the quantification of mitochondrial distribution, by measuring fluorescent intensity, in relation to the distance from the nucleus (Fig. 3.1 A). The ratio of the mitochondrial fluorescent intensities localized within 2 μm from the nuclear periphery showed that, at 8 hours post-infection (h p.i.) 27.7 \pm 1% were located in this region, significantly less than the 32.9 \pm 1% observed in mock infected cells (Fig. 3.1 B). In agreement, 8.4% more mitochondria were located at the cell periphery by assessment of an increase in intensity in mitochondria staining localized more than 4 μm away from the cell nucleus (Fig. 3.1 C). Taken together, these results suggest that infection leads to a shift in mitochondrial distribution in the cell, leading to their expansion towards the periphery as illustrated in Figure 3.1 D.

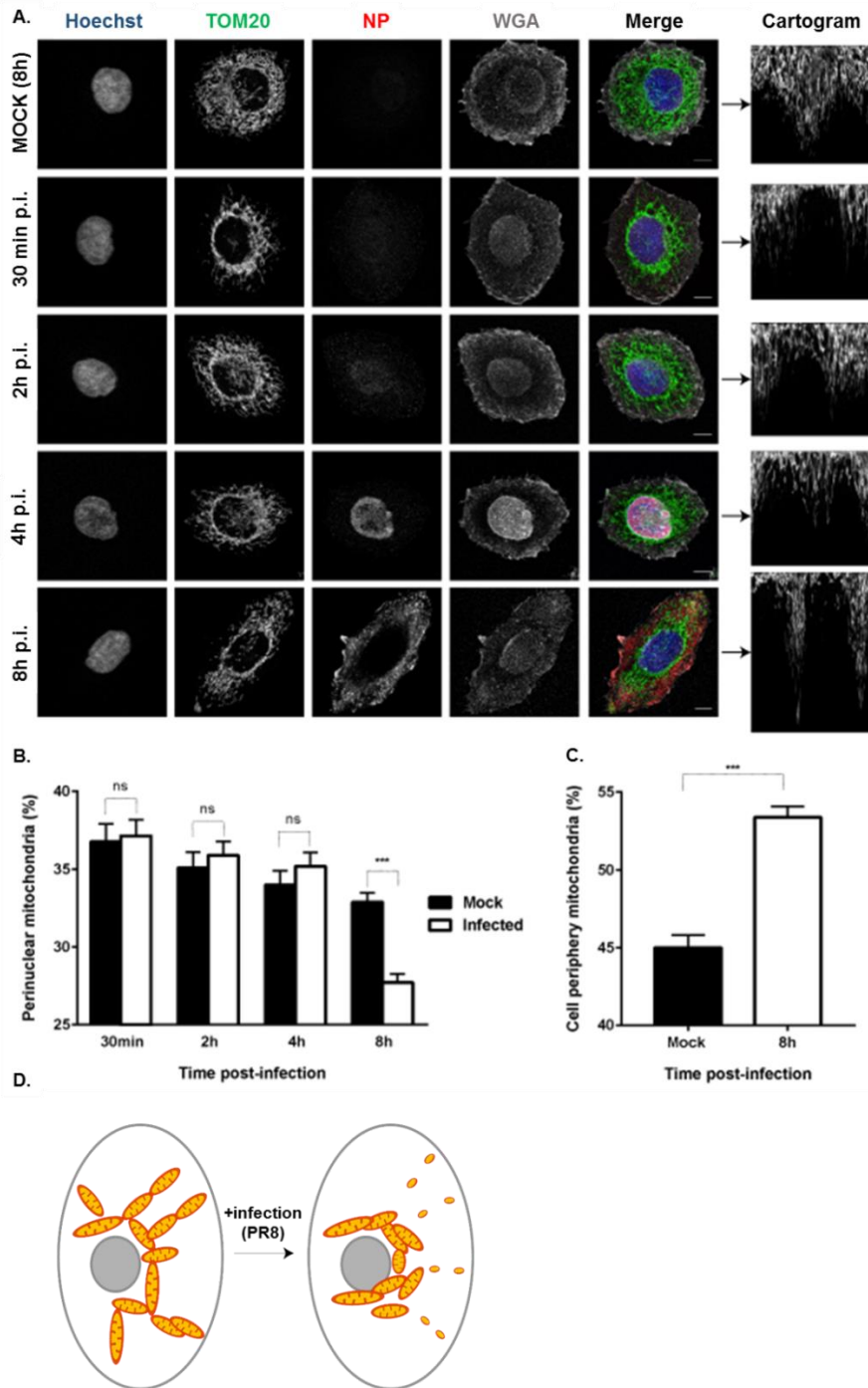


Fig. 3.1 | Quantification of mitochondrial distribution during IAV infection. HeLa cells were infected or mock infected with PR8 at a MOI of 3. (A.) At the indicated times p.i. cells were fixed and stained for nucleus (Hoeschst), mitochondria (TOM20), vRNPs (using NP as a proxy) and cell membrane (WGA). Images were acquired using Leica SP5. The error bar represents 10 μ m. Each confocal image was converted from polar to Cartesian system by an automated tool which also quantified the percentage of mitochondria that are perinuclear (within 2 μ m of the nucleus) or cell peripheral (\geq 4 μ m from the nucleus). Upon establishing the center of the polar coordinate as the periphery of the cell nucleus, and circulating clockwise, the signal of each channel was displayed one degree apart in a XY graph. The analysis continues repeating the process upon increments of a fixed width, towards the cell surface. The organelle distribution map in this format provides means to accurately quantify polarization, redistribution towards the perinuclear region or expansion to the cell periphery, thus allowing a systematic analysis. The automated system is powerful because it allows to image and process a statistical significant number of cells using the indicated procedure. (B.) The percentage of perinuclear mitochondria was plotted over the course of infection. (C.) The percentage of cell peripheral mitochondria at 8h p.i. was also plotted. An average of 100 cells per time-point was processed to obtain the graphs in (B.) and (C.) Error bars represent the standard error of the mean (S.E.M.). Statistical analysis of data was performed using non-parametric Mann-Whitney test (**p<0.001; ns, non-significant). (D.) Schematic representation of mitochondria distribution in the cell. PR8 infection leads to a shift in mitochondrial relocation towards the periphery.

The data on mitochondria redistribution to the periphery is consistent with observations substantiating that influenza A virus infection induces an alteration in mitochondria dynamics. However, to prove the initial observations of the CBV lab, other topics will be analysed and subdivided in the first chapter of results as follows:

- I. Analysis of levels of fragmented mitochondria over the course of IAV infection;
- II. Identification of viral factors that promote mitochondria fragmentation. Candidates include NS1, PB1-F2 and vRNPs.

3.2 | Characterization of mitochondria's morphology throughout a time course of IAV infection: mitochondria becomes more fragmented in PR8 infected cells over time

Complying with the necessity to use an automated analytical method to measure many cells picked randomly by applying an uniform set of parameters, we opted to use the automated tool SQUASSH ⁸¹ to quantify mitochondria shape and size in IAV infected cells. This analytical software was described as adequate for segmentating and quantifying shapes in fluorescence microscopy. However, this method presented many limitations. First, many cells had mitochondria aggregated at the perinuclear region. This phenomenon was read by the SQUASSH method as an increase in mitochondria size as the segmentation process was unable to resolve these mitochondria as individual organelles. Second, during IAV infection the levels of fragmented mitochondria at the periphery are subtle, with most mitochondria remaining unaltered, and the software was not sensitive enough to account for these small differences.

To overcome the above mentioned limitations of the SQUASSH analysis, a qualitative classification system was developed to categorize different mitochondrial morphologies. Mitochondria shape of at least 100 cells per condition were ranked in three different categories that are represented in Figure 3.2: 1) network-like mitochondria; 2) network-like mitochondria but presenting clear fragments at the cell periphery; 3) fragmented mitochondria with no network visible. For convenience, only cells presenting mitochondria in category 1) will be referred to as network henceforward. In addition, for higher accuracy, images of cells within category 2) (known as periphery fragmented) were further divided into two subcategories: 2.1.) Presenting more than 10 fragments at the periphery, but fewer than 40 (+10 fragments); and 2.2.) Presenting more than 40 fragments at the periphery (+40 fragments).

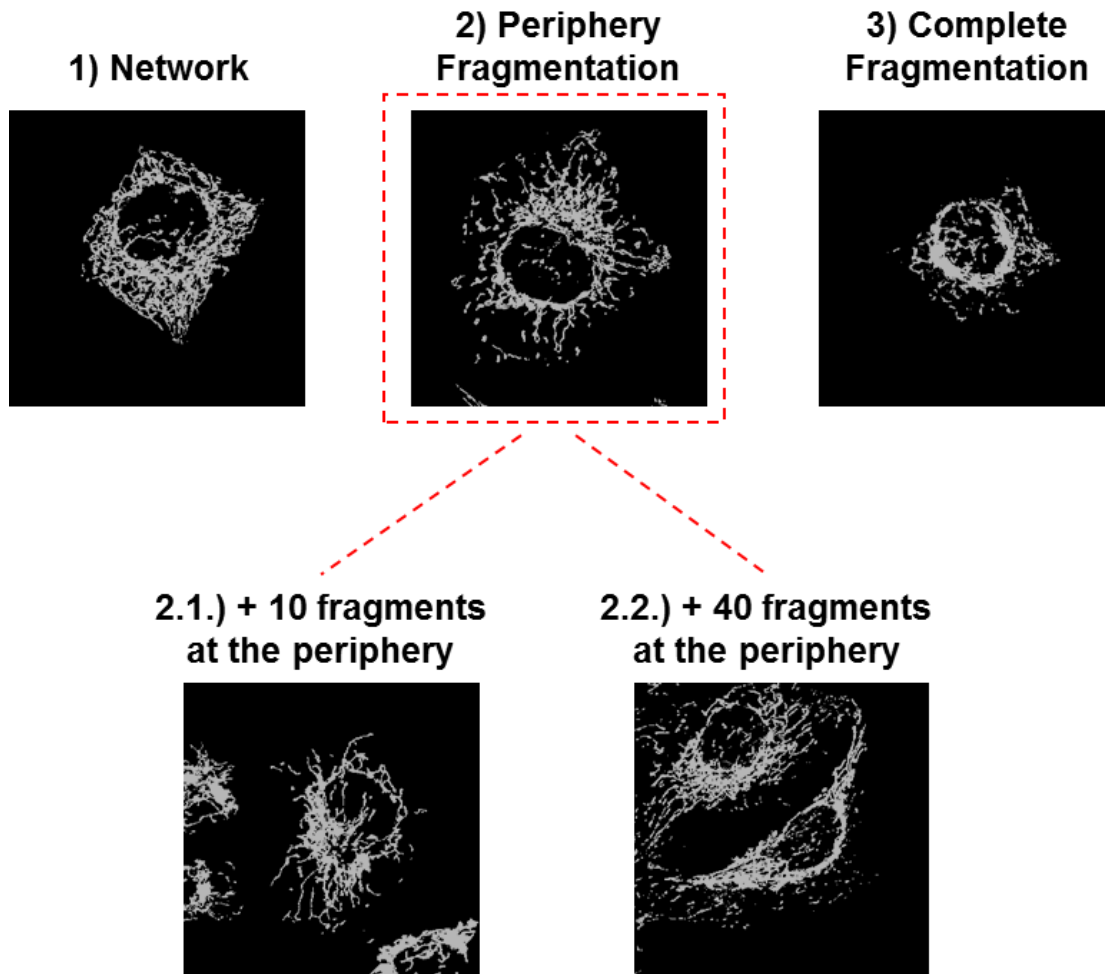


Fig. 3.2 | Classification system of mitochondria morphology. Qualitative system developed to categorize different mitochondrial morphologies throughout this project. Over 100 immunofluorescence images of cells stained for mitochondria (TOM20) and acquired using Leica SP5 were ranked in three different categories, according to their morphology. 1) network-like mitochondria. 2) network-like mitochondria presenting clear fragments at the cell periphery. 3) completely fragmented mitochondria with no network visible. Images of cells with mitochondria fragmented at the periphery were further divided into two subcategories, accordingly to the number of fragments visible near the plasma membrane: 2.1.) Presenting more than 10 fragments at the periphery, but fewer than 40 (+10 fragments); 2.2.) Presenting more than 40 fragments at the periphery (+40 fragments). Representative of mitochondria morphology of each group are displayed.

Such classification was used to rank the mitochondria morphology of cells infected and mock infected with PR8 at a MOI of 3 that were fixed at 6, 8 and 16h p.i. as indicated in Figure 3.3. Cells were stained for TOM20 as the mitochondria marker and the viral protein NP, as proxy of the stage in viral infection. Mock infected cells did not exhibit NP staining, as expected, whilst in infected cells, NP localized in the cytoplasm from 6h onwards. Representative images of viral progression and mitochondria morphology are depicted in Figure 3.3.

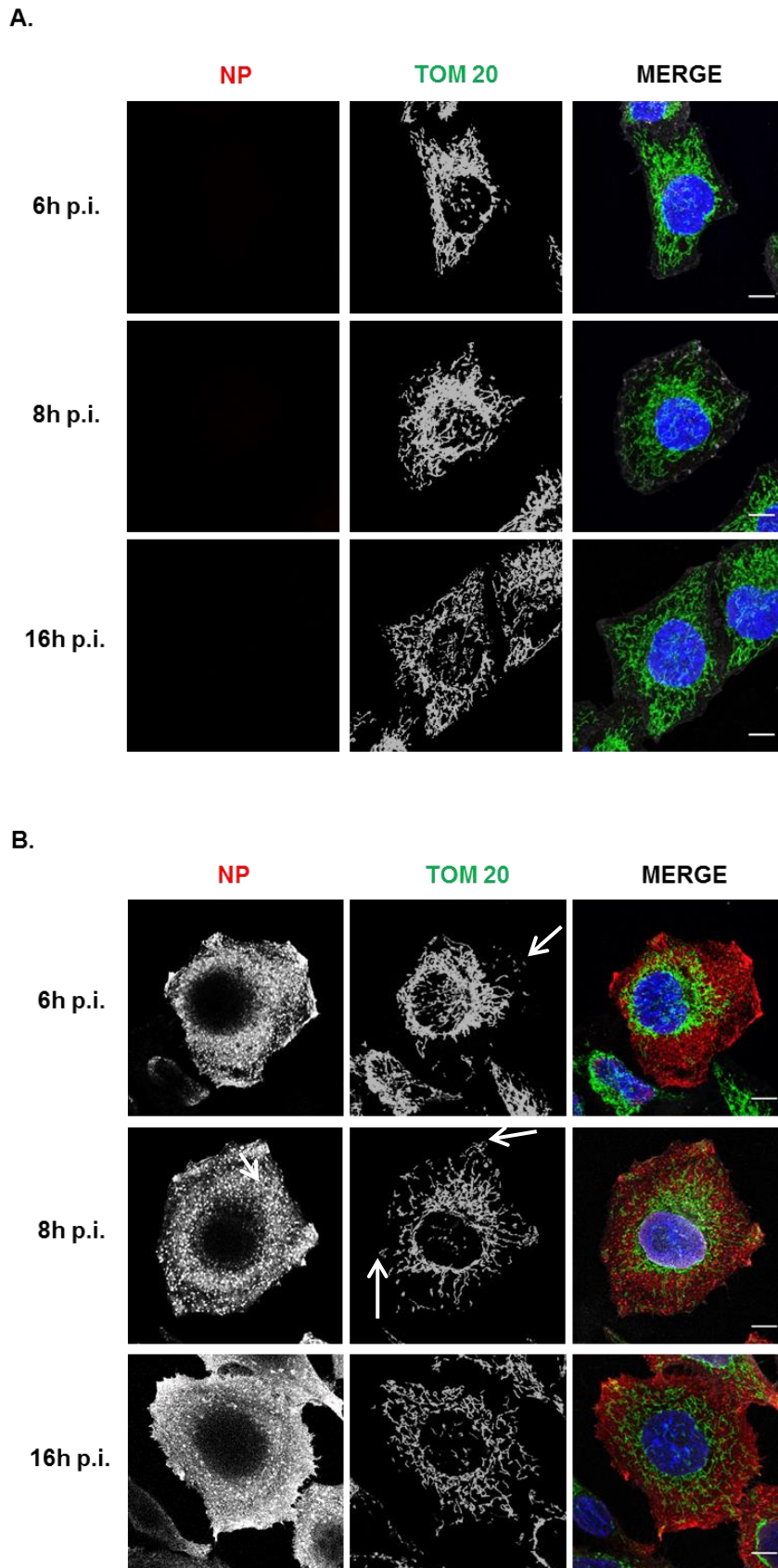


Fig. 3.3 | Mitochondria morphology changes during PR8 infection. HeLa cells were infected or mock infected with PR8 at a MOI of 3. At the indicated times p.i. cells were fixed and stained for nucleus (Hoeschst), mitochondria (TOM20) and vRNPs (using NP as a proxy). Images were acquired using Leica SP5. Bar=10µm. (A.) Mock infected cells. (B.) Infected cells.

By implementing the classification system described above, the majority of mock cells presented a network-like mitochondria or peripheral fragmentation. Only less than 9% of cells exhibited complete fragmentation of mitochondria. Out of all the cells that had peripheral segmentation, 56% presented between 10 and 40 fragments (Fig. 3.4). In PR8 infected cells, as infection progressed, the number of cells with peripheral fragmentation and complete fragmentation increased, concomitantly with a marked decrease in cells presenting network of mitochondria. The number of fragments found at the periphery also increased, with 80% of all cells presenting more than 40 mitochondrial fragments at 16h p.i. (Fig. 3.4).

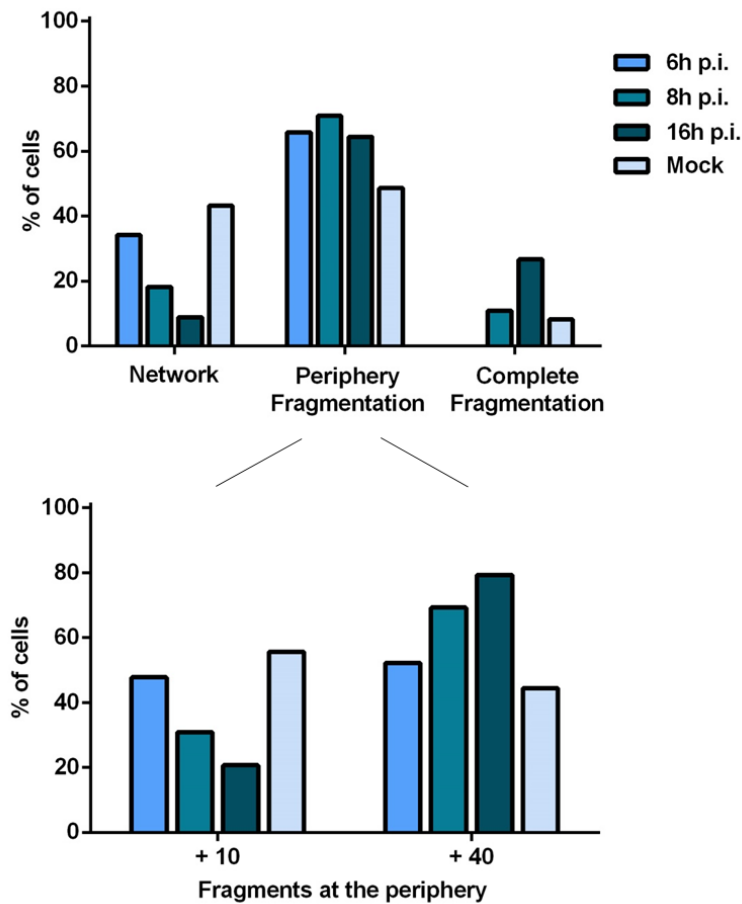


Fig. 3.4 | PR8 infection induces mitochondria fragmentation. HeLa cells represented in Fig. 3.3 were infected or mock infected with PR8 at a MOI of 3. At the indicated times p.i. cells were fixed and stained for nucleus (Hoeschst), mitochondria (TOM20) and vRNPs (using NP as a proxy). Images were acquired using Leica SP5. Over 100 images of the TOM20 channel were ranked using the three categories system described in Fig. 3.2. Top graph plots the percentage of cells that presented mitochondria within one of following morphological categories: 1) Network-like mitochondria; 2) Network-like mitochondria presenting peripheral fragments; 3) Completely fragmented mitochondria. Bottom graph represents a sub-division of category 2) Periphery fragmentation. All cells considered for peripheral fragmentation were divided into more than 10 and more than 40 fragments sub-categories and the percentages of cells determined plotted.

These results indicate that the fragmentation induced by PR8 infection that was observed by others³³ progressively increased with infection. In addition, our work determined that infection originated two types of fragmentation: complete and peripheral localized. However, the mechanisms responsible for this shift in mitochondrial dynamics remain unknown, including the viral factor that trigger mitochondria fragmentation. Literature reports that the viral proteins PB1-F2 and NS1 are involved in mitochondria fragmentation^{33,69}. In order to understand the individual contribution of each viral protein in promoting the two types of fragmentation identified, mutant viruses lacking the full-length version of the referred proteins were evaluated next.

3.3 | Viral proteins that modulate mitochondrial dynamics: NS1 and PB1-F2 participate in shaping mitochondrial morphology in PR8 infected cells

It has been reported that upon recognition of foreign genetic material, RIG-I binds and activates MAVS which triggers mitochondrial elongation as a means to activate IFN response and antiviral signaling⁸² (Fig. 3.5 A). Two viral proteins were shown to interfere with mitochondria morphology and activation of IFN response. Their mode of action is depicted in Figure 3.5 B-C. NS1 is a multifunctional viral protein reported to inhibit RIG-I activation by directly associating with it, and consequently block IFN response⁶⁹. NS1 expression therefore indirectly avoids mitochondrial elongation (Fig. 3.5 B). In addition, the viral protein PB1-F2 has been reported to enter mitochondria through the TOM40 channel and cause mitochondrial fission by Drp1 recruitment, presumably also reducing interferon activation³³ (Fig. 3.5 C.).

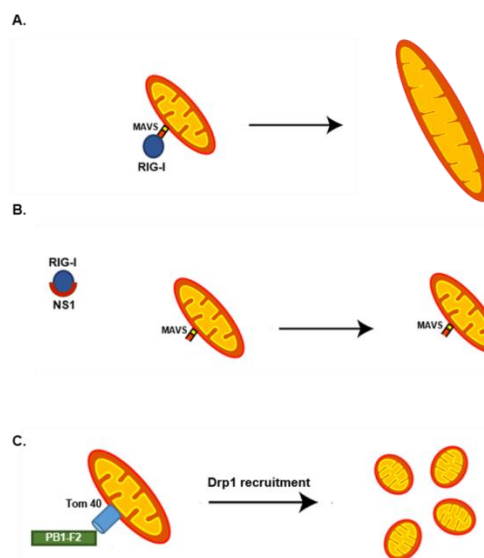


Fig. 3.5 | Predicted modulation of mitochondrial morphology by NS1 and PB1-F2 viral proteins. (continues in the next page)

Fig. 3.5 | Predicted modulation of mitochondrial morphology by NS1 and PB1-F2 viral proteins. NS1 and PB1-F2 are two viral proteins previously implicated in shaping mitochondrial morphology. (A.) In normal conditions, when the cell

detects foreign material, RIG-I is activated and binds MAVS triggering a signaling cascade that leads to interferon response and antiviral signaling. MAVS signal propagation relies on mitochondrial elongation. (B.) NS1 protein directly inhibits RIG-I and blocks MAVS activation indirectly avoiding mitochondrial elongation. (C.) PB1-F2 enters mitochondria through TOM40 channels and triggers a cascade of events that inflect Drp1 recruitment to the mitochondria and consequential fission.

In order to assess the role of NS1 and PB1-F2 in the alterations of mitochondrial morphology during infection, viral mutants devoid of full-length versions of these proteins were grown by reverse genetics, using plasmids depleted of these factors ^{42,83} (Fig. 3.6 A-B). PR8 Δ NS1 virus was made using a mutated version of segment 8 that lacked full-length NS1 (Fig. 3.6 A). For PR8 Δ 8 virus a plasmid with a mutated segment 2 lacking PB1-N40 and PB1-F2 expression was used (Fig. 3.6 B).

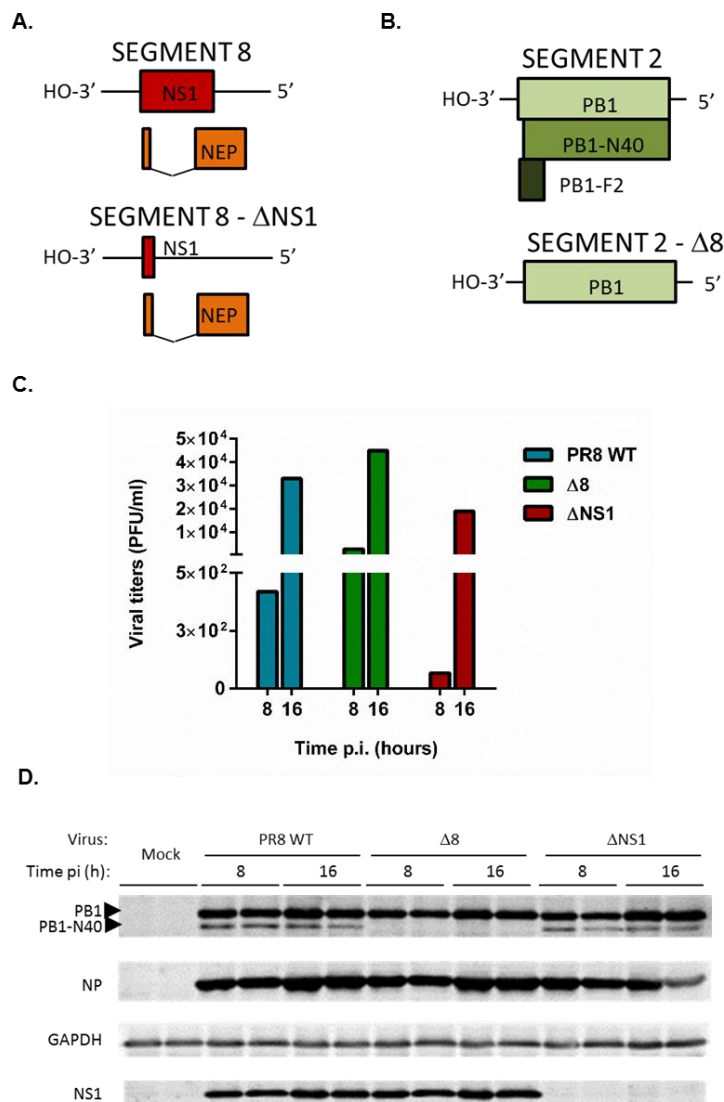


Fig. 3.6 | Characterization of Δ NS1 and Δ 8 viruses. (A.) Schematic representation comparing segment 8 in PR8 WT virus (top) and in Δ NS1 virus (bottom). (B.) Schematic representation comparing segment 2 in PR8 WT virus (top) and in Δ 8 virus (bottom). (C.) Growth of PR8 WT, Δ 8 and Δ NS1 viruses at 8 and 16h p.i.. Viral titers were measured in MDCK cells infected with each of the viruses. (D.) Western blotting confirms viral protein depletion of mutants used at 8 and 16h p.i.. Sample replicates were analyzed for PR8 WT, Δ NS1 and Δ 8 viruses on membranes stained for viral proteins NP, PB1, NS1 (identifier of Δ NS1 virus) and PB1-N40. GAPDH was used as a loading control.

Growth rates for PR8 WT, Δ 8 and Δ NS1 were analyzed by plaque assays (Fig. 3.6 C). Note that PR8 Δ NS1 growth rate was, as expected lower than that of WT and Δ 8 viruses (Fig. 3.6 C). To

determine if depletion was successful and if revertant mutants emerged, viral protein expression for each virus was confirmed by western blotting (Fig. 3.6 D). Depletion of viral proteins was successful for all cases analyzed (Fig. 3.6 D). Given the lack of an antibody to detect PB1-F2, its expression was not analyzed. However, the lack of PB1-N40 strongly suggests that the virus did not revert and will behave as published ⁴².

HeLa cells were infected at a MOI of 3 with one of the following viruses: PR8 Δ NS1 (henceforward Δ NS1) or PR8 Δ 8 (Δ 8). Cells were fixed at 6, 8 and 16h p.i. and stained for TOM20 as a mitochondrial marker and for NP as a proxy of infection as indicated in Figures 3.7 A and 3.8 A. Cells infected with Δ NS1 viruses exhibited a delayed progression of infection and many cells had NP in the nucleus at 8h p.i. (Fig. 3.7 A) whilst in the Δ 8 infected cells, NP was detected exclusively in the cytoplasm from 8h onwards (Fig. 3.8 A).

When mitochondrial morphology of cells infected with Δ NS1 virus was ranked in the three categories, we observed that infected cells (from 6 to 16h p.i.), did not alter dramatically mitochondrial morphology. The majority of cells presented mitochondria with peripheral fragmentation and over 30% had network-like mitochondria. The number of the fragments, however increased with the progression of infection (Fig. 3.7 B).

For cells infected with the Δ 8 virus, the same pattern was maintained throughout infection with the majority of the cells presenting peripheral fragmentation and around 20% of the cells network-like mitochondria (Fig. 3.8 B).

For a comparative analysis, mock cells values described above were subtracted to those obtained for mitochondrial morphology with Δ NS1 and Δ 8 viruses, as well as with PR8 WT (presented in Fig. 3.4) and are depicted in Figure 3.9. Comparison between the three conditions suggests that infection with all viruses lead to an increase in mitochondria fragmentation at the periphery that, however, is milder in Δ NS1 infection. While infection with WT virus decreased up to 40% network-like mitochondria at 16h p.i., infection with the mutant viruses Δ NS1 and Δ 8 caused a 10% and 20% drop, respectively, in the number of cells presenting network-like mitochondria, value that remained stable throughout infection. Complete fragmentation was also less evident, although not abolished, in cells infected with Δ NS1 and Δ 8 viruses.

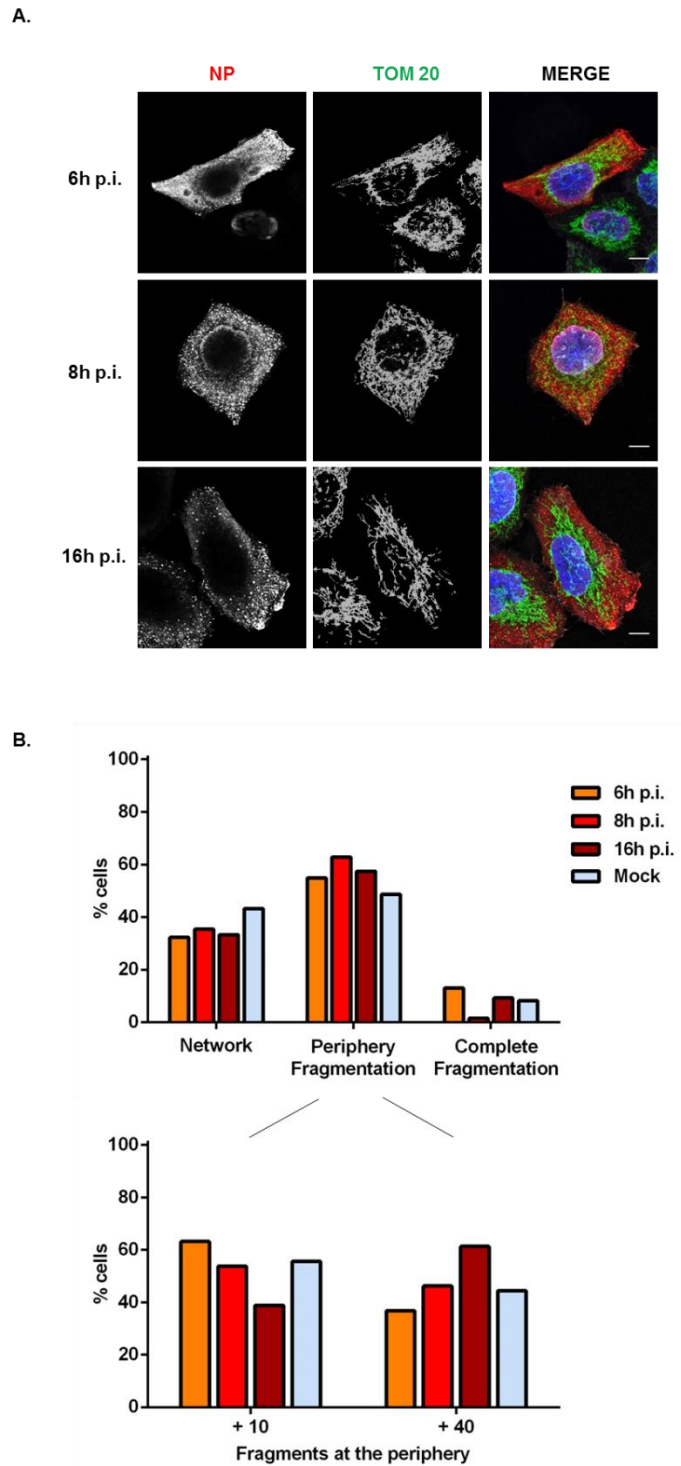
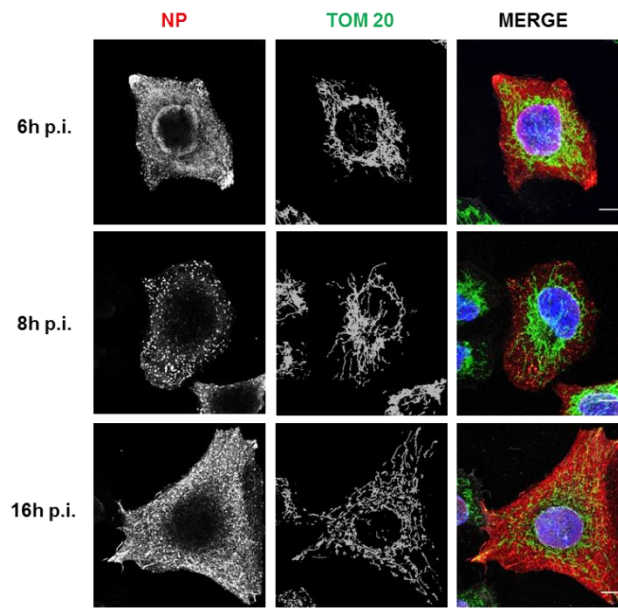


Fig. 3.7 | Δ NS1 viral infection mildly increases mitochondria fragmentation. HeLa cells were infected with Δ NS1 virus at a MOI of 3. At the indicated times p.i. cells were fixed and stained for nucleus (Hoeschst), mitochondria (TOM20) and vRNPs (using NP as a proxy). Images were acquired using Leica SP5. Bar=10 μ m. (A.) Immunofluorescence images representative of each stage of infection and mitochondrial morphology. (B.) Over 100 images of the TOM20 channel were ranked using the three categories system described in Fig. 3.2. Top graph plots the percentage of cells that presented mitochondria within one of following morphological categories: 1) Network-like mitochondria; 2) Network-like mitochondria presenting peripheral fragments; 3) Completely fragmented mitochondria. Bottom graph represents a subdivision of category 2) Periphery fragmentation. All of the cell images accounted for in 2) were further classified in 2.1.) mitochondria presenting between 10 to 40 fragments at the cell periphery (+10 fragments at the periphery) or 2.2.) mitochondria presenting more than 40 fragments at the cell periphery (+ 40 fragments at the periphery). Mock results depicted in the graphs are those of Figures 3.3 and 3.4.

A.



B.

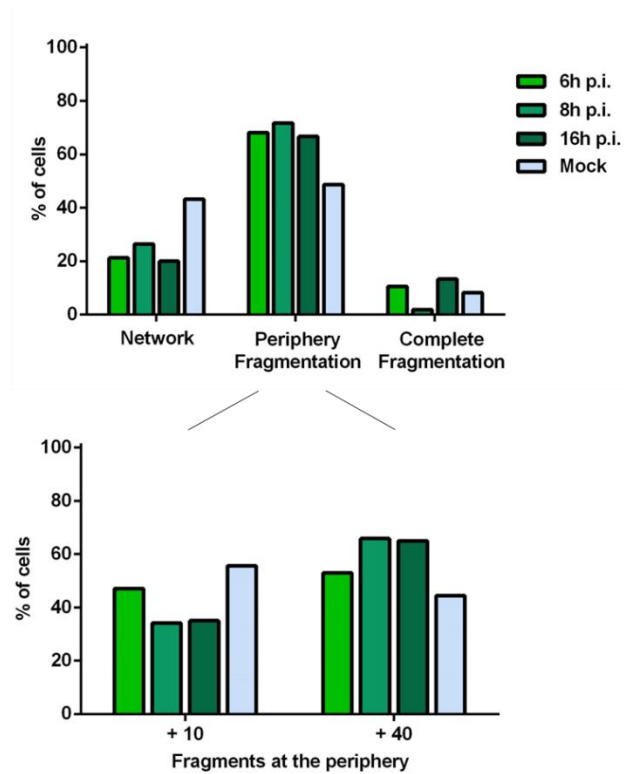


Fig. 3.8 | $\Delta 8$ viral infection modestly increases mitochondria fragmentation. HeLa cells were infected with $\Delta 8$ virus at a MOI of 3. At the indicated times p.i. cells were fixed and stained for nucleus (Hoeschst), mitochondria (TOM20) and vRNPs (using NP as a proxy). Images were acquired using Leica SP5. Bar=10 μ m. (A.) Immunofluorescence images representative of each stage of infection and mitochondrial morphology. (B.) Over 100 images of the TOM20 channel were ranked using the three categories system described in Fig. 3.2. Top graph plots the percentage of cells that presented mitochondria within one of following morphological categories: 1) Network-like mitochondria; 2) Network-like mitochondria presenting peripheral fragments; 3) Completely fragmented mitochondria. Bottom graph represents a subdivision of category 2) Periphery fragmentation. All of the cell images accounted for in 2) were further classified in 2.1.) mitochondria presenting between 10 to 40 fragments at the cell periphery (+10 fragments at the periphery) or 2.2.) mitochondria presenting more than 40 fragments at the cell periphery (+ 40 fragments at the periphery). Mock results depicted in the graphs are those of Figures 3.3 and 3.4.

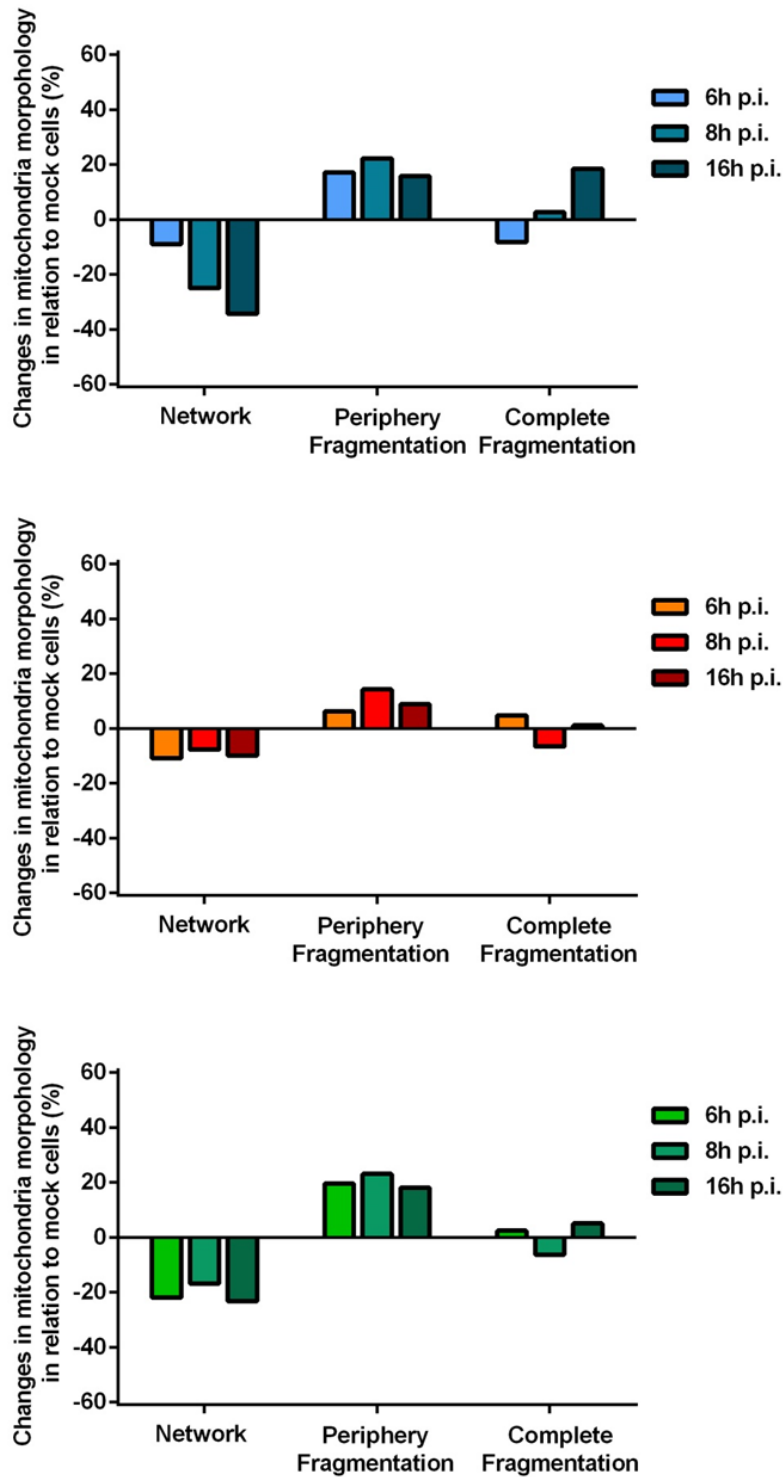


Fig. 3.9 | PR8 WT viral infection leads to higher fragmentation levels at the mitochondria than Δ NS1 and Δ 8 viruses infection. HeLa cells were mock infected or infected with either PR8 WT, Δ NS1 or Δ 8 virus at a MOI of 3. At the indicated times p.i. cells were fixed and stained for nucleus (Hoeschst), mitochondria (TOM20) and vRNPs (using NP as a proxy). Images were acquired using Leica SP5. Over 100 images of the TOM20 channel were ranked per condition using the three categories system described in Fig. 3.2: cells presenting either 1) Network-like mitochondria; 2) Network-like mitochondria presenting peripheral fragments; 3) Completely fragmented mitochondria. To the percentage of cells obtained for each category and each virus assessed, the percentage of mock cells at the same time within each category was subtracted. Graph represents variations in mitochondrial morphology in infected cells, at different time-points and in each of the three categories in comparison to mock cells. Negative values represent a decrease and positive represent an increase. Top graph is relative to PR8 WT infected cells. Middle graph is relative to Δ NS1 infected cells. Bottom graph is relative to Δ 8 infected cells.

Infections without PB1-F2 or NS1 modestly decreased viral induced effects in mitochondrial segmentation. Care has to be taken when analyzing these results as Δ NS1 infection is delayed and many cells present vRNPs in the nucleus. However, our results confirm that both viral proteins modulate mitochondrial dynamics during infection. Nevertheless, each viral protein on its own does not totally eliminate the modulation in mitochondrial dynamics induced by infection and hence there is room for postulating a combinatory role of several viral proteins including vRNPs that will be evaluated next.

3.4. Pulling the system to a maximum: targeting vRNPs to mitochondria increases mitochondrial fission

The CBV lab developed an artificial targeting system to identify the factors attracted by Rab11 that was published as the MitoRab11 method. The MitoRab11 method is a system by which Rab11a is targeted to the mitochondria thus assessing Rab11-mediated recruitment if enquired factors change their localization to the mitochondria ⁴⁹. Constitutively active (CA) Rab11 protein was tagged with cherry at the N-terminus. Mitochondria was chosen as an organelle to target Rab11 by fusion of the mitochondrial targeting sequence (MTS) of TOM20 to the Cherry-Rab11 protein. The system aimed to test the capacity of Rab11a to recruit vRNPs during IAV infection (Fig. 3.10 A). The system was initially tested by measuring the colocalization between the mitochondrial marker TOM20 and MitoCherryRab11aCA (Fig. 3.10 B), indicating that Rab11 is being efficiently targeted to mitochondria. In PR8 infected cells, the viral protein NP was shown to relocate to the mitochondria, in cells transfected with MitoCherryRab11aCA, thus demonstrating that the MitoRab11 system was functional (Fig. 3.10 B).

In my case, the MitoRab11 method was used to evaluate if binding of vRNPs to the mitochondria modulates mitochondria morphology. By pushing the system whereby vRNP association with the mitochondria is amplified, we expected to maximize mitochondria fragmentation if vRNPs would be involved in modulating mitochondrial dynamics as predicted by our working model (Fig. 3. 10 C). The experimental design included assessment of mitochondria fragmentation in mock and infected cells expressing individually mitochondrial targeted Rab11 wild-type (WT), constitutively active (CA) and dominant negative (DN) forms as well as mcherry. If the working model were correct, WT and CA Rab11 were expected to efficiently recruit vRNPs to the mitochondria and increase mitochondrial fission. The DN form of Rab11 would not attract vRNPs and mitochondria morphology would remain intact (Fig. 3.10 C).

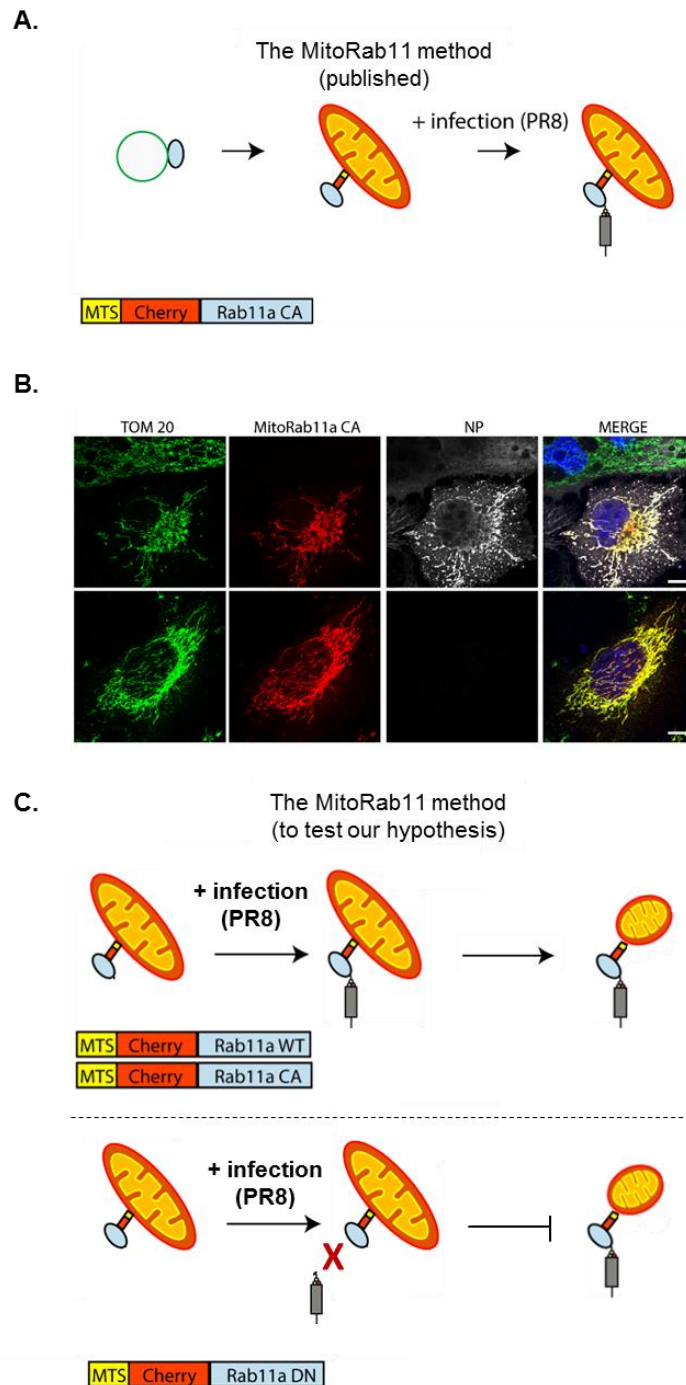


Fig. 3.10 | The MitoRab11 method used to recruit vRNPs to the mitochondria and study mitochondrial morphology. The MitoRab11 method is an artificial system by which Rab11a is targeted to the mitochondria to assess Rab11 mediated recruitment of enquired factors. (A.) The CBV lab had previously tested this method by transfecting cells with a CA form of the Rab11 protein tagged with cherry at the N-terminus fused with the mitochondrial targeting sequence (MTS) of TOM20. The system aimed to test the capacity of Rab11a to recruit vRNPs during IAV infection. (B.) Functional demonstration of the MitoRab11 method. Immunofluorescence images of pMitoCherryRab11aCA transfected cells stained for mitochondria (TOM20 used a marker) and vRNPs (NP used a proxy). TOM20 and MitoRab11a CA colocalize indicating that Rab11 is being efficiently targeted to mitochondria. NP relocated to the mitochondria, demonstrating that the MitoRab11 system was functional. (C.) To test our working model, in this project MitoCherryRab11aCA and MitoCherryRab11aWT were used to maximize the recruitment of vRNPs to the mitochondria and exploit mitochondrial fragmentation. The DN form of Rab11 was used to assure that the fragmentation pattern would be due to vRNP recruitment and not Rab11 insertion into mitochondria. MitoRab11aDN would not recruit vRNPs to mitochondria and mitochondria fragmented would not be induced.

HeLa cells were infected with PR8 virus at a MOI of 20 and concomitantly infected with one of the following plasmids: 1) Cherry, 2) MitoCherryRab11aWT (henceforward MitoRab11a WT), 3) MitoCherryRab11aCA (MitoRab11a CA) or 4) MitoCherryRab11aDN (MitoRab11a DN). Cells were fixed at 14h p.i. and stained for TOM20 as a mitochondrial marker and for NP as a proxy of infection. Regardless of infection, MitoRab11a WT, CA and DN colocalized with TOM20 and, as expected, cherry was scattered throughout the cell (Fig. 3.11 A-B). NP was not present in mock infected cells (Fig. 3.11 A) and, in infected cells, NP colocalized with TOM20 and Cherry in cells transfected with MitoRab11a WT and CA whilst it was diffused in the cytoplasm in cells transfected with Cherry or MitoRab11 DN (Fig. 3.11 B).

Mock infected cells transfected with all plasmids presented mainly mitochondria with peripheral fragmentation, although the levels varied from 90% with cherry, to 60% with MitoRab11a WT or CA and 51% for MitoRab11a DN. The number of fragments at the periphery was similar for all conditions (Fig. 3.12 A). Decrease in mitochondria with peripheral fragmentation was mostly accompanied by a proportional increase in the level of network mitochondria and indirectly proportional to completely fragmented mitochondria (Fig. 3.12 A).

Infection in cells transfected with Cherry increased complete fragmentation to 20%. Cells transfected with the DN form of Rab11 showed a mitochondrial morphology pattern similar to that of Cherry transfected cells, indicating that infection induces some level of fragmentation. When we pushed the system to the maximum, by increasing the association of vRNPs with the mitochondria, in infected cells transfected with MitoRab11 WT or CA complete fragmentation increased to 40% in the case of MitoRab11WT and 75% in the case of CA (Fig. 3.12 B). MitoRab11CA is predicted to recruit higher levels of vRNPs, as it is always switched on. This was accompanied by a proportional reduction in peripheral fragmentation. However, in the cases with peripheral fragmentation, an increase (more pronounced in the CA form) was observed in the number of cells presenting more than 40 fragments (Fig. 3.12 B).

For convenience, the values for mock cells were subtracted to the trends and values of the conditions upper described and are depicted in Figure 3.12 C. These results show that, the condition in which recruitment of vRNPs to the mitochondria was more efficient (MitoRab11CA) presented higher levels of mitochondrial fission immediately followed by MitoRab11WT, the second highest condition in vRNPs recruitment. These observations support our working hypothesis that the vRNP-mitochondria association modulates mitochondrial dynamics by increasing fragmentation. Still, the question remains on which cellular proteins mediate vRNP association with mitochondria or simply has an impact in mitochondria fragmentation.

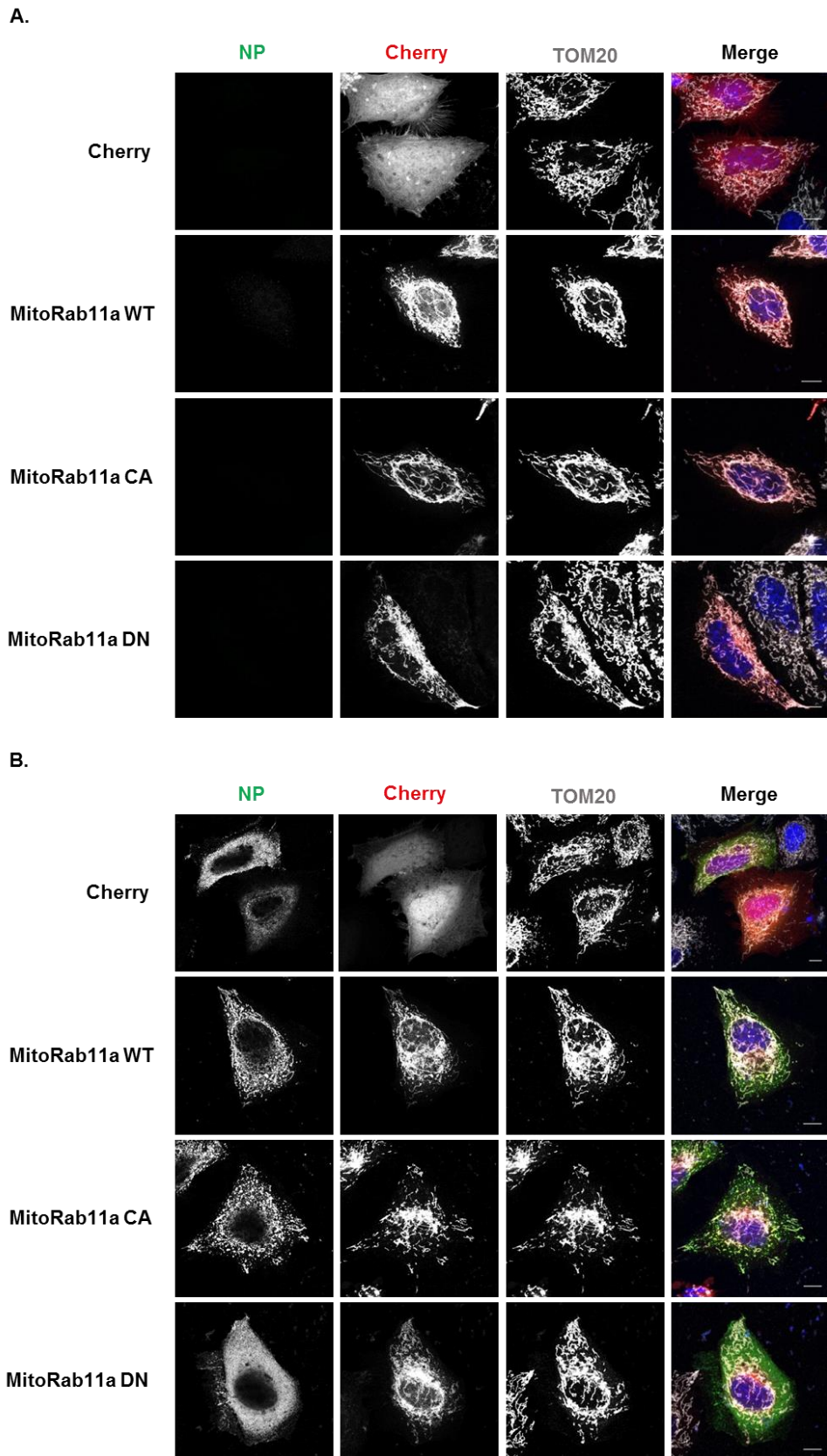
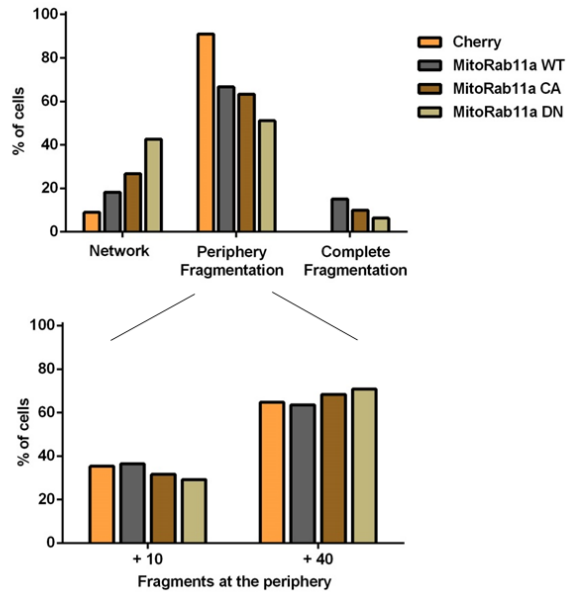
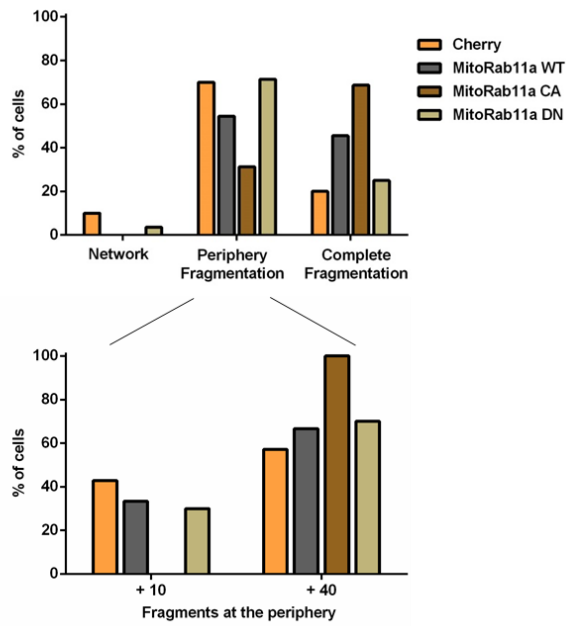


Fig.3.11 | Mitochondria morphology changes during PR8 infection when using the MitoRab11 method to obligatorily bind vRNPs to mitochondria. HeLa cells were infected or mock infected with PR8 at a MOI of 20 and concomitantly infected with mcherry, MitoCherryRab11aWT (MitoRab11a WT), MitoCherryRab11aCA (MitoRab11a CA) or MitoCherryRab11aDN (MitoRab11a DN). 14h p.i. cells were fixed and stained for nucleus (Hoeschst), mitochondria (TOM20) and vRNPs (using NP as a proxy). Images were acquired using Leica SP5. Bar=10µm. (A.) Mock infected cells. (B.) Infected cells.

A.



B.



C.

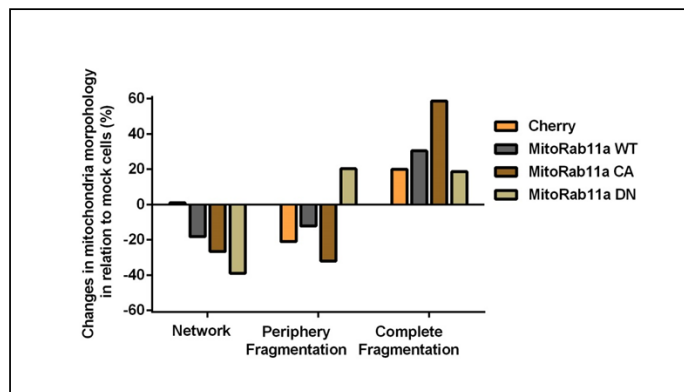


Fig. 3.12 | Using the MitoRab11 method to obligatorily bind vRNPs to mitochondria during PR8 infection increases mitochondrial fragmentation. (continues in the next page)

Fig. 3.12 | Using the MitoRab11 method to obligatorily bind vRNPs to mitochondria during PR8 infection increases mitochondrial fragmentation. HeLa cells were infected or mock infected with PR8 at a MOI of 20 and concomitantly infected with mcherry, MitoCherryRab11aWT (MitoRab11a WT), MitoCherryRab11aCA (MitoRab11a CA) or MitoCherryRab11aDN (MitoRab11a DN). 14h p.i. cells were fixed and stained for nucleus (Hoeschst), mitochondria (TOM20) and vRNPs (using NP as a proxy). Images were acquired using Leica SP5. Over 100 images of the TOM20 channel were ranked using the three categories system described in Fig. 3.2. Top graphs plot the percentage of cells that presented mitochondria within one of following morphological categories: 1) Network-like mitochondria; 2) Network-like mitochondria presenting peripheral fragments; 3) Completely fragmented mitochondria. Bottom graphs represent a subdivision of category 2) Periphery fragmentation. All of the cell images accounted for in 2) were further classified in 2.1.) mitochondria presenting between 10 to 40 fragments at the cell periphery (+10 fragments at the periphery) or 2.2.) mitochondria presenting more than 40 fragments at the cell periphery (+ 40 fragments at the periphery). (A.) Mock infected cells. (B.) Infected cells. (C.) To the percentage of infected cells obtained for each category the percentage of mock cells was subtracted. Graph represents variations in mitochondrial morphology in infected cells.

4. Results

Host factors involved in mitochondria modulation in PR8 infection

4.1. Building up a working hypothesis

Preliminary work done by the CBV lab in infected cells analyzed by immunofluorescence and stained for mitochondria (using TOM20 as marker), vRNPs (using NP as proxy) and the GTPase Drp1, indicated that, at the cell periphery, fragmented mitochondria associated with vRNPs. Interestingly, Drp1 was consistently found between vRNPs and mitochondria, as seen in Figure 4.1 A. Our working hypothesis is that Drp1 is recruited to the mitochondria, and vRNPs that are associated with Rab11 vesicles as well. Upon fragmentation, the small mitochondria-Drp1-vRNP-Rab11 complex is transported to the cell periphery by a yet unidentified mechanism (Fig. 4.1 B).

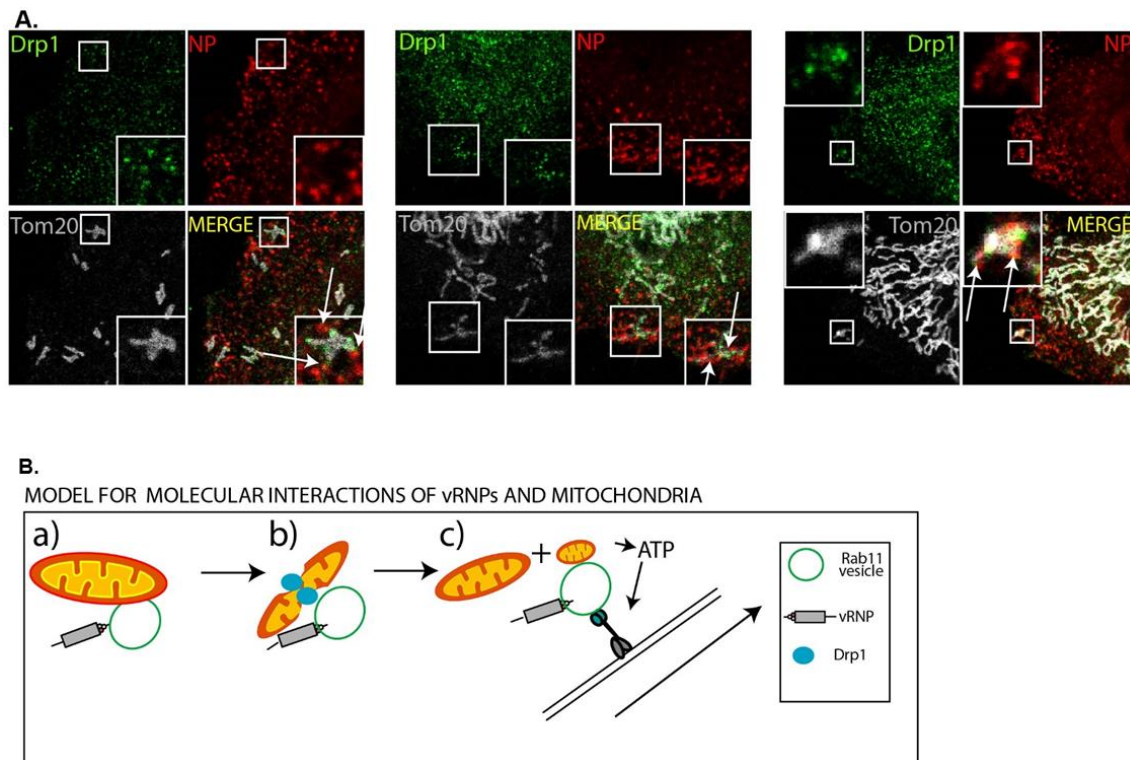


Fig. 4.1 | Predicted working model for vRNP-mitochondria association at the cell periphery via Drp1 intermediate. (A.) Immunofluorescence images of PR8 infected cells stained for mitochondria (TOM20), vRNPs (using NP as a proxy) and Drp1. Images of the cell periphery show side by side localization of the three components analyzed. Zoom ins allow to observe that fractions of mitochondria are found in close proximity to vRNPs, and DRP1 appears to be localized in between the two structures. (B.) Schematic representation of the model for molecular interactions between vRNPs and mitochondria. Our working model predicts that vRNPs bound to Rab11 vesicles come into close proximity of mitochondria (a) which leads to the recruitment of Drp1 to a specific place in the mitochondrial membrane (b) by an unknown chain of events that culminates in the formation of smaller mitochondrial fragments that might be required for localized energy production necessary to transport vRNPs to the plasma membrane (c).

The purpose of this part of the project is to analyze the host factors involved in modulating mitochondria dynamics. However, due to time constraints this part was limited to evaluate if Drp1 contributed to viral production and antiviral response.

The main reason for this modest analysis was the identification of a second candidate that could be involved in modulating mitochondrial dynamics. In a large screen carried out by Dr. M. Amorim and B. Kellen, several ADP-ribosylation factors (ARFs) were analyzed in the MitoRab11 system, described in chapter 3.4., for their potential to disturb the recruitment of vRNPs by Rab11 (Fig. 4.2 A). The ARF family is a subset of the small GTPase superfamily with important roles in vesicular traffic. In total, it comprises: 5 ARFs, 21 ARF-Like proteins (ARLs), two SAR1 isoforms, an ARF-related protein 1 (ARFRP1) and TRIM protein 23 in humans⁸⁴.

As a note, the ARF-family proteins generally are able to interconvert from an inactive GDP-bound to an active GTP-bound state and to bind specific effectors while in the “on” or “off” status. The GDP/GTP switch is generally very slow, requiring catalysis by guanine exchange factors (GEFs) and relying on GTPase activating proteins (GAPs) for inactivation due to a negligible GTPase activity^{84,85}. ARFs and ARLs participate in initial steps of a signaling cascade of events that culminates in the biogenesis of vesicles. In very simplified terms, upon activation and recruitment to the donor membrane, ARFs/ARLs recruit coating molecules to the surface of the budding vesicle, cargo from the cytoplasm and scission factors that take part in the process of vesicle biogenesis^{84,85}.

In the MitoRab11 based assay, one amongst all the ARFs tested originated a surprising result. The CBV lab found that the GFP tagged Arl17 (Arl17-GFP) did not interfere with vRNP recruitment by MitoRab11, as observed in Figure 4.2 B and confirmed with a Pearson correlation value of 0.51 for MitoRab11a and vRNPs (Fig. 4.2 C). Intriguingly, Arl17-GFP colocalized with MitoRab11 WT, as seen in Figure 4.2 C and determined by a Pearson correlation of 0.56. Yet, what stood out in the images of cells overexpressing Arl17-GFP was that mitochondria, especially in infected cells, were highly fragmented (Fig. 4.2 E). Over 80% of non-infected cells overexpressing Arl17-GFP had mitochondria fragmented at the periphery. Infection, in the same conditions, led to complete fragmentation of all cells analyzed (Fig. 4.2 D).

These initial observations suggested that Arl17 localized to the mitochondria where it impacted mitochondrial dynamics. Infection of cells overexpressing Arl17 accentuated mitochondrial fission (Fig. 4.2 D). Due to the fact that the GTPase localized to the mitochondria and that it modulated its morphology especially during infection, Arl17 became an interesting candidate for this study and therefore the second part of this chapter is devoted to the analysis of its role in infection mainly by assessing its contribution to viral production; mitochondrial fragmentation; and infection progression. Hence, this chapter will initially study the effects of depleting Drp1 and subsequently of depleting Arl17 for the viral infection.

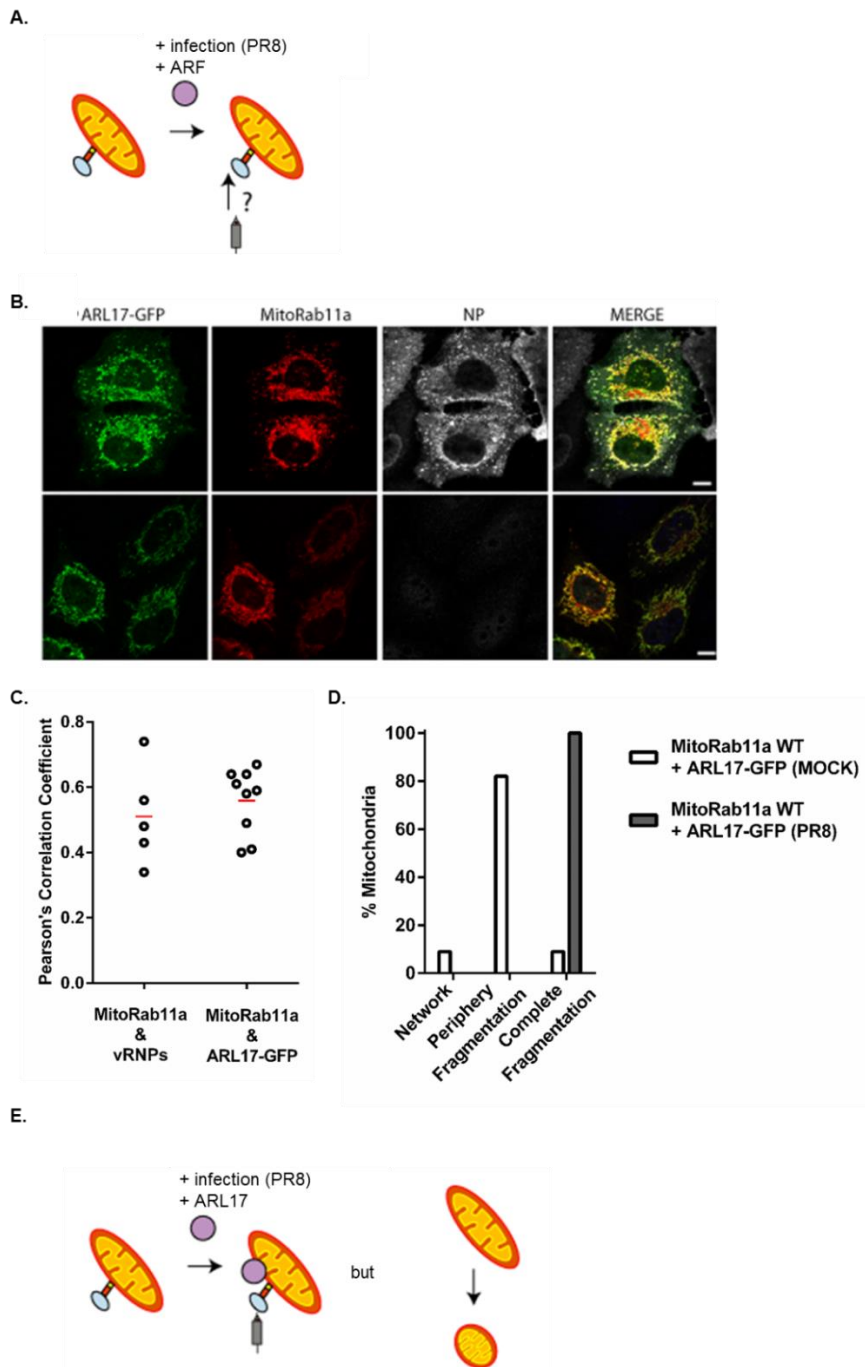


Fig. 4.2 | The analysis of a large screen testing ARF proteins for their potential to disturb recruitment of vRNPs identified Arl17 as a potential mitochondrial modulator in infection. (A.) A large screen was performed by the CBV lab using the MitoRab11 method to identify ARFs capable of disrupting the recruitment of vRNPs by MitoRab11a WT. (B.) Immunofluorescence images obtained in the screen analysis of cells transfected with pMitoRab11a WT, overexpressing Arl17-GFP and stained for vRNPs (using NP as a proxy). Merge pictures shows that Arl17 is localized in the mitochondria, and, in infected cells, the viral complexes come into close proximity of mitochondria. Scale bar represents 10µm. (C.) Pearson's correlation analysis between MitoRab11a and vRNPs (0.51) and MitoRab11a and Arl17-GFP (0.53) indicate colocalization between MitoRab11a at the mitochondria with vRNPs and Arl17. (D.) Analysis of mitochondria morphology in cells overexpressing Arl17. Images of cells were ranked according to the fragmentation levels of mitochondria. 80% of mock infected cells had mitochondria with peripheral fragmentation. Infected cells were completely fragmented. (E.) Arl17 allowed vRNP association with MitoRab11a and was identified as a potential modulator of mitochondrial morphology as its overexpression during infection increased mitochondrial fragmentation.

4.2. Drp1 is required for normal viral production

Drp1 plays a major role in mitochondrial fission by oligomerizing around mitochondria and forming a constriction ring that divides mitochondria into smaller portions⁹. Others have postulated that, in infection, Drp1 is either activated or recruited to the mitochondria and it increases fragmentation⁹. However, confocal images suggest that Drp1 may be acting as the link between vRNPs and mitochondria (Fig. 4.1). Our working hypothesis predicts that vRNP association with Drp1 and the mitochondria results in the relocalization of smaller mitochondrial fragments to the cell periphery, mediated by Rab11 vesicles (Fig. 4.3 A). Such hypothesis predicts that Drp1 would have a role in infection and that its depletion would reduce viral titers (Fig. 4.3 B).

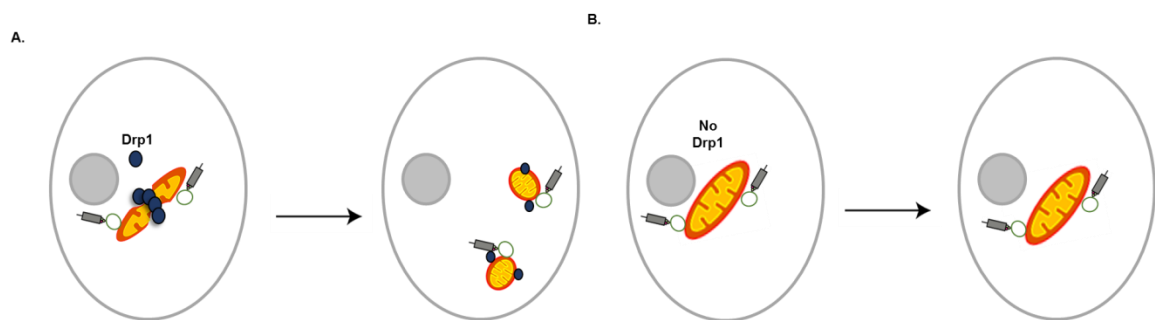


Fig. 4.3 | Schematic model for predicted Drp1 role in IAV infection. (A.) In IAV infection, vRNPs come in close proximity with mitochondria and Drp1 is recruited to the mitochondrial membrane which leads to mitochondrial fragmentation. Smaller mitochondrial fractions travel alongside vRNPs bound to the Rab11 vesicles towards the cell periphery. (B.) In the case of Drp1 depletion, vRNPs will not be able to recruit Drp1 and mitochondria will not become fragmented. Motility of vRNPs bound to Rab11 vesicles would become impaired and less vRNPs would be able to reach the cell periphery to form new virions.

Hence, Drp1 was depleted from HeLa cells using two different siRNAs (siDrp1 #4 and siDrp1 #10) or a mix of both (siDrp1 Mix). A non-targeting sequence (siNT) was used as a transfection control. Upon 48h of transfection, cells were infected with PR8 virus at a MOI of 0.001. For this experiment a multicycle infection protocol was used, which means that several rounds of infection can take place.

Supernatants and cells were collected separately to evaluate viral production and isolate RNA at 4, 8, 12, 24, 32 and 48h p.i. as indicated in Figure 4.4. RNA samples were used to measure Drp1 levels of mRNA by qPCR (Fig. 4.4 A) and the supernatants harvested were then used to infect MDCK cells and evaluate viral production by plaque assay (Fig. 4.4 B).

Results depicted in Figure 4.4 A show that the levels of Drp1 mRNA were 70% reduced with all siRNAs tested. Figure 4.4 B shows the progression in viral production. At 4 to 8h p.i. viral titers for all conditions were similar, however from 12h onwards, cells depleted of DRP1 presented reduced levels of viral production. In cells expressing Drp1, viral production grew exponentially until 32h and still increased until 48h. Viruses grown in cells treated with siDrp1 #4 and mix exhibited reduced viral titers of almost 10x at 24h p.i. and 100x at 32h p.i., when compared to viruses grown in the presence of Drp1. Although presenting a similar trend, siRNA #10 treatment

resulted in a milder reduction in viral production to that observed with other siDrp1 (Fig. 4.4 B). Given that the reduction in Drp1 mRNA levels for this siRNA was similar to that observed for the other depletions, care has to be taken as to whether decrease in viral production does not reflect additional off target effects of the treatment.

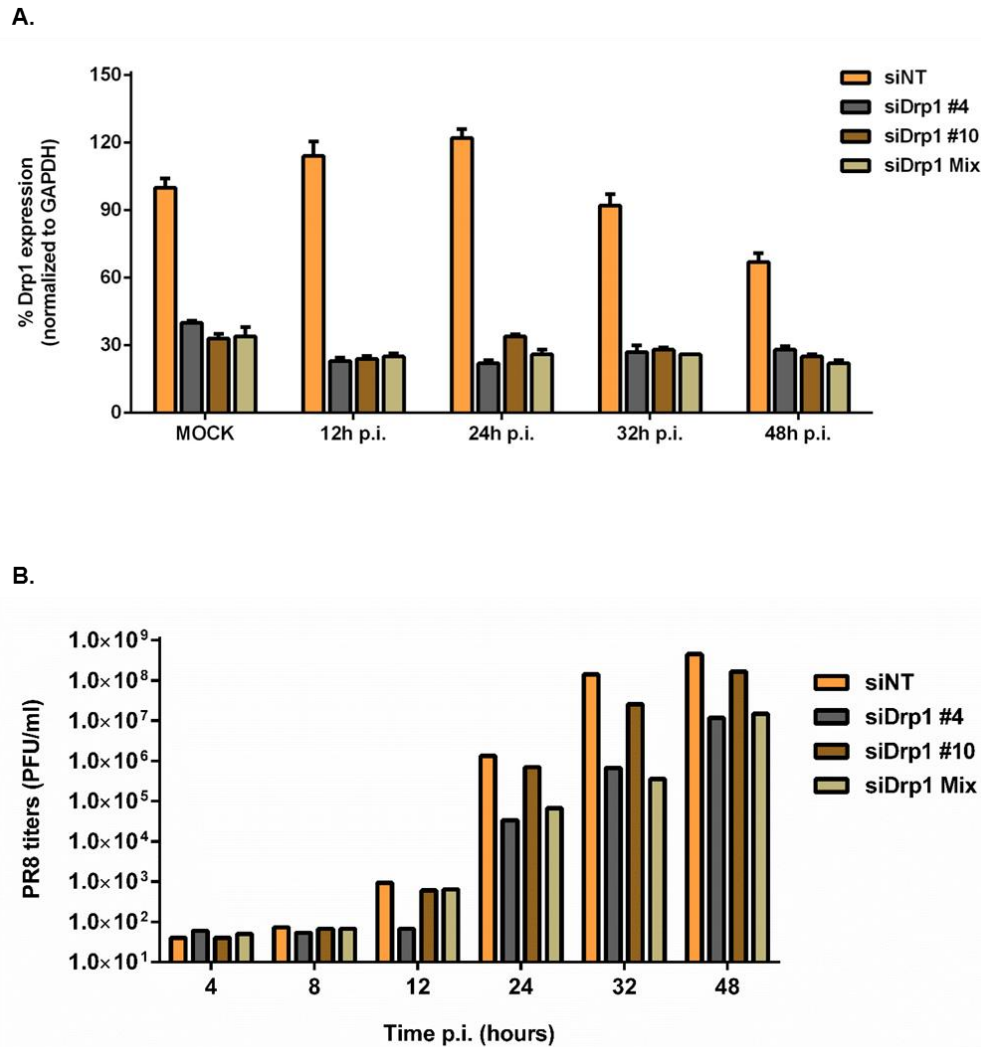


Fig. 4.4 | Drp1 depletion causes a decrease in viral production. HeLa cells were transfected with siRNA sequences targeting endogenous Drp1 (siDrp1 #4, siDrp1 #10 and a mix of both). A non-targeting RNA sequence (siNT) was used as a negative control. 36 hours after transfection cells were infected with PR8 virus at a MOI of 0.001 in a multicycle infection. At the indicated times p.i., supernatants were collected and cells were harvested. (A.) RNA was extracted from cells and reverse transcribed into cDNA. Quantification of Drp1 expression was evaluated by qRT-PCR and normalized to GAPDH values in each condition. All siDrp1 sequences used were able to successfully deplete Drp1. (B.) MDCK cells were infected with the supernatant samples in serial dilution sets. 36 hours p.i. cells were fixed and stained using a 4% PFA – 0.2% toluidine blue solution. Plaque forming units were counted for each dilution and viral titers were estimated. PR8 viral production was deficient for cells transfected with siDrp1 #4 or with the mix of both siRNAs from 24h p.i. onwards.

These results suggest that Drp1 is playing a functional role in the viral life cycle. In order to understand if the drop in viral titers was due to an increase in antiviral signaling when Drp1 was not being expressed, expression of IFN β 1 mRNA levels was measured.

4.3. IFN β 1 mRNA levels accompanied viral progression

IFN β 1 is a pro-inflammatory cytokine expressed as a result of activation of antiviral response. IFN β 1 levels increase when sensing molecules, like RIG-I, activate the MAVS signaling pathway [19].

The mRNA levels of IFN β 1 were measured by qPCR using the same RNA extracted from the Drp1 depleted cells and controls above. It became relevant to quantify antiviral signal activation, through IFN β 1 expression, in order to determine if the drop in viral titers in cells depleted of Drp1 were caused by an increased immune response activation.

In cells expressing Drp1, infection with PR8 virus resulted in an increase in mRNA levels for IFN β 1 of 100x from 12 to 24h p.i.. From 24 to 32h p.i. the increase was less pronounced and stabilized until 48h (Fig. 4.5). For cells depleted of Drp1 that produced a decrease in virus titres, IFN β 1 mRNA levels were at all times inferior to those observed in control cells (Fig. 4.5). The siDrp1#10, whose depletion was of roughly 70%, but that originated a smaller drop in virus titres also gave rise to higher levels of IFN β 1. Levels of IFN β 1 mRNA thus accompany viral production and not Drp1 depletion.

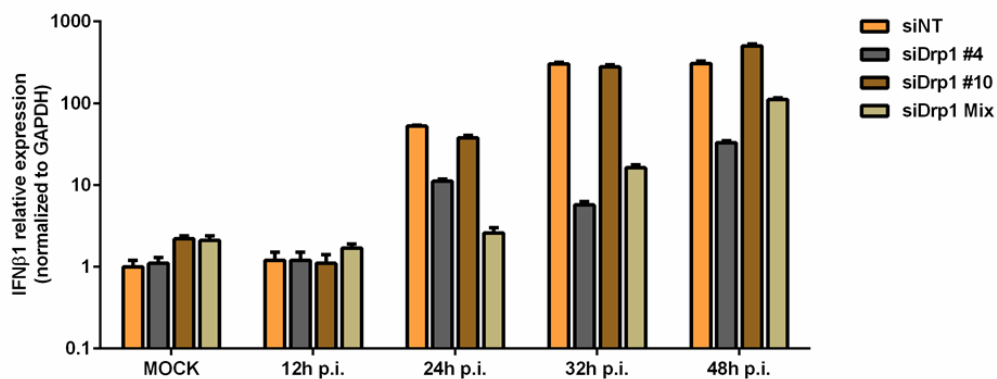


Fig. 4.5 | Drp1 depletion did not increase activation of innate immunity. HeLa cells were transfected with siRNA sequences targeting Drp1 mRNA (siDrp1 #4, siDrp1 #10 and a mix of both). A non-targeting RNA sequence (siNT) was used as a negative control. 36 hours after transfection, cells were infected with PR8 virus at a MOI of 0.001 in a multicycle infection. At the indicated times p.i. cells were harvested, RNA was and reverse transcribed into cDNA. Quantification of IFN β 1 mRNA levels was evaluated by qRT-PCR and normalized to GAPDH values in each condition. Relative levels of IFN β 1 accompanied levels of viral production depicted in Fig. 4.4.

These results indicate that the lack of Drp1 in infected cells is not triggering a more pronounced innate immune response and that the drop in viral titers in cells depleted of Drp1 does not result from increased antiviral signaling. Whether Drp1 plays a role in the association of vRNPs to the mitochondria and in modulating its morphology remains to be analyzed and will be discussed in future perspectives.

4.4. Arl17 is required for normal viral production

One of the proteins tested and relevant for this MSc thesis was Arl17 (Fig. 4.6). Arl17 is found in only one publication where it arises as a possible genetic factor involved in Anthrax vaccine induced antibody response in a clinical trial ⁸⁶ and hence the information regarding this protein is almost inexistent. Dr. M. Alenquer analyzed its sequence and using different softwares publicly available, was able to identify three conserved domains: a GTP binding domain, a mitochondria targeting signal at the corresponding N-terminus of the protein and a transmembrane domain at the C-terminus (Fig. 4.6).

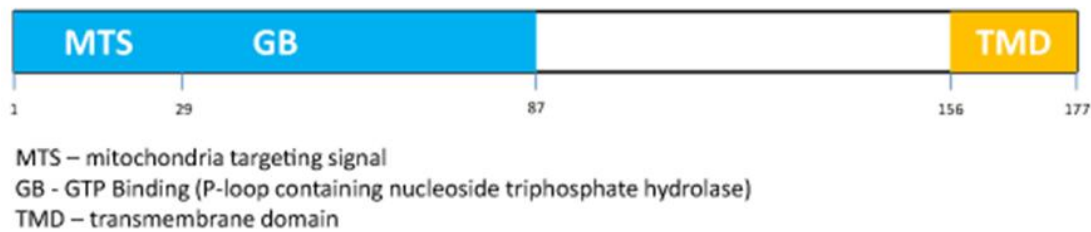
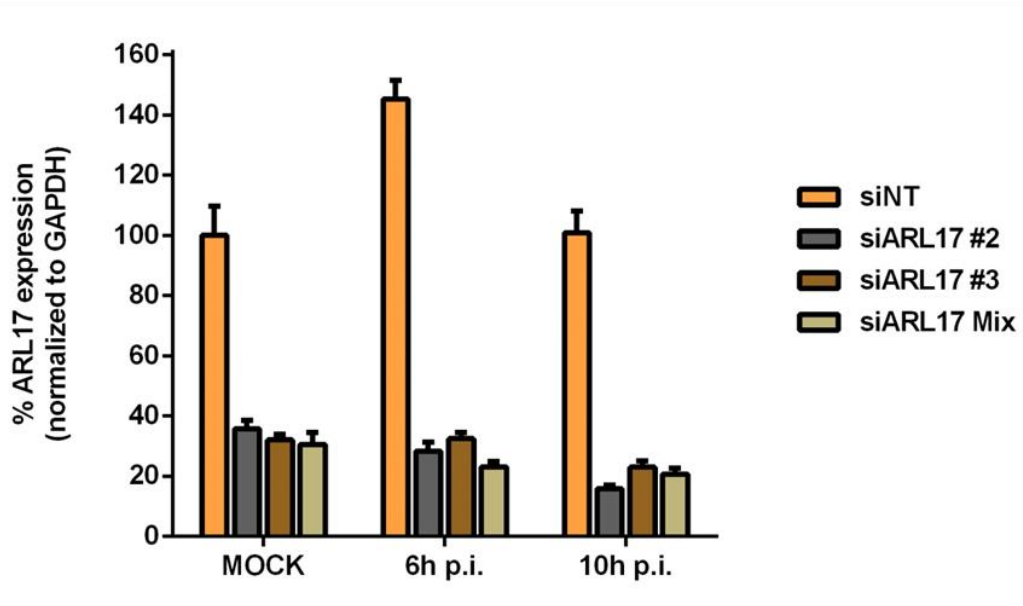


Fig. 4.6 | Arl17 has a mitochondria targeting signal. Illustrative image of Arl17 protein. The small GTPase is 177 amino acid long and has a mitochondria targeting signal downstream of the GTP binding domain and a transmembrane domain in the correspondent N-terminus. TMD was predicted by TM-Pred (www.ch.embnet.org/software/TMPRED_form.html). MTS was predicted by iPSORT (iSORT.hgc.jp) and GB was predicted by InterPro (www.ebi.ac.uk/interpro).

In order to understand if Arl17 was playing a relevant role in IAV infection, A549 cells were depleted of endogenous Arl17 using two different siRNAs (siArl17 #2 and siArl17 #3) or a mix of both (siArl17 Mix). A non-targeting sequence (siNT) was used as a transfection control. Upon 48h of transfection, cells were infected with PR8 virus at a MOI of 5 and samples of the supernatant and cells were harvested separately at 6 and 10h p.i.. Cells were processed to purify RNA, and samples were used to measure Arl17 mRNA levels by qPCR (Fig. 4.7 A). Results depicted in Figure 4.7 A show that Arl17 mRNA levels was reduced by 60-80% with all siRNAs tested. We then tested viral titers by plaque assays in samples depleted of Arl17. Figure 4.7 B shows viral production at 6 to 10h p.i. Results normalized to viral titers of cells treated with NT, demonstrate that depletion of siArl17 #2 and mix, resulted in a 90% drop in viral titres, whilst that of siArl #3 was less efficient, reducing viral titers only 60%, (Fig. 4.7 B).

A.



B.

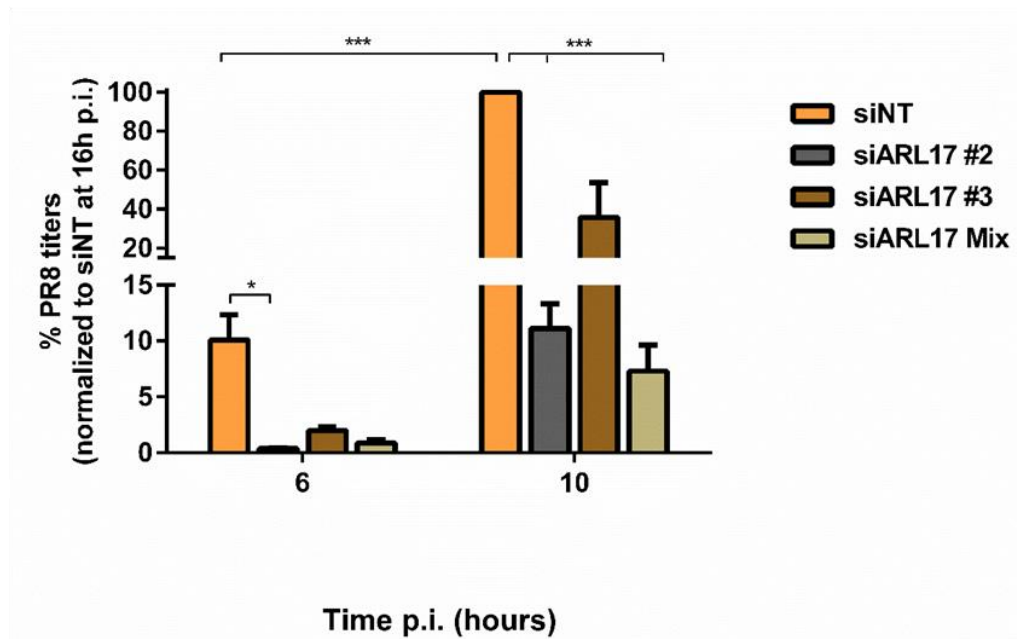


Fig. 4.7 | Arl17 depletion causes a decrease in viral production. A549 cells were transfected with siRNA sequences targeting endogenous Arl17 mRNA (siArl17 #2, siArl17 #3 and a mix of both). A non-targeting RNA sequence (siNT) was used as a negative control. 36 hours after transfection cells were infected with PR8 virus at a MOI of 5. At the indicated times p.i., supernatants were collected and cells were harvested. (A.) RNA was extracted from cells collected at each time p.i. and reverse transcribed into cDNA. Quantification of Arl17 mRNA levels was evaluated by qRT-PCR and normalized to GAPDH values in each condition. All siArl17 sequences used were able to successfully deplete Arl17. (B.) MDCK cells were infected with the supernatant samples in serial dilution sets. 36 hours p.i. cells were fixed and stained using a 4% PFA – 0,2% toluidine blue solution. Plaque forming units were counted for each dilution and viral titers were calculated. Error bars represent the standard deviation. Statistical analysis of data was performed using unpaired t-test with 95% confidence (**p<0.001). PR8 viral production was deficient for cells transfected with siArl17 #2 or with the mix of both siRNAs at all times tested.

4.5. Depleting Arl17 causes mitochondrial fractioning

In order to better comprehend what was happening in infection in cells depleted of Arl17, cells were fixed at 10 h p.i. and processed for immunofluorescence, by staining for TOM20 as the mitochondria marker and the viral protein NP, as proxy of the stage in viral infection. Given the lack of available commercial antibodies that efficiently recognize Arl17 it was not possible to stain for this protein and hence detect which cells exhibited reduced levels of expression. To overcome this limitation, many cells were analyzed per sample, picked randomly to limit the bias of analysis, and enquired for statistical significance. Analysis consisted of scoring mitochondria according to the three categories: network, fragmented at the periphery and completely fragmented. As before, fragmentation at the periphery was subdivided into two categories: more than 10 but less than 40 and more than 40 fragments near the plasma membrane.

Mock infected cells did not exhibit NP staining (Fig. 4.8 A), as expected. In cells transfected with siNT, 80% of the mitochondria presented peripheral segmentation with about 60% of cells with less than 40 fragments. 18% had mitochondria with network like morphology and 2% were completely fragmented (Fig. 4.8 B). Interestingly, these cells presented higher levels of fragmentation than the mock cells previously described (Fig 4.2), which might be due to the stress generated by siRNA transfection. Mock infected cells treated with siArl17 lost the Network-like mitochondria and instead showed more fragmented mitochondria either at the periphery (with siArl17#2) or completely fragmented with both (siArl17#3 and mix) as seen in Figure 4.8 B. Our results indicate that depletion of Arl17 disturbs mitochondrial dynamics leading to its fragmentation. Representative images are shown in Figure 4.8 A.

Knocking down Arl17 expression lead to a significant drop in viral production with all siRNAs tested. This data indicates that Arl17 might be playing an important role in IAV life cycle, at a yet unidentified step. In order to further understand the role of Arl17 in mitochondria during infection, an immunofluorescence analysis was performed.

Infected cells shifted mitochondrial morphology towards fragmentation at 10h p.i. (Fig. 4.9 A-B), with more than 50% of all cells presenting completely fragmented mitochondria. However, this phenotype was not caused by Arl17 depletion, since siNT depleted cells also presented complete fragmentation of mitochondria in the majority of cells analysed. If we analyse the cells with peripheral mitochondria localization, which represent 20-40% of all cells depending on the condition, we can see that 60% of siNT-treated cells present more than 10 fragments. siARL17 treatment, however, increased the number of cells with more than 40 fragments at the periphery. Taken together, the results indicate that infection leads to a shift towards fragmentation and that depletion of Arl17 does not change this phenotype (Fig. 4.10). This might also indicate, although confirmation is required, that Arl17 is not involved in infection induced mitochondria fragmentation.

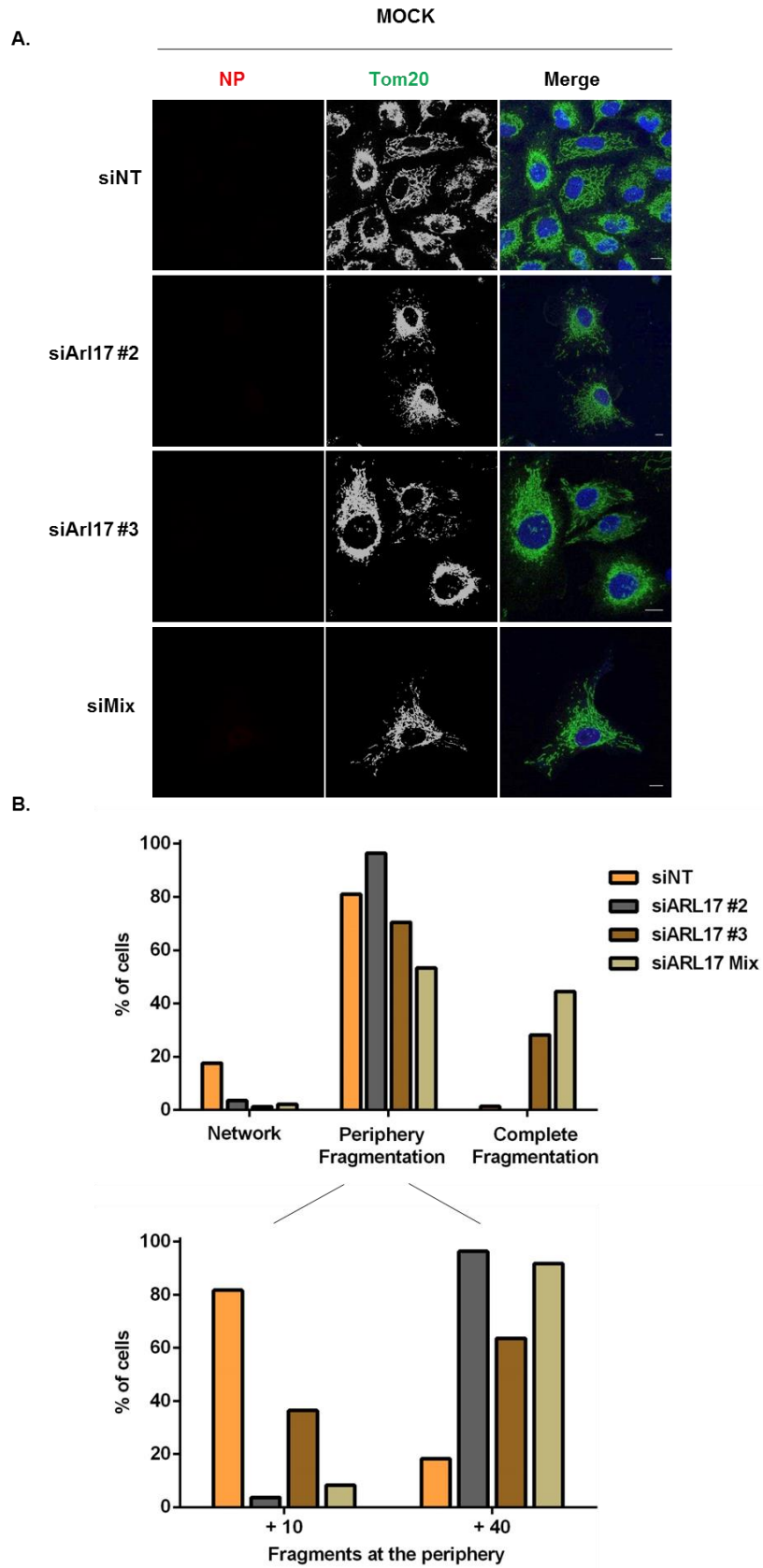


Figure legend is in page 46.

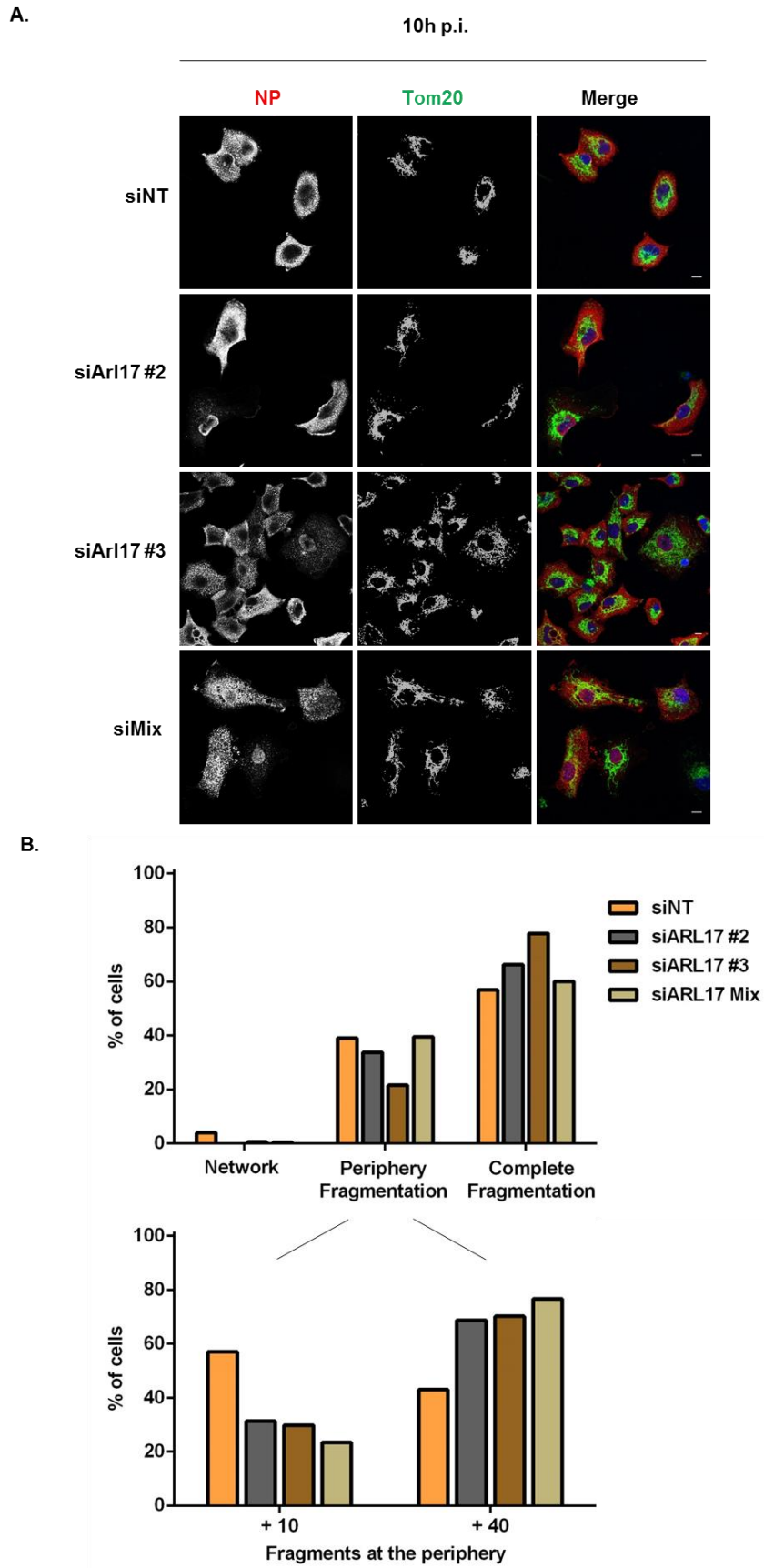


Figure legend is in page 46.

Fig. 4.8 | Arl17 depletion increases mitochondrial fragmentation. A549 cells were transfected with siRNA sequences targeting endogenous Arl17 (siArl17 #2, siArl17 #3 and a mix of both). A non-targeting RNA sequence (siNT) was used as a negative control. (A.) 36 hours after transfection, cells were mock infected and 10h latter cells were fixed and stained for nucleus (Hoeschst), mitochondria (TOM20) and vRNPs (using NP as a proxy). Images were acquired using Leica SP5. Scale bar represents 10µm. (B.) Over 100 images of the TOM20 channel were ranked using the three categories system described in Fig. 3.2. Top graph plots the percentage of cells that presented mitochondria within one of following morphological categories: 1) Network-like mitochondria; 2) Network-like mitochondria presenting peripheral fragments; 3) Completely fragmented mitochondria. Bottom graph represents a sub-division of category 2) Periphery fragmentation. All of the cell images accounted for in 2) were further classified in 2.1.) mitochondria presenting between 10 to 40 fragments at the cell periphery (+10 fragments at the periphery) or 2.2.) mitochondria presenting more than 40 fragments at the cell periphery (+ 40 fragments at the periphery).

Fig. 4.9 | Infection in Arl17 depleted cells does not lead to significant changes in mitochondrial fragmentation. A549 cells were transfected with siRNA sequences targeting endogenous Arl17 (siArl17 #2, siArl17 #3 and a mix of both). A non-targeting RNA sequence (siNT) was used as a negative control. (A.) 36 hours after transfection, cells were infected with PR8 virus at a MOI of 5 and 10h latter cells were fixed and stained for nucleus (Hoeschst), mitochondria (TOM20) and vRNPs (using NP as a proxy). Images were acquired using Leica SP5. Scale bar represents 10µm. (B.) Over 100 images of the TOM20 channel were ranked using the three categories system described in Fig. 3.2. Top graph plots the percentage of cells that presented mitochondria within one of following morphological categories: 1) Network-like mitochondria; 2) Network-like mitochondria presenting peripheral fragments; 3) Completely fragmented mitochondria. Bottom graph represents a sub-division of category 2) Periphery fragmentation. All of the cell images accounted for in 2) were further classified in 2.1.) mitochondria presenting between 10 to 40 fragments at the cell periphery (+10 fragments at the periphery) or 2.2.) mitochondria presenting more than 40 fragments at the cell periphery (+ 40 fragments at the periphery).

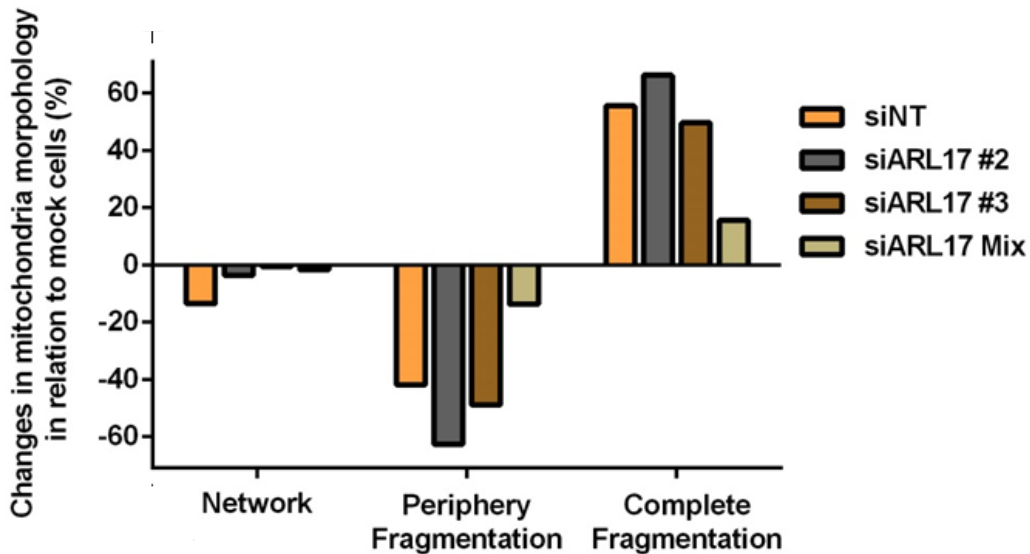


Fig. 4.10 | Infection causes mitochondrial fragmentation in an Arl17 independent manner. To the percentage of infected cells obtained for each category in Fig. 4.9 B the percentage of mock cells in Fig. 4.8 B was subtracted. Graph represents variations in mitochondrial morphology in infected cells (positive values in Y axis) in comparison to mock cells. Negative values represent a decrease and positive represent an increase.

4.6. Depletion of Arl17 delays nuclear export of NP

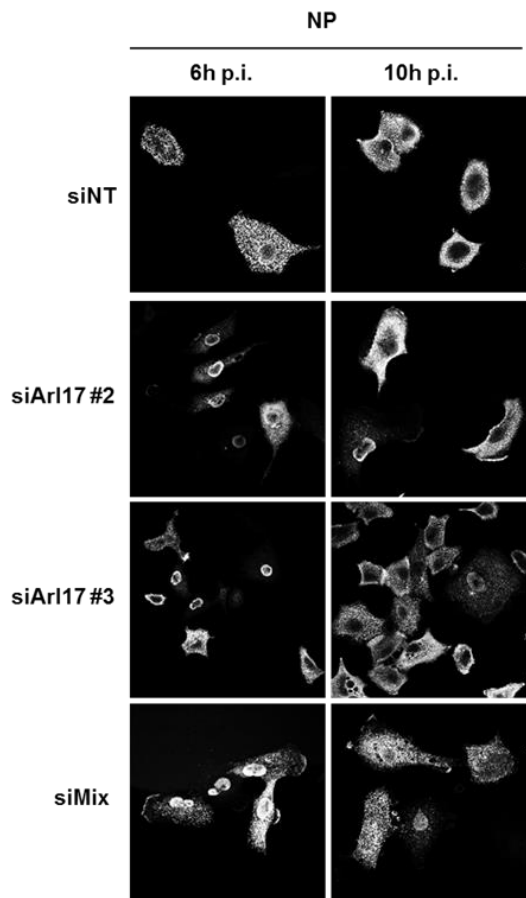
One other interesting observation was made by analyzing progression of infection using NP. NP cellular localization was measured by scoring the number of cells presenting NP at the nucleus, both at the nucleus and the cytoplasm or only in the cytoplasm and the percentages were plotted in a graph (Fig. 4.11 B.).

NP protein contains two nuclear localization signals⁸⁷, and vRNPs are synthesized in the nucleus, hence in the first 4 hours of infection NP is predominantly found in this location. As vRNPs exit the nucleus, NP (that coats vRNPs) is found in the cytoplasm, being prevalently in this location from 8 h p.i. onwards. Representative images of infected cells stained for NP in siNT treated cells are presented in Figure 4.11 A. At 6h p.i. 70% of cells showed NP in the cytoplasm, and at 10 h p.i. this value increased to 100%. In cells depleted of Arl17, this pattern was delayed (Fig. 4.11 A-B). By 6h p.i., a minority of 10-20% of the cells presented NP in the cytoplasm and by 10h p.i. the percentage of cells with cytoplasmic NP was reduced to 70-50% (Fig. 4.10 B).

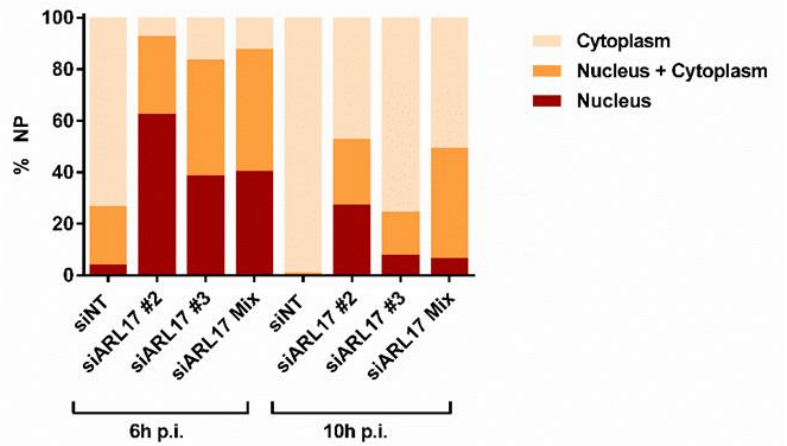
Different stages of the viral lifecycle could be impaired by Arl17 depletion, thus explaining the visible delay in viral progression. In order to determine if the delay was observed in the initial stages of viral infection, a western blot of Arl17 expressing and depleted cells infected or mock infected was performed using cellular extracts harvested in Laemmli buffer. For all viral proteins tested, expression increased from 6 to 10 h p.i., in all conditions. However, no differences were observed between expression of each viral protein between siNT and siArl17 treated samples at either 6 or 10 h p.i. (Fig. 4.11 C). This result indicates that all viral proteins tested are being produced at equal rates in cells with or without Arl17. Therefore, delays in viral entry or viral replication can be excluded at this stage. Impairment in nuclear export upon Arl17 depletion is currently being investigated.

Fig. 4.11 | Infection in Arl17 depleted cells is stalled at the nucleus. A549 cells were transfected with siRNA sequences targeting endogenous Arl17 (siArl17 #2, siArl17 #3 and a mix of both). A non-targeting RNA sequence (siNT) was used as a negative control. 36 hours after transfection cells were infected with PR8 virus at a MOI of 5. At the indicated times p.i., cells were fixed and stained for nucleus (Hoeschst), mitochondria (TOM20) and vRNPs (using NP as a proxy). Images were acquired using Leica SP5. Bar=10µm. (A.) NP channel images showing localization of vRNPs. In cells depleted of Arl17, normal viral progression is delayed at the nucleus. (B.) Quantification of the number of cells presenting NP 1) in the nucleus, 2) in the nucleus and in the cytoplasm or 3) exclusively in the cytoplasm. In Arl17 depleted cells, comparatively to cells transfected with a siNT sequence, vRNPs are delayed in the nucleus. (C.) In parallel to the immunofluorescence assay, cells in the same conditions were harvested at the indicated times p.i., separated by electrophoresis and transferred to membranes that were stained for viral proteins PB1, NS1, NP and M1. GAPDH and Lamin B were loading controls. Red boxes delineate conditions in which Arl17 was not depleted from cells. Comparatively with the other conditions at the same time p.i. the expression levels of the viral proteins are similar, indicating that in all conditions, transcription and translation of viral components is identical. Blue dashed lines are assisting the interpretation of the image by dividing mock and infected cells as well as time of infection.

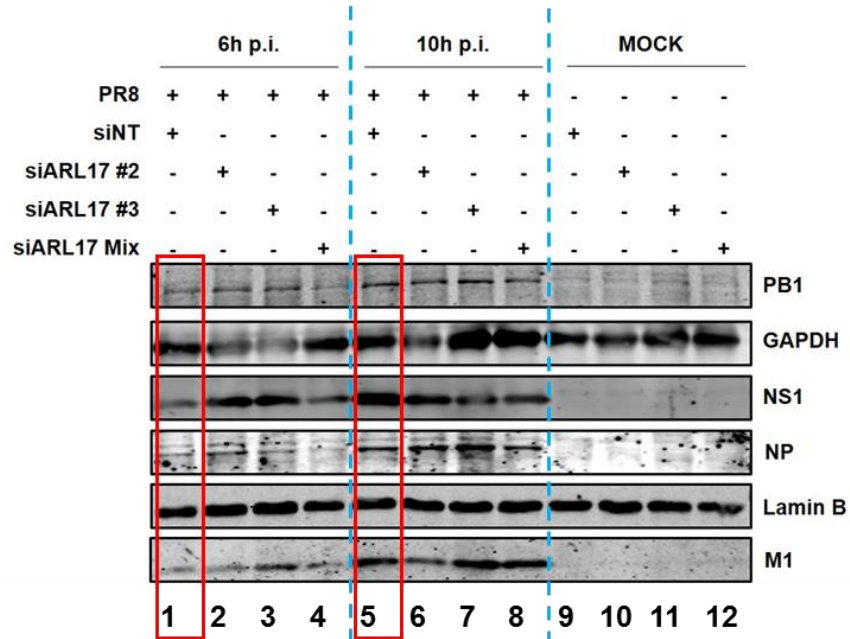
A.



B.



C.



5. Discussion

Mitochondria take part in fundamental reactions in the cell responding to external stimuli and to mitochondrial damage by dynamic changes in shape and distribution. Amongst other roles, these complex organelles are involved in energy and ROS production, amino acid and lipid synthesis, immune response and antiviral signaling, calcium regulation and apoptosis ¹. Because mitochondria are involved in so many pathways, communication with other organelles is fundamental and a tight regulation of mitochondrial quality is necessary.

Several viruses have been reported to take over the mitochondrial dynamics machinery ¹⁵. In the case of IAV, two reports analyzed the interplay between mitochondria and IAV infection, and so this interplay is not well explored. One stated that mitochondria fragmented during infection on account of changes in membrane potential, somehow induced by PB1-F2³³ and the second whereby incoming vRNPs associated with mitochondria to escape innate immunity sensors ³². In addition, preliminary data from the CBV lab, indicated that, at late stages of infection, mitochondria were detected at the cell periphery (Fig. 3.1). These mitochondria, as analyzed by immunofluorescence, were fragmented. These observations suggested that IAV infection modulated mitochondria dynamics at least in two ways: localization and morphology.

Analysis of mitochondrial morphological alterations were the focus of this project. To confirm that IAV infection induces mitochondrial fragmentation, infected cells were stained for mitochondria and classified in a three category ranking system: 1) network-like mitochondria, 2) network mitochondria presenting peripheral fragmentation and 3) completely fragmented mitochondria (Fig. 3.2). Our results indicate that PR8 induced mitochondrial fragmentation (Fig. 3.3 and Fig. 3.4). Our observations are in agreement with the work of Yoshizumi et al. ³³. However, our study conveys two original messages: 1) fragmentation increased progressively with infection from 6 to 16h p.i. and that 2) two types of fragmentation are observed: a) peripheral fragmentation, in which most of the mitochondria present a network-like structure but the periphery is occupied with many fragmented mitochondria and b) complete fragmentation.

Given these differences, and in order to elucidate which viral proteins were responsible for the shift in each type of mitochondria morphology, we decided to evaluate this parameter in cells infected with two mutants: Δ NS1 and Δ 8. These viruses lack either full length NS1 or PB1-F2 and PB1-N40, respectively. The usage of these mutants is justified as these viral proteins were reported to modulate mitochondrial morphology through RIG-I pathway inhibition (NS1) or through Drp1 recruitment (PB1-F2), respectively^{33,69}.

When compared to WT virus infection, Δ NS1 and Δ 8 viruses, lead to a lesser complete fragmentation morphology and a greater network structure, yet, the majority of cells presented mitochondrial fragmentation at the periphery (similarly to WT infection) (Fig. 3.9 compares levels of the three categories in each graph). Our results confirm that both viral proteins modulate

mitochondrial dynamics in infection, but, on their own, NS1 and PB1-F2, do not eliminate, entirely, infection derived mitochondrial modulation.

In addition, we assessed the role of vRNPs as potential modulators of mitochondrial shape in infection, because when evaluating mitochondria morphology during infection it became apparent that vRNPs were, in many occasions, seen in close proximity to fragmented mitochondria at the periphery (Fig 3.3). If vRNPs would be responsible for modulating mitochondria dynamics, then increasing the levels of vRNPs at the mitochondria would increase fragmentation. The lab had developed the perfect system to address this question ⁴⁹. By using the MitoRab11 method that is able to recruit vRNPs directly to mitochondria the effects in mitochondria morphology would be maximized (Fig. 3.10). After assessing the efficient recruitment of vRNPs to the mitochondria when using MitoRab11 CA and WT, morphology levels were analyzed using the three category ranking system. The condition in which recruitment of vRNPs to the mitochondria was more efficient (CA) presented higher levels of mitochondrial fission, immediately followed by MitoRab11 WT (fig 3.12). These observations indicate vRNP-mitochondria association modulates mitochondria morphology by increasing fragmentation. However, results were obtained using an experimental design that pushed the system to a maximum, and requires additional validation, as is very far from natural infection.

We then designed a working model based on the above described observations and in confocal images suggesting that Drp1 may be acting as the link between vRNPs and mitochondria (Fig. 4.1 A). Drp1 plays a major role in mitochondrial fission by oligomerizing around mitochondria and forming a constriction ring that divides mitochondria into smaller portions ⁹. Others have postulated that in infection, Drp1 is either activated or recruited to the mitochondria leading to an increase in fragmentation ³³. Our working hypothesis predicts that vRNPs associate with Drp1 and the mitochondria. If vRNPs are involved in mitochondria fragmentation, then vRNPs should impact in Drp1 recruitment to the mitochondria. The mechanism governing this interaction is currently unknown. However, an association between Drp1 and Rab11a has been reported, in which Rab11a-FIP1C modulated the trafficking of Drp1, and impacted in mitochondria dynamics ¹⁰. Whether a similar process operates here is unknown, although at late stages of infection, when vRNPs and mitochondria were seen in close contact, vRNPs are found in association with Rab11a ⁷⁰. Alternatively, vRNP association with the mitochondria leading to fragmentation is an artefact of our very artificial system.

Our working model further predicts that this association results in fragmented mitochondria that are then relocated to the cell periphery (Fig 4.1 B). Such hypothesis predicts that Drp1 would have a role in infection and that its depletion would reduce viral titers. When tested, Drp1 was important for viral production but for reasons other than increasing antiviral response as the mRNA levels of IFNB1 were not higher in cells depleted of Drp1. However, with one of the siRNAs tested, depletion was efficient but did not result in the same level of reduction in viral titres. It is

therefore possible that the effects observed in viral production result from off target effects of the siRNAs. Rescue experiments should confirm the effect of Drp1 in viral infection.

An interesting question relates with the functional role of relocating fragmented mitochondria to the periphery. Three hypothesis could be considered. Incoming vRNPs were shown to associate with mitochondria by attaching to RIG-I, which resulted in the suppression of type I IFN signaling³² (Fig 2E-a)). In addition, it was recently shown that vRNP association with Rab11 vesicles alters the cellular architecture, promoting vesicular clustering⁷⁴. Such alteration could reduce interferon activation, via modulating mitochondria fragmentation (Fig 5.1a)). Alternatively, the processes of vRNP trafficking on Rab11 vesicles and virion budding require high demand of energy, for which additional recruitment of mitochondria could be advantageous (Fig 5.1b)). Other functional possibilities include mitochondrial redistribution to the periphery might to supplying membrane for virion budding (Fig 5.1c))⁸⁸.

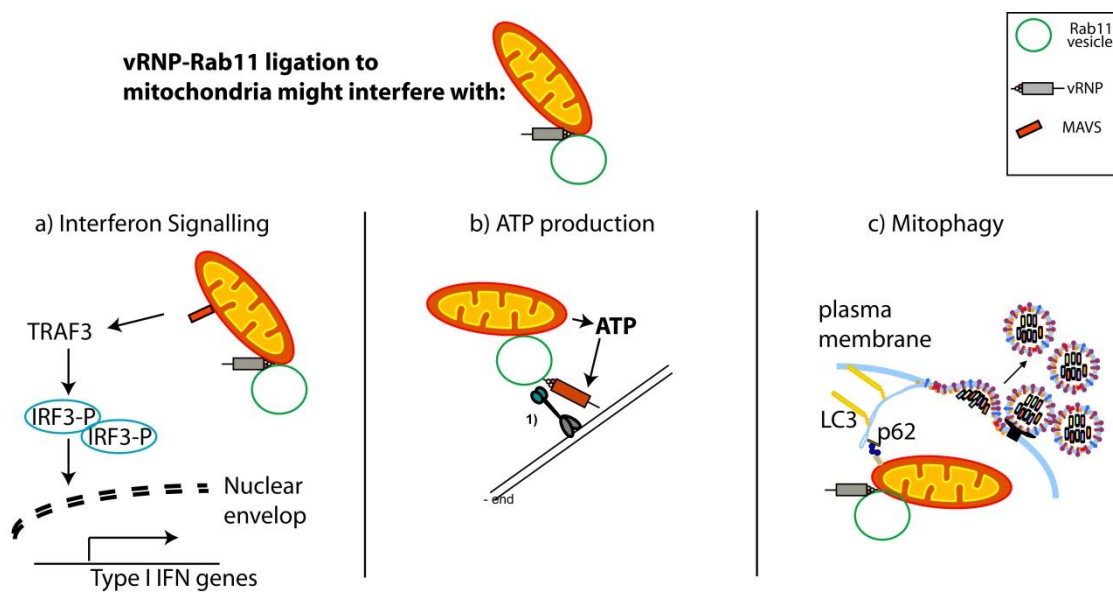


Fig. 5.11 | Models proposed for the role of mitochondria fragmentation and localization at the periphery, modulated by viral infection. Association might interfere (positively or negatively) with interferon response and antiviral signaling (a); provide ATP for trafficking, assembly and budding (b) or induce mitophagy and provide membrane to support viral budding that requires host-derived membranes (c).

Another GTPase targeted to mitochondria is Arl17. Although almost nothing is known about this protein or its function in the cell, Arl17 was identified in a screen as a potential modulator of mitochondrial morphology during infection. Using the MitoRab11 method in cells overexpressing Arl17 mitochondria became completely fragmented.

However, when mitochondria morphology was analyzed in infected cells depleted of Arl17, the results were not as expected. Arl17 depletion gave rise to an increase in mitochondrial fragmentation, regardless of infection (Fig. 4.8). The analysis of viral progression, however,

showed that infected cells depleted of Arl17 exhibited a delayed progression in NP from the nucleus to the cytoplasm, without altering the initial steps in infection, namely viral entry and protein expression (Fig. 4.11). Ongoing experiments are testing whether Arl17 depletion leads to vRNP nuclear retention, although a role of Arl17 in viral RNA synthesis could not be ruled out.

Arl proteins are normally involved in cellular trafficking and participate in initial steps of a signaling cascade of events that culminates in the biogenesis of vesicles ^{84,85}. Since Arl17 has a mitochondrial targeting signal it is tempting to assume that Arl17 may be involved in mitochondrial vesicular transport and development of mitochondrial derived vesicles (MDVs).

MDVs have been reported to establish a bridge between mitochondria and other organelles, namely late endosomes (and lysosomes) and a subpopulation of peroxisomes. The fate of the cargo transported to late endosomes is lysosomal degradation but the fate of the cargo transported to the peroxisomes remains unclear ³.

Ayumu Sugiura, et. al. hypothesize that MDV transport to lysosomes may contribute to mitochondrial quality control in a stage downstream of mitophagy ³. The removal of mitochondrial damaged patches through the generation and transport of MDVs to lysosomes would help maintain mitochondrial integrity. Consequently, only in cases of complete mitochondrial dysfunction would the entire organelle be targeted for mitophagy ³.

If Arl17 is somehow involved in the biogenesis of MDVs, mitochondrial clearance of damaged molecules would have become impaired by Arl17 depletion, which would lead to cellular stress, known to abrogate nuclear export of vRNPs ⁸⁹. Alternatively, accumulation of damaged mitochondria activates mitophagy and mitochondrial fragmentation mediated by Drp1. Mitophagy activates several nuclear transcription factors whose upregulated transcripts are exported from the nucleus using CRM1 ⁶⁴. Since vRNP nuclear export is dependent on CRM1⁹⁰, retention of vRNPs in the nucleus could as well be explained by direct competition for CRM1.

In order to make sure that the effects mediated by Arl17 depletion were not caused by off-target effects of the siRNA used, the ability of Arl17 to rescue viral titers in cells depleted of Arl17 was tested (supplementary data). An Arl17-GFP plasmid resistant to siArl17 treatment (due to the lack of the 3'UTR targeted by the siArl17) was used. Results showed a minor trend of viral titer rescue. Three hypotheses could explain this modest rescue observed. The expression of Arl17-GFP detected by western blotting using an antibody against GFP, revealed that transfection efficiency was low. Alternatively, the GFP tag was hindering the enzymatic activity of Arl17. The molecular weight of this small GTPase is 19kDa whilst GFP molecular weight is 27kDa. Since the tag added to Arl17 is bigger than the protein itself, it is possible that this plasmid encodes for a non-functional protein. The third hypothesis is that the siArl17 may be causing off-target effects and these would be responsible for the lower viral production and delay in infection observed.

Taking all these hypotheses together, Arl17 seems to be maintaining mitochondrial integrity, which might be required for successful viral infection.

6. Future perspectives

This project was designed to evaluate 1) influenza A virus mediated modulation of mitochondria morphology, and identify the 2) viral proteins and 3) the host factors involved.

In relation to the morphological analysis of mitochondria, our data corroborated that PR8 infection induces mitochondrial fragmentation and peripheral localization. In addition, we have shown for the first time that fragmentation is progressive and of two types: complete mitochondria fragmentation and a special kind in which fragments appear at the periphery.

To complete this study, identical analyzes of mitochondrial dynamics should be performed using other strains of IAV with a different pathogenicity to determine if the fragmentation observed was specific of PR8 infection or a general effect of infection. Then, to approximate the system to a real infection, lower MOIs should be used in multicycle infections.

The second aim of the project was to identify viral factors contributing to mitochondria fragmentation. Data obtained in this study indicates that mitochondrial dynamics may be modulated by viral components like PB1-F2 and NS1. Infection with viruses lacking these proteins induced milder fragmentation levels than PR8 WT infection. Complementarily to this analysis, other viral proteins could be tested for their ability to modulate mitochondrial dynamics by using mutated viruses lacking other viral proteins.

Besides mitochondrial modulation by viral proteins, vRNPs were also assessed for their ability to trigger infection induced mitochondrial fragmentation when in association with the organelle. In an artificial system in which vRNPs were obligatorily recruited to the mitochondria via Rab11a that was targeted to the organelle, fragmentation levels increased. However, these results are not conclusive and to further understand the real implications of these modulators in mitochondrial dynamics another type of analyses must be carried out.

First, by inhibiting nuclear export of vRNPs using leptomycin B, mitochondrial fragmentation levels in infected cells over the course of infection should not increase because vRNPs would be enclosed in the nucleus and could not get into close contact with mitochondria. This strategy would prove our hypothesis that vRNP-mitochondria association leads to mitochondrial fragmentation in a viral infection scenario closer to natural conditions. Second, this study could be complemented with super-resolution microscopy analysis of infected cells to improve image resolution and better measure colocalization between vRNPs and mitochondria. Third, biochemical isolation of mitochondria in infected cells and analysis of material co-precipitated, including the vRNP components NP, PB1, PB2 and PA could provide invaluable information as to which percentage of vRNPs associates with mitochondria, and at which time post-infection.

The last chapter of this project focused on the identification of host mechanisms involved in the modulation of mitochondria dynamics in infection. Both GTPases studied, Drp1 and Arl17, can localize to the mitochondria and, when depleted, decrease viral titers. In order to affirm that Drp1

and Arl17 are positively affecting IAV infection, rescue assays should be performed in cells depleted of each of the proteins in which overexpression of the GTPases, using plasmids resistant to the depletion, would completely rescue PR8 viral titers. This result would allow us to firmly say that Drp1 and Arl17 depletion leads to a decrease in viral titers that is not a result of off target effects of the siRNAs used. After viral rescue confirmation, innumerable analysis could be performed to further study the roles of these GTPases in infection. Due to time restrictions, this part of the work was less explored experimentally.

First, starting by Drp1, cells depleted of the protein could be analyzed, by immunofluorescence for infection progression, for expression of viral proteins by western blotting and for vRNA synthesis by primer extension analysis to determine the step in infection where Drp1 participates. Second, by isolating the mitochondrial and cytosolic fractions of infected cells with and without Drp1, it would be possible to analyze, by western blotting, if the viral proteins that make part of vRNPs still co-precipitated with in the mitochondrial fraction. Such analysis would indicate whether Drp1 provides a link between vRNPs and mitochondria.

Regarding Arl17, increased fragmentation of mitochondria was detected in cells depleted of the GTPase, independently of infection. Our working hypothesis regarding Arl17 is that it is involved in the biogenesis of mitochondrial derived vesicles, able to mitigate mitochondrial damage. To verify our hypothesis, mock transfected cells and cells depleted of Arl17 would have to be analyzed, by electron microscopy, for MDV formation. These cells should also be depleted of Drp1 in order to inhibit fission and allow better visualization of vesicle formation. Subsequently, to assess if the mitochondrial fragmentation levels in cells knocked down of Arl17 were due to increased levels of mitophagy activation, the activation of signaling pathways triggered by redox signals, increase in ROS synthesis or cytosolic calcium accumulation should be tested as these are signs of increased mitochondrial stress.

7. References

1. Zong, W. X., Rabinowitz, J. D. & White, E. Mitochondria and Cancer. *Mol. Cell* **61**, 667–676 (2016).
2. Palikaras, K. & Tavernarakis, N. Mitochondrial homeostasis: The interplay between mitophagy and mitochondrial biogenesis. *Exp. Gerontol.* **56**, 182–188 (2014).
3. Sugiura, A., McLelland, G.-L., Fon, E. a & McBride, H. M. A new pathway for mitochondrial quality control: mitochondrial-derived vesicles. *EMBO J.* **33**, 1–15 (2014).
4. Wallace, D. C. HHS Public Access. *Nat Rev, Cancer* **12**, 685–698 (2012).
5. Horvath, S. E. *et al.* Role of membrane contact sites in protein import into mitochondria. *Protein Sci.* **24**, 277–297 (2015).
6. Hockenbery, D. M. Targeting mitochondria for cancer therapy. *Environ. Mol. Mutagen.* **51**, 476–489 (2010).
7. Kim, H.-E., Du, F., Fang, M. & Wang, X. Formation of apoptosome is initiated by cytochrome c-induced dATP hydrolysis and subsequent nucleotide exchange on Apaf-1. *Proc. Natl. Acad. Sci. U. S. A.* **102**, 17545–17550 (2005).
8. Chandel, W. S. E. . L. A. S. and N. S. Mitochondria in the regulation of innate and adaptive immunity. *Immunity* **6**, 356–372 (2015).
9. Chang, C. R. & Blackstone, C. Dynamic regulation of mitochondrial fission through modification of the dynamin-related protein Drp1. *Ann. N. Y. Acad. Sci.* **1201**, 34–39 (2010).
10. Landry, M. C. *et al.* A functional interplay between the small GTPase rab11a and mitochondria-shaping proteins regulates mitochondrial positioning and polarization of the actin cytoskeleton downstream of Src family kinases. *J. Biol. Chem.* **289**, 2230–2249 (2014).
11. Yamada, T., Adachi, Y., Iijima, M. & Sesaki, H. Making a Division Apparatus on Mitochondria. *Trends Biochem. Sci.* **41**, 209–210 (2016).
12. Chan, D. C. Fusion and Fission: Interlinked Processes Critical for Mitochondrial Health. *Annu. Rev. Genet.* **46**, 120830114430006 (2011).
13. Varadi, A. *et al.* Cytoplasmic dynein regulates the subcellular distribution of mitochondria by controlling the recruitment of the fission factor dynamin-related protein-1. *J. Cell Sci.* **117**, 4389–4400 (2004).
14. Sanchez-Madrid, F. & Serrador, J. M. Mitochondrial redistribution: adding new players to the chemotaxis game. *Trends Immunol.* **28**, 193–196 (2007).
15. Khan, M., Syed, G. H., Kim, S. J. & Siddiqui, A. Mitochondrial dynamics and viral infections: A close nexus. *Biochim. Biophys. Acta - Mol. Cell Res.* **1853**, 2822–2833 (2015).
16. Kim, S. J. *et al.* Hepatitis B Virus Disrupts Mitochondrial Dynamics: Induces Fission and Mitophagy to Attenuate Apoptosis. *PLoS Pathog.* **9**, 1–12 (2013).
17. Takeuchi, O. & Akira, S. Innate immunity to virus infection. *Immunol. Rev.* **227**, 75–86 (2009).
18. Zhou, R., Yazdi, A. S., Menu, P. & Tschopp, J. A role for mitochondria in NLRP3 inflammasome activation. *Nature* **469**, 221–5 (2010).
19. Seth, R. B., Sun, L., Ea, C. K. & Chen, Z. J. Identification and characterization of MAVS, a mitochondrial antiviral signaling protein that activates NF- κ B and IRF3. *Cell* **122**, 669–682 (2005).
20. Kawai, T. *et al.* IPS-1, an adaptor triggering RIG-I- and Mda5-mediated type I interferon induction. *Nat Immunol* **6**, 981–988 (2005).
21. Meylan, E. *et al.* Cardif is an adaptor protein in the RIG-I antiviral pathway and is targeted by hepatitis C virus. *Nature* **437**, 1167–1172 (2005).
22. Xu, L. G. *et al.* VISA is an adapter protein required for virus-triggered IFN- β signaling. *Mol. Cell* **19**, 727–740 (2005).
23. Jacobs, J. L. & Coyne, C. B. Mechanisms of MAVS regulation at the mitochondrial membrane. *J. Mol. Biol.* **425**, 5009–5019 (2013).
24. Castanier, C., Garcin, D., Vazquez, A. & Arnoult, D. Mitochondrial dynamics regulate the RIG-I-like receptor antiviral pathway. *EMBO Rep.* **11**, 133–138 (2010).
25. Strahle, L., Garcin, D. & Kolakofsky, D. Sendai virus defective-interfering genomes and the activation of interferon-beta. *Virology* **351**, 101–111 (2006).
26. Ichinohe, T., Yamazaki, T., Koshiba, T. & Yanagi, Y. Mitochondrial protein mitofusin 2 is

- required for NLRP3 inflammasome activation after RNA virus infection. *Proc. Natl. Acad. Sci. U. S. A.* **110**, 17963–8 (2013).
27. Kim, S.-J. *et al.* Hepatitis C virus triggers mitochondrial fission and attenuates apoptosis to promote viral persistence. *Proc. Natl. Acad. Sci. U. S. A.* **111**, 6413–8 (2014).
 28. Kim, S. J., Syed, G. H. & Siddiqui, A. Hepatitis C Virus Induces the Mitochondrial Translocation of Parkin and Subsequent Mitophagy. *PLoS Pathog.* **9**, (2013).
 29. Meng, G. *et al.* Mitophagy promotes replication of oncolytic Newcastle disease virus by blocking intrinsic apoptosis in lung cancer cells. *Oncotarget* **5**, 6365–6374 (2014).
 30. Xia, M. *et al.* Mitophagy enhances oncolytic measles virus replication by mitigating DDX58/RIG-I-like receptor signaling. *J. Virol.* **88**, 5152–64 (2014).
 31. Wang, Q. *et al.* NIH Public Access. **27**, 380–392 (2014).
 32. Liedmann, S. *et al.* Viral suppressors of the RIG-I-mediated interferon response are pre-packaged in influenza virions. *Nat. Commun.* **5**, 5645 (2014).
 33. Yoshizumi, T. *et al.* Influenza A virus protein PB1-F2 translocates into mitochondria via Tom40 channels and impairs innate immunity. *Nat. Commun.* **5**, 4713 (2014).
 34. Bouvier, N. M. & Palese, P. The biology of influenza viruses. *Vaccine* **26**, (2008).
 35. Ducatez, M. F., Pelletier, C. & Meyer, G. Influenza d virus in cattle, France, 2011-2014. *Emerg. Infect. Dis.* **21**, 368–371 (2015).
 36. Szewczyk, B., Bienkowska-Szewczyk, K. & Król, E. Introduction to molecular biology of influenza A viruses. *Acta Biochim. Pol.* **61**, 397–401 (2014).
 37. Tognotti, E. Influenza pandemics: A historical retrospect. *J. Infect. Dev. Ctries.* **3**, 331–334 (2009).
 38. Cheng, V. C. C., To, K. K. W., Tse, H., Hung, I. F. N. & Yuen, K. Y. Two years after pandemic influenza A/2009/H1N1: What have we learned? *Clin. Microbiol. Rev.* **25**, 223–263 (2012).
 39. Carrat, F. & Flahault, A. Influenza vaccine: The challenge of antigenic drift. *Vaccine* **25**, 6852–6862 (2007).
 40. Jagger, B. W. *et al.* An overlapping protein-coding region in influenza A virus segment 3 modulates the host response. *Science* **337**, 199–204 (2012).
 41. Chen, W. *et al.* A novel influenza A virus mitochondrial protein that induces cell death. *Nat. Med.* **7**, 1306–1312 (2001).
 42. Wise, H. M. *et al.* A complicated message: Identification of a novel PB1-related protein translated from influenza A virus segment 2 mRNA. *J. Virol.* **83**, 8021–31 (2009).
 43. Amorim, M. J. & Digard, P. Influenza A virus and the cell nucleus. *Vaccine* **24**, 6651–6655 (2006).
 44. Wise, H. M. *et al.* Identification of a Novel Splice Variant Form of the Influenza A Virus M2 Ion Channel with an Antigenically Distinct Ectodomain. *PLoS Pathog.* **8**, (2012).
 45. Jackson, D. & Lamb, R. A. The influenza A virus spliced messenger RNA M mRNA3 is not required for viral replication in tissue culture. *J. Gen. Virol.* **89**, 3097–3101 (2008).
 46. Muramoto, Y., Noda, T., Kawakami, E., Akkina, R. & Kawaoka, Y. Identification of novel influenza A virus proteins translated from PA mRNA. *J. Virol.* **87**, 2455–62 (2013).
 47. Yamayoshi, S., Watanabe, M., Uraki, R., Goto, H. & Kawaoka, Y. Identification of a novel viral protein expressed from the PB2 segment of Influenza A Virus. *16th Int. Congr. Virol. Montr. Canada* **90**, 375 (2014).
 48. Eisfeld, A. J., Neumann, G. & Kawaoka, Y. At the centre: influenza A virus ribonucleoproteins. *Nat. Rev. Microbiol.* **13**, 28–41 (2014).
 49. Vale-costa, S., Alenquer, M., Sousa, A. L., Kellen, B. & Ramalho, J. Influenza A virus ribonucleoproteins modulate host recycling by competing with Rab11 effectors. 1697–1710 (2016). doi:10.1242/jcs.188409
 50. Huang, Q. *et al.* Early steps of the conformational change of influenza virus hemagglutinin to a fusion active state: Stability and energetics of the hemagglutinin. *Biochim. Biophys. Acta - Biomembr.* **1614**, 3–13 (2003).
 51. Sun, X. & Whittaker, G. R. Role of the actin cytoskeleton during influenza virus internalization into polarized epithelial cells. *Cell. Microbiol.* **9**, 1672–1682 (2007).
 52. de Conto, F. *et al.* Highly dynamic microtubules improve the effectiveness of early stages of human influenza A/NWS/33 virus infection in LLC-MK2 cells. *PLoS One* **7**, 1–11 (2012).
 53. Hutchinson, E. C. & Fodor, E. Nuclear import of the influenza A virus transcriptional machinery. *Vaccine* **30**, 7353–7358 (2012).
 54. Wu, W. W. H., Sun, Y.-H. B. & Panté, N. Nuclear import of influenza A viral ribonucleoprotein complexes is mediated by two nuclear localization sequences on viral

- nucleoprotein. *Viol. J.* **4**, 49 (2007).
55. Nakada, R., Hirano, H. & Matsuura, Y. Structure of importin- α bound to a non-classical nuclear localization signal of the influenza A virus nucleoprotein. *Sci. Rep.* **5**, 15055 (2015).
 56. Poon, L. L., Pritlove, D. C., Sharps, J. & Brownlee, G. G. The RNA polymerase of influenza virus, bound to the 5' end of virion RNA, acts in cis to polyadenylate mRNA. *J. Virol.* **72**, 8214–9 (1998).
 57. Pflug, A., Guilligay, D., Reich, S. & Cusack, S. Structure of influenza A polymerase bound to the viral RNA promoter. *Nature* **516**, 355–60 (2014).
 58. Dias, A. *et al.* The cap-snatching endonuclease of influenza virus polymerase resides in the PA subunit. *Nature* **458**, 914–918 (2009).
 59. Poon, L. L., Pritlove, D. C., Fodor, E. & Brownlee, G. G. Direct evidence that the poly(A) tail of influenza A virus mRNA is synthesized by reiterative copying of a U track in the virion RNA template. *J. Virol.* **73**, 3473–3476 (1999).
 60. Rossman, J. & Lamb, R. Influenza virus assembly and budding. *Virology* **411**, 229–236 (2011).
 61. Matsuoka, Y. *et al.* A comprehensive map of the influenza A virus replication cycle. *BMC Syst. Biol.* **7**, 97 (2013).
 62. Noton, S. L. *et al.* Identification of the domains of the influenza A virus M1 matrix protein required for NP binding, oligomerization and incorporation into virions. *J. Gen. Virol.* **88**, 2280–2290 (2007).
 63. Akarsu, H. *et al.* Crystal structure of the M1 protein-binding domain of the influenza A virus nuclear export protein (NEP/NS2). *EMBO J.* **22**, 4646–4655 (2003).
 64. Elton, D. *et al.* Interaction of the Influenza Virus Nucleoprotein with the Cellular CRM1-Mediated Nuclear Export Pathway Interaction of the Influenza Virus Nucleoprotein with the Cellular CRM1-Mediated Nuclear Export Pathway. *J. Virol.* **75**, 408–419 (2001).
 65. Bui, M., Wills, E. G., Helenius, A. & Whittaker, G. R. Role of the influenza virus M1 protein in nuclear export of viral ribonucleoproteins. *J. Virol.* **74**, 1781–6 (2000).
 66. Neumann, G., Hughes, M. T. & Kawaoka, Y. Influenza A virus NS2 protein mediates vRNP nuclear export through NES-independent interaction with hCRM1. *EMBO J.* **19**, 6751–6758 (2000).
 67. Lamb, R. a, Choppin, P. W., Chanock, R. M. & Lai, C. J. Mapping of the two overlapping genes for polypeptides NS1 and NS2 on RNA segment 8 of influenza virus genome. *Proc. Natl. Acad. Sci. U. S. A.* **77**, 1857–1861 (1980).
 68. Robb, N. C., Jackson, D., Vreede, F. T. & Fodor, E. Splicing of influenza A virus NS1 mRNA is independent of the viral NS1 protein. *J. Gen. Virol.* **91**, 2331–2340 (2010).
 69. Talon, J. *et al.* Activation of Interferon Regulatory Factor 3 Is Inhibited by the Influenza A Virus NS1 Protein. **74**, 7989–7996 (2000).
 70. Amorim, M. J. *et al.* A Rab11- and microtubule-dependent mechanism for cytoplasmic transport of influenza A virus viral RNA. *J. Virol.* **85**, 4143–4156 (2011).
 71. Eisfeld, A. J., Kawakami, E., Watanabe, T., Neumann, G. & Kawaoka, Y. RAB11A is essential for transport of the influenza virus genome to the plasma membrane. *J. Virol.* **85**, 6117–26 (2011).
 72. Avilov, S. V., Moisy, D., Naffakh, N. & Cusack, S. Influenza A virus progeny vRNP trafficking in live infected cells studied with the virus-encoded fluorescently tagged PB2 protein. *Vaccine* **30**, 7411–7417 (2012).
 73. Momose, F. *et al.* Apical transport of influenza A virus ribonucleoprotein requires Rab11-positive recycling endosome. *PLoS One* **6**, 1–15 (2011).
 74. Vale-costa, S., Alenquer, M., Sousa, A. L., Kellen, B. & Ramalho, J. Influenza A virus ribonucleoproteins modulate host recycling by competing with Rab11 effectors. (2016). doi:10.1242/jcs.188409
 75. Leser, G. P. & Lamb, R. A. Influenza virus assembly and budding in raft-derived microdomains: A quantitative analysis of the surface distribution of HA, NA and M2 proteins. *Virology* **342**, 215–227 (2005).
 76. Nayak, D. P., Hui, E. K. W. & Barman, S. Assembly and budding of influenza virus. *Virus Res.* **106**, 147–165 (2004).
 77. Chen, B. J., Leser, G. P., Jackson, D. & Lamb, R. A. The influenza virus M2 protein cytoplasmic tail interacts with the M1 protein and influences virus assembly at the site of virus budding. *J. Virol.* **82**, 10059–10070 (2008).
 78. Steinhauer, D. a. Role of hemagglutinin cleavage for the pathogenicity of influenza virus.

- Virology* **258**, 1–20 (1999).
79. Chen, J. *et al.* Structure of the hemagglutinin precursor cleavage site, a determinant of influenza pathogenicity and the origin of the labile conformation. *Cell* **95**, 409–417 (1998).
 80. Topf, U., Wrobel, L. & Chacinska, A. Chatty Mitochondria: Keeping Balance in Cellular Protein Homeostasis. *Trends Cell Biol.* **xx**, 1–10 (2016).
 81. Rizk, A. *et al.* Segmentation and quantification of subcellular structures in fluorescence microscopy images using Squassh. *Nat. Protoc.* **9**, 586–96 (2014).
 82. Ohman, T., Rintahaka, J., Kalkkinen, N., Matikainen, S. & Nyman, T. a. Actin and RIG-I/MAVS signaling components translocate to mitochondria upon influenza A virus infection of human primary macrophages. *J. Immunol.* **182**, 5682–5692 (2009).
 83. García-Sastre, a *et al.* Influenza A virus lacking the NS1 gene replicates in interferon-deficient systems. *Virology* **252**, 324–330 (1998).
 84. Manuscript, A. & Proteins, A. F. G. NIH Public Access. **12**, 362–375 (2012).
 85. Kahn, R. A. Arfs and Arls: Models for Arf family members in membrane traffic at the Golgi. *Golgi Appar. State Art 110 Years after Camillo Golgi's Discov.* **6**, 106–119 (2008).
 86. Falola, M. I. *et al.* Genomic Copy Number Variants: Evidence for Association with Antibody Response to Anthrax Vaccine Adsorbed. *PLoS One* **8**, (2013).
 87. O'Neill, R. E., Jaskunas, R., Blobel, G., Palese, P. & Moroianu, J. Nuclear Import of Influenza Virus RNA Can Be Mediated by Viral Nucleoprotein and for Protein Import. *J. Biol. Chem.* **270**, 22701–22704 (1995).
 88. Munz, C. Influenza a virus lures autophagic protein LC3 to budding sites. *Cell Host Microbe* **15**, 130–131 (2014).
 89. Dudek, S. M. *et al.* Abl tyrosine kinase phosphorylates nonmuscle Myosin light chain kinase to regulate endothelial barrier function. *Mol. Biol. Cell* **21**, 4042–4056 (2010).
 90. Nguyen, K. T., Holloway, M. P. & Altura, R. A. The CRM1 nuclear export protein in normal development and disease. *Int. J. Biochem. Mol. Biol.* **3**, 137–151 (2012).

8. Supplementary data

Quantification of mitochondria size using the SQUASH software

To quantify changes in mitochondria size over the course of IAV infection, HeLa cells were infected or mock-infected with PR8 WT, or the mutant viruses Δ NS1 and Δ 8, at a MOI of 3 and, at the indicated times p.i., cells were harvested and stained for the mitochondrial marker TOM20. Using confocal images, an average of 100 cells per condition were automatically analysed by the SQUASH software⁸¹, which measured mitochondrial areas. We then assigned mitochondria into 4 categories according to size (Figure S1). No significant differences were found in mitochondrial size distribution for any of the viruses analysed in comparison to mock cells. These results may be due to software limitations that are discussed in chapter 3.2.

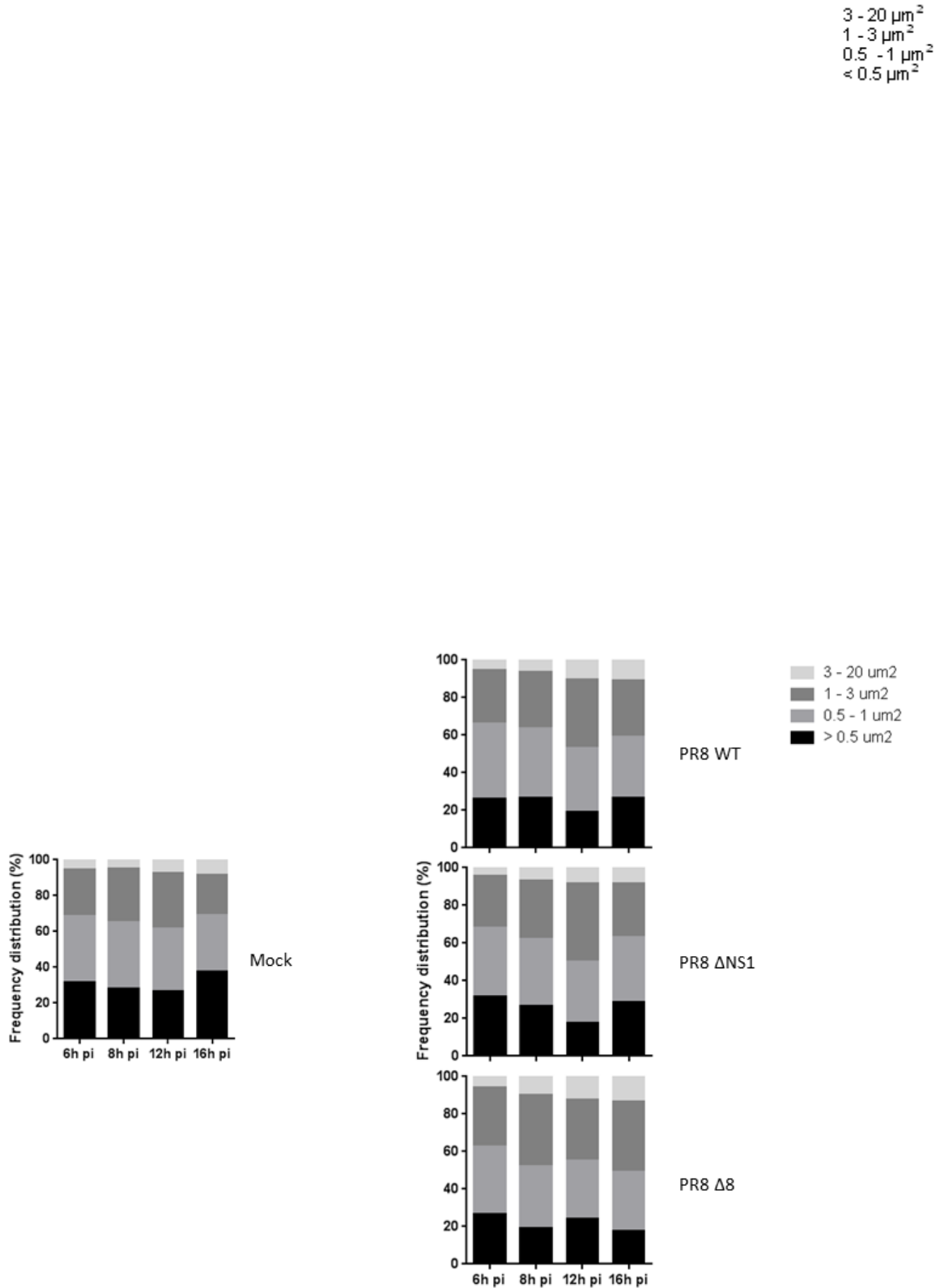


Fig. S1 | Quantification of mitochondrial area during IAV infection using the SQUASSH automated tool. HeLa cells were infected or mock infected with PR8 WT, D8 or DNS1 at a MOI of 3 and, at the indicated times p.i., cells were fixed and stained for the mitochondrial marker TOM20. Each confocal image was automatically analysed by the SQUASH software that quantified the area (in μm^2) of each mitochondria within the cell. The frequency distribution of four size categories in mitochondrial areas was plotted over the course of infection. An average of 100 cells was analysed per time point.

Rescue of viral titers

Our results demonstrate that Arl17 plays a relevant role in mitochondria morphology and its down regulation has a negative impact on IAV viral production. When Arl17 was depleted, mitochondria became more fragmented, regardless of infection. In Arl17 depleted cells, viral titers dropped. However, the degree in titer drop varied with the sequence of siArl17 used. If Arl17 is required for normal viral production, then, by overexpressing Arl17 in cells depleted of the same protein, viral titers should return to their normal values. In order to address this issue, a rescue assay was performed in HeLa cells co-transfected with siArl17 and a plasmid encoding Arl17 tagged with GFP at the N-terminus. ARL17 ectopically expressed by the plasmid is resistant to siArl17 treatment because the sequence used in siArl17#2 targets the 3'UTR of ARL17 that is not present in this plasmid.

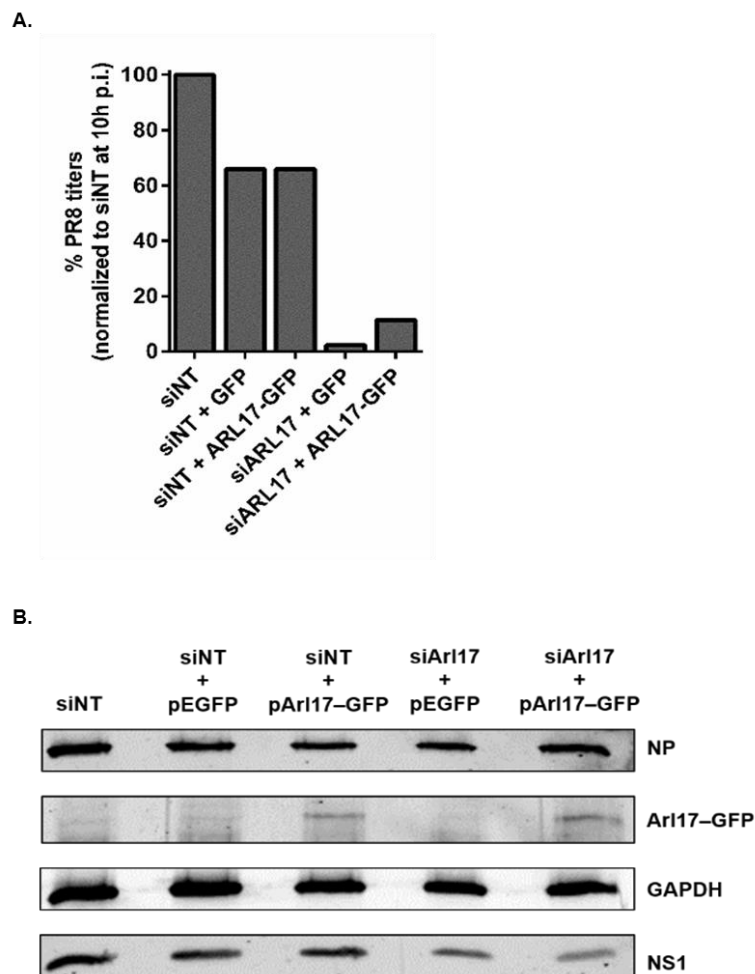


Fig. S2 | Arl17 rescue assay. HeLa cells were co-transfected with the plasmids and siRNAs indicated and incubated for 48h. Cells were then infected or mock infected with PR8 at a MOI of 5 and incubated for further 10h before processing (A.)

Viral titers were normalized to the percentage of the condition siNT control; (B.) Viral and host cell expression by western blot stained for NP, NS1 and GFP (Arl17-GFP) and GAPDH (n=1).

HeLa cells were concomitantly co-transfected with one of the following: 1) siNT, 2) siNT + pEGFP, 3) siNT + pArl17-GFP, 4) siArl17 #2 + pEGFP, 5) siArl17 #2 + pArl17-GFP. 48h after transfection, cells were infected with PR8 virus and supernatants and cells were harvested. Viral titres analysis revealed that treatment with siArl17#2 resulted in a reduction of 95% in viral titres as compared to the control siNT. However, overexpression of Arl17-GFP, resulted in a mild increase in viral titers. The expression of Arl17-GFP detected by western blotting using an antibody against GFP, revealed that low levels of Arl17-GFP were being expressed in cells transfected with its coding plasmid (Fig. S2).